

POLITECNICO DI TORINO

Department of Environment, Land, and Infrastructure Engineering

Master of Science in Petroleum Engineering

ESTIMATION OF LAMINATED RESERVOIR PROPERTIES (A CASE STUDY/ TORTONIAN OIL RESERVOIR)



Supervisors:

prof. Vera Rocca

Dr. Zakaria Hamdi

POLITECNICO DI TORINO

HERIOT WATT UNIVERSITY

Candidate

Ibrahim Ahmed

July 2021

ABSTRACT

The lack of information for reservoir characterization has been a common problem nowadays due to the current economic limitations on companies' capital expenses. Therefore, the reservoir engineer has to fully exploit all available data and estimate the unavailable reservoir characteristics. For lack of core data, the porosity is usually used to estimate the permeability through classical correlations. However, predicting permeability from porosity only and using classical relationships becomes unreliable due to lithology and pore geometry effects. The objective of this study is to test the integration between Flow Zone Indicator (FZI), Artificial Neural Network (ANN), and Convergent Interpolation (CI) techniques to enhance the Tortonian reservoir description in the Gamma oil field using the data of one exploratory well and four appraisal wells.

The reservoir description is done through 1) modeling the non-linear relationship between the Tortonian reservoir properties, 2) calculating the effective porosity after considering the effect of shale on well-log porosity measurements, 3) estimating the permeability of appraisal wells (uncored wells), and 4) creating a permeability map for the Tortonian oil reservoir.

The results showed that three rock types present within the Tortonian reservoirs. The effective porosity and permeability logs were successfully estimated, and the comparison between the created permeability log and quality check logs (GR and porosity logs) reflected the high model quality. A permeability map has been created and showed a direct relationship with the porosity map, which validates the methodology. The reliability of the porosity/permeability relationship has increased up to 90% after using the integrated techniques presented in the study.

The integration between FZI, ANN, and Convergent Interpolation techniques has successfully modeled the non-linear intercourse between the porosity and permeability of the Tortonian reservoir. The study enabled improving the complex reservoir description economically with the minimum capital budget and available data.

ACKNOWLEDGEMENTS

Full thanks to Allah for the gifts which Allah gives me. Firstly, from my heart, I would be honored to declare my full thanks to my supervisors; Professor Vera Rocca, for her help, motivation, and tracking of my work; definitely my full recognition to Dr. Zakaria Hamdi for his gold tips, counseling, which leads to significant, clear, and polished work.

I'm so eager to appreciate my parents, my sons (Adam and Younis), my wife for their patience, face complex situations, especially in Covid-19 age. I'm eager to thank all my colleagues, friends for their support.

Finally, thanks to the ENI scholarship official sponsors for their support and providing all the necessary needs for the smooth and successful completion of the educational process

TABLE OF CONTENTS

ABSTRACT.....	i
ACKNOWLEDGEMENTS.....	ii
LIST OF FIGURES	vi
LIST OF TABLES.....	viii
NOMENCLATURE	ix
1 INTRODUCTION	1
1.1 Introduction.....	1
1.2 Statement of the Problem	1
1.3 Objectives.....	2
2 LITERATURE REVIEW	3
2.1 Reservoir properties.....	3
2.1.1 Porosity	3
2.1.1.1 Porosity classification.....	3
2.1.2 Permeability	4
2.1.2.1 Permeability classification.....	5
2.2 Reservoir properties evaluation.....	5
2.2.1 Coring & core analysis (CA):	5
2.2.1.1 (RCA)	6
2.2.1.2 SCAL	6
2.2.2 Open hole-logs.....	7
2.2.2.1 Gamma-ray logs	7
2.2.2.2 Porosity logs	8
2.2.2.3 Resistivity log.....	10
2.3 Rock typing	11
2.3.1 Flow zone indicator	11
2.3.1.1 FZI validation	14
2.4 Artificial neural networks (ANN)	15
2.4.1 ANN applications in the oil & gas industry.....	17
3 METHODOLOGY	18

3.1	Activity workflow	18
3.2	Input description.....	19
3.2.1	Core data	19
3.2.1.1	Messenian sand core.....	19
3.2.1.2	Tortonian sand core	20
3.2.2	Log data	20
3.2.2.1	Gamma-EX open hole logs	21
3.2.2.2	Gamma-1 open hole logs.....	23
3.2.2.3	Gamma-2 open hole logs.....	25
3.2.2.4	Gamma-3 open hole logs.....	27
3.2.2.5	Gamma-4 open hole logs.....	29
3.2.2.6	Well logs correlation	30
3.3	Estimation of FZI	31
3.3.1	Estimation of FZI flowchart	31
3.4	Effective porosity estimation	32
3.4.1	Effective porosity estimation flow chart for Tortonian reservoir	32
3.5	Estimation permeability logs for uncored appraisal wells	33
3.5.1	Activity flow chart to assess the permeability for the appraisal wells.....	33
3.5.2	ANN model for Gamma oil field.....	34
3.5.2.1	Data processing of Gamma-EX dataset.....	34
3.5.2.2	Building the ANN model.....	34
3.5.2.3	Training the ANN on the training set of Gamma-EX	36
3.5.2.4	Predicting the FZI for the test set of Gamma-EX.....	37
3.5.2.5	Predicting the FZI for the appraisal wells	37
3.6	Creating the permeability map of the Tortonian reservoir.....	38
4	RESULTS	39
4.1	Tortonian's rock types	39
4.1.1	FZI statistical analysis	39
4.2	FZI, effective porosity, and permeability logs for uncored wells	40

4.2.1	Gamma-1	40
4.2.2	Gamma-2	41
4.2.3	Gamma-3	42
4.2.4	Gamma-4	43
4.3	Developed Tortonian's porosity and permeability relationship for the three rock types	44
4.4	Permeability & effective porosity maps of the Tortonian reservoir	45
4.4.1	Tortonian's permeability map	45
4.4.2	Tortonian's effective porosity map	46
5	CONCLUSION.....	47
	REFERENCES	48
	APPENDICES	52
	Appendix A tables of core data.....	52
	Appendix B tables of well-logs	53
	Appendix C tables of results.....	75

LIST OF FIGURES

Figure 2-1 Engineering classification schematic	4
Figure 2-2 GR log vs. lithology	7
Figure 2-3 deep vs. shallow resistivity	10
Figure 2-4 conventional K vs. PHI cross-plot	12
Figure 2-5 RQI – Φ_z Cross-plot	14
Figure 2-6 General ANN architecture	15
Figure 2-7 Cost function VS. NO of epochs.....	16
Figure 3-1 Methodology flow chart.....	18
Figure 3-2 Traditional cross-plot for Messenian sand	19
Figure 3-3 Traditional cross-plot for Tortonian sand	20
Figure 3-4 Tortonian reservoir (cored interval) log data	22
Figure 3-5 Statistical analysis of gamma-ray vs. depth	22
Figure 3-6 Gamma-1 log data for Tortonian reservor	23
Figure 3-7 Statistical distribution of gamma-ray vs. depth	25
Figure 3-8 Gamma-2 log data for Tortonian formation.....	26
Figure 3-9 Statistical distribution of gamma-ray values for upper Tortonian body sand for well Gamma-3	27
Figure 3-10 Gamma-3 logs data for Tortonian formation	28
Figure 3-11Gamma-4 logs data for Tortonian formation	29
Figure 3-12 Well logs correlation	30
Figure 3-13 Flowchart for FZI estimation	31
Figure 3-14 Effective porosity estimation flow chart.....	32
Figure 3-15 Permeability estimation flow chart	33
Figure 3-16 ANN architecture for Gamma oil field	35
Figure 3-17 Python code to build ANN model.....	35
Figure 3-18 Training the ANN code.....	36
Figure 3-19 Gamma-field ANN cost function plot.....	36
Figure 3-20 FZI Pred VS FZI Obs.....	37
Figure 3-21 FZI prediction code	37
Figure 3-22 Permeability map creation workflow.....	38

Figure 4-1 Tortonian's rock types	39
Figure 4-2 FZI statistical analysis.....	39
Figure 4-3 Created logs vs. quality check logs for Gamma-1	40
Figure 4-4 Created logs vs. quality check logs for Gamma-2	41
Figure 4-5 Created logs vs. quality check logs for Gamma-3	42
Figure 4-6 Created logs vs. quality check logs for Gamma-4	43
Figure 4-7 Porosity-permeability relationship of RT-1	44
Figure 4-8 Porosity-permeability relationship of RT-2	44
Figure 4-9 Porosity-permeability relationship of RT-3	45
Figure 4-10 Tortonian's permeability map	45
Figure 4-11 Tortonian's effective porosity map.....	46

LIST OF TABLES

Table 1 Messenian sand core data	52
Table 2 Tortonian reservoir core data.....	52
Table 3 Messenian sand (cored interval) log data.	53
Table 4 Tortonian sand (cored interval) log data.....	53
Table 5 Gamma-1 logs data for interesting intervals of Tortonian FM.....	54
Table 6 Gamma-2 logs data for interesting intervals of Tortonian FM.....	61
Table 7 Gamma-3 log data for interesting intervals of Tortonian FM	64
Table 8 Gamma-4 logs data for interesting intervals of Tortonian FM.....	71
Table 9 FZI and its relevant log data of Gamma-EX	75
Table 10 FZI, effective porosity, and permeability logs of Gamma-1	76
Table 11 FZI, effective porosity, and permeability logs of Gamma-2	81
Table 12 FZI, effective porosity, and permeability logs of Gamma-3	84
Table 13 FZI, effective porosity, and permeability logs of Gamma-4	89

NOMENCLATURE

v	Apparent Flow Velocity, cm/s
k	Permeability, Darcys,mD,m ²
μ	Fluid Viscosity, cp
$\frac{dp}{dl}$	Pressure Drop, atm/cm
Φ	Total Porosity, fraction
pV	Pore Volume, cm ³
BV	Bulk Volume, cm ³
I_{sh}	Shale Index, dimensionless
v_{sh}	Volumetric Shale, dimensionless
Φ_D	Density Derived Porosity, fraction
ρ_l	Fluid Density, g/cm ³
ρ_b	Bulk Density, g/cm ³
ρ_{ma}	Matrix Density, g/cm ³
$\rho_{b,c}$	Corrected Bulk Density, g/cm ³
ρ_{sh}	Shale Density, g/cm ³
Φ_{Dc}	Corrected Density Porosity, fraction
Φ_{Nc}	Corrected Neutron Porosity, fraction
Φ_{Nsh}	Neutron Porosity / Shaly Intervals, fraction
Φ_e	Effective Porosity, fraction
τ	Tortuosity
F_s	Shape Factor
S_{gv}	Surface Area Per Grain Volume, μm^2
RQI	Reservoir Quality Index, μm
Φ_z	Pore Volume Per Grain Volume
FZI	Flow Zone Indicators, μm

1 INTRODUCTION

1.1 Introduction

Nowadays, there is an inadequate information due to expensive operations to identify reservoir characterization, especially for complex structure reservoirs. The reservoir simulation software could not precisely simulate the reservoir structure and the grain distribution within it. Therefore, the reservoir engineer should exploit the available data to manage the reservoir in the optimal way to maximize hydrocarbons recovery.

The core analysis and lab correlations produce non-unique equations, which describe the intercourses between the reservoir variables. Predicting one variable from the other one using the direct relationship that comes from the lab analysis is unreliable due to the complex geological structure of the reservoir. Hence, if the degree of the non-linearity is reduced and correlates the independent variable with the reliant variable, it is feasible to understand and manage such as a complex reservoir.

1.2 Statement of the Problem

Gamma field is an oil field consist of five wells. One of them is exploratory, and the others are appraisal wells to appraise the entire area of interest. Tortonian sand is the target reservoir penetrated by the five wells. Tortoninan sand shows a lamination phenomenon; hence the geological reservoir structure is complex.

The exploratory well is cored and logged; However, the appraisal wells are logged but uncored due to the economic limitations and the shortage of the available exploration budget.

The porosity/permeability relationship of Tortonian sand was derived from the routine core analysis test of the exploratory well. However, there is a high degree of non-linearity between the porosity and permeability because the variation in permeability depends not only on the porosity but also on the geological facies and the pore geometry; hence there is no unique mathematical equation that can describe the classical relationship between permeability and porosity.

A full description of the Tortonion reservoir is required to maximize the oil recovery, which is a big challenge since:

1. The core data for the appraisal wells is not available
2. The classical porosity-permeability relationship drove from the core analysis test of Gamma-EX is unreliable due to the complexity of the reservoir structure

1.3 Objectives

The objective of this study is to test the integration between Flow Zone Indicator (FZI), Artificial Neural Network (ANN), and Convergent Interpolation (CI) techniques for the sake of:

1. Modeling the non-linear relationship between the Tortonian reservoir properties belong to the Gamma oil field
2. Calculating the effective porosity after considering the impact of shale on well-log porosity measurements
3. Estimating the permeability of appraisal wells (uncored wells)
4. Creating a permeability map for the Tortonian oil reservoir

2 LITERATURE REVIEW

2.1 Reservoir properties.

The petroleum domain consists of three fundamental elements (Alyafei, 2019); these elements are:

- Source rock
- Cap-rock
- Reservoir rock

The essential element in the petroleum system is the reservoir rock, which is the rock that has sufficient storage capacity to store a significant amount of hydrocarbons and can transmit the fluid (Amyx et al., 1960). The rock's ability to hold the fluid is the porosity (void space), and permeability is a porous medium property that measures fluid transmission capability for the formation (Ahmed, 2001).

The diagenetic process determines the structure of the inner reservoir and identifies the porosity, permeability, and other physical characteristics of the reservoir rock (Bjorlykke et al., 2011; Clark, 1960). Carbonates and sandstones are generally reservoir rocks that contain hydrocarbons. Tissot and Welte report that around 10% of petroleum occurrences founded in fractured shale, igneous, and metamorphic rock (Dandekar, 2015).

2.1.1 Porosity

From a mathematical standpoint, the porosity is fractional of the bulk volume of the rock (Ahmed, 2001). Once the water plays an essential role in the transmission and depositional processes, the water employs a part of the void space, isolating this part of the void space. However, most pore space still has a movable fluid, water, oil, or gas (Clark, 1960).

2.1.1.1 *Porosity classification*

- (1) In terms of origin mode (Amyx et al., 1960)
 - Original
 - Induced

(2) Engineering classification (Alyafei, 2019)

- Total porosity
- Effective porosity
- Ineffective porosity

The distinction among the subdivision of the porosity: total, effective, and ineffective porosity highlighted through Figure 2-1.

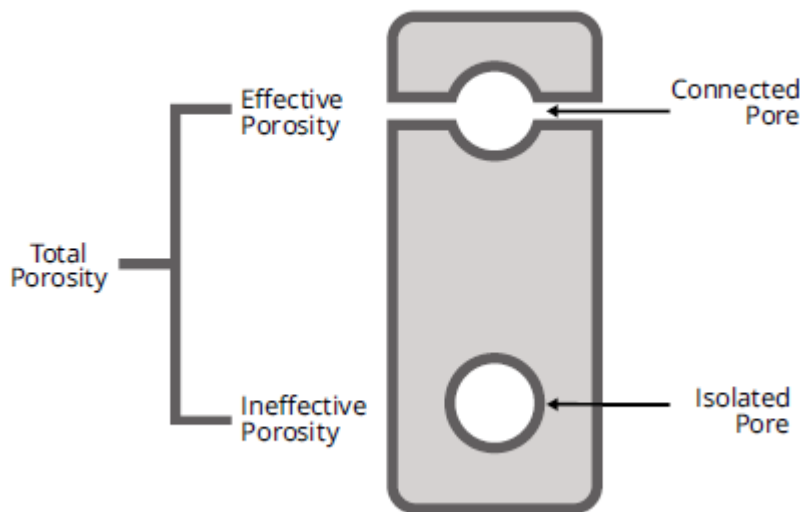


Figure 2-1 Engineering classification schematic

(source: (Alyafei, 2019))

2.1.2 Permeability

The facility to move the fluid through rock spaces reflects the degree of rock permeability (Clark, 1960). The rock permeability, which guides the fluid and controls the flow rate, is an essential rock property. Henry Darcy mathematically defined this rock characterization in 1856 (Ahmed, 2001). Indeed, in terms of mathematical calculations, the equation that describes permeability is called - Darcy's Law (Amyx et al., 1960) see equation (2-1)

$$v = - \left[\frac{k}{\mu} \right] \frac{dp}{dl} \quad (2-1)$$

Where v = apparent flow velocity, cm/s

k = permeability, Darcys

μ = fluid viscosity, cp

$\frac{dp}{dl}$ = pressure drop, atm/cm

2.1.2.1 Permeability classification

The classification according to the number of phases saturates the rock's porous (Alyafei, 2019). These classifications are:

- Effective permeability
- Absolute permeability
- Relative permeability (rock and fluid interaction)

2.2 Reservoir properties evaluation

2.2.1 Coring & core analysis (CA):

Core quality material is crucial for the success of an assessment of rock characterization (Ubani & Adeboye, 2013). The coring program must minimize rock damage and maximize rehabilitation. Core handling and preservation procedures used before the core's arrival in the laboratory are equally important (Skopec, 1994).

There are two essential classes of testing for CA performed on core specimens concerning the reservoir characteristics (Ahmed, 2001). These classes are:

(1) Routine CA tests

- Porosity (Φ)
- Permeability (K)
- Saturation (S)

(2) Special CA tests

- Relative Permeability
- Wettability
- Capillary pressure (CP)
- Interfacial tension
- Overburden pressure

2.2.1.1 (RCA)

RCA measures the essential rock characteristics under near-ambient conditions: Porosity and intrinsic permeability (Ubani & Adeboye, 2013).

Porosity evaluation:

Porosity is a function in bulk volume & pore volume described by equation (2-2) (Dandekar, 2015) as follows:

$$\Phi = \frac{pV}{BV} \quad (2-2)$$

Where Φ = total porosity

pV = pore volume, cm^3

BV = bulk volume, cm^3

Vacuum saturation and Helium expansion are the main methods for measuring the void spaces. However, the bulk volume is determined by calibrating the plug sample or through the Archimedes principle (Dandekar, 2015; Ubani & Adeboye, 2013).

Permeability evaluation:

The intrinsic permeability of reservoir rock is measured directly by utilizing gas flowing through the core plug under steady-state or transient conditions, such as air, nitrogen, or helium. However, due to economic constraints, the liquid flowing through the core plug is unpreferable (Dandekar, 2015; Ubani & Adeboye, 2013).

By injecting the air, nitrogen, or helium through the core plug under a controlled flow rate, pressure, and well-known core plug geometry, it is easy to estimate the permeability by using the proper form of Darcy's law (Ubani & Adeboye, 2013).

2.2.1.2 SCAL

The crucial task of SCAL is to identify the rock-fluid interaction properties, which are embedded in the reservoir modeling to describe the fluid flow within the reservoir, displacement processes, and transition zone thickness (Baker et al., 2015b).

2.2.2 Open hole-logs

Lithology, porosity, permeability, formation water salinity, and rock stiffness are the fundamental rock characteristics that affect logging measurements. The interpretation of the logging tool response is essential to identify these properties (Asquith & Krygowski, 2014). The most crucial logging tool are:

- Gamma-ray (GR) logs
- Porosity logs
- Resistivity logs

2.2.2.1 *Gamma-ray logs*

Radionuclides, mainly potassium, uranium, and thorium decay, originate the present application of the gamma-ray logs. Radio-active minerals mainly concentrate on the shaly formation, which gives high gamma-ray values. However, the sandy formation or free shale rock gives low gamma-ray readings (Asquith & Krygowski, 2014; Killeen, 1982). See Figure 2-2

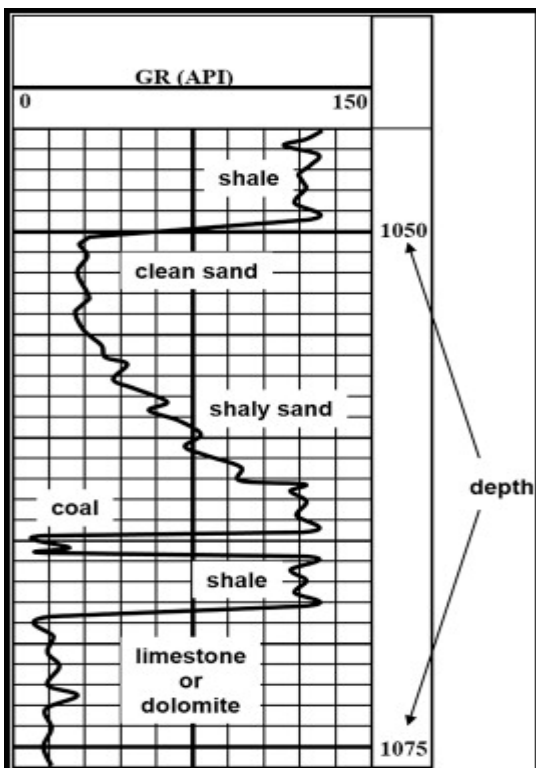


Figure 2-2 GR log vs. lithology

(source: (Baker et al., 2015a))

Shale volume evaluation

The shaly formation contains clay minerals, organic matter as well. The structure, laminar, and dispersed shale within reservoir rocks reduce the reservoir's storage capacity, flow capacity, and effective porosity. Also, the shale affects the open-hole logs measurements (Bassiouni, 1994; MK, 2017).

Gamma-ray index gives the first indication of the shale volume, which calculated by the following equation (Asquith & Krygowski, 2014; Bassiouni, 1994):

$$I_{sh} = \frac{GR_{log} - GR_{min}}{GR_{max} - GR_{min}} \quad (2-3)$$

Where I_{sh} = shale index, dimensionless

GR_{log} = the GR value from the log, API

GR_{min} = the minimum GR reading from the log, API

GR_{max} = the maximum GR value from the log, API

The shale volume directly relates with the gamma-ray index through non-linear empirical equations, which gives low shale volume compared to the linear relationship(Asquith & Krygowski, 2014). Larionov (1969) represents the non-linear relationship between the shale volume and the gamma-ray index for tertiary rock equation (2-4) (Asquith & Krygowski, 2014; Bassiouni, 1994) as follows:

$$v_{sh} = 0.083(2^{3.7I_{sh}} - 1) \quad (2-4)$$

Where: v_{sh} = shale volume, dimensionless

0.032 & 3.71 are the correlation constants for tertiary rocks

2.2.2.2 Porosity logs

Porosity logs measure the porosity indirectly based on nuclear measurements such as density and neutron logs or acoustic measurements such as sonic logs (Asquith & Krygowski, 2014).

Neutron logs (Φ_n , NPHI) measure the hydrogen amount retained into the porous media in the absence of the shale. However, the density logs (Φ_d) measure the bulk density (BHOB or RHO); the combination between neutron and density logs enhances the estimation of rock lithology and detects hydrocarbon-bearing zone (Asquith & Krygowski, 2014).

Effective porosity evaluation

The integration between fluid type, matrix nature, shale volume enhances reliable porosity estimation (Kamel & Mohamed, 2006). Therefore, the first step to evaluate rock porosity from the porosity logs is to correct the readings because the shale content affects the logging tool response (Bassiouni, 1994).

The equation (2-5) (Bassiouni, 1994; HLS, 2007) is used for calculating rock porosity from the density log:

$$\Phi_D = \frac{\rho_{ma} - \rho_b}{\rho_{ma} - \rho_l} \quad (2-5)$$

Where Φ_D = density derived porosity

ρ_l = fluid density, g/cm³

ρ_b = observed bulk density, g/cm³

ρ_{ma} = bulk density of the rock matrix, for sand 2.64 g/cm³ (Asquith & Krygowski, 2014).

The equation(2-6) (Miah, 2014) gives the corrected bulk density as:

$$\rho_{b,c} = \rho_b + v_{sh}(\rho_{ma} - \rho_{sh}) \quad (2-6)$$

Where $\rho_{b,c}$ = corrected bulk density, g/cm³

ρ_{sh} = observed bulk density for shale interval, g/cm³

The formulation of calculating the corrected density derived porosity and adjusted neutron porosity (HLS, 2007; Miah, 2014) as follows:

$$\Phi_{Dc} = \frac{\rho_{ma} - \rho_{b,c}}{\rho_{ma} - \rho_l} \quad (2-7)$$

$$\Phi_{Nc} = \Phi_N - v_{sh} \times \Phi_{Nsh} \quad (2-8)$$

Where Φ_{Nc} = corrected neutron porosity, fractional

Φ_N = neutron porosity observed from neutron log, fractional

Φ_{Nsh} = neutron porosity observed for shale interval, fractional

Finally, the following equation (HLS, 2007) determines the effective porosity:

$$\Phi_e = \frac{\Phi_{Nc} + \Phi_{Dc}}{2} \quad (2-9)$$

2.2.2.3 Resistivity log

The rock skeleton is a high resistive material to transmit electric current. However, the bulk resistivity of the formation depends on the fluid that saturates the bore space. The hydrocarbons are non-conductive. The ability of the layer to conduct electric current depends on the water content and water salinity as well. The main tasks of the resistivity logs are (Asquith & Krygowski, 2014):

- Identify fluids contact
- Indicate permeable layers

Figure 2-3 highlights how the resistivity logs indicate the permeable layers

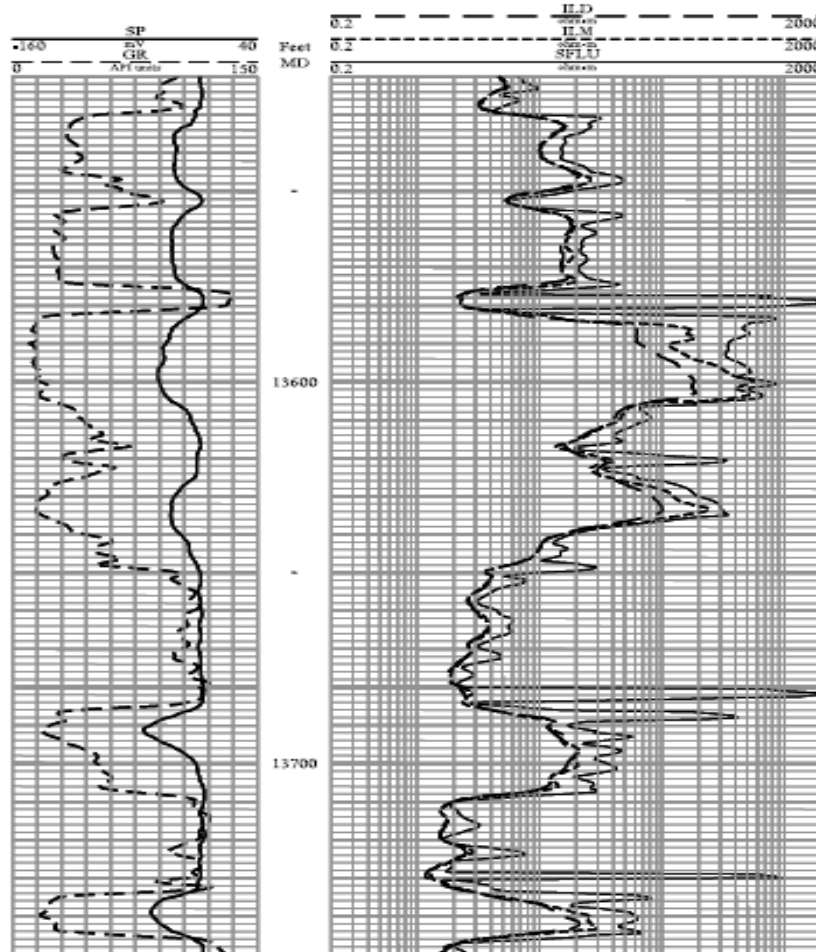


Figure 2-3 deep vs. shallow resistivity
(source: (Asquith & Krygowski, 2014))

2.3 Rock typing

The process by which reservoir rock is divided into geological units as a reservoir building block is called rock typing; each block has the same geological facies, flow capacity, and storage capacity. In the permeability-porosity framework, the integration between the diagenesis properties and the depositional environment defines the rock type. The supreme rock type has similar geological facies and the same reservoir characteristic (Tavakoli, 2018).

There are four main rock typing techniques (Haikel et al., 2018), these are:

- Lucia
- Winland R35
- Flow zone indicator (FZI)
- Pore geometry structure (PGS)

2.3.1 Flow zone indicator

The most relevant approach of rock typing techniques is FZI, which depends on the core data. The method divides the rock into hydraulic units(Amaefule et al., 1993). Gunter (1997) defined the hydraulic unit as a volume of rock that has the same characteristics and geological features; Tiab and Donaldson (2015) believed that the reservoir unit is mappable, correlative, identifiable by wireline logs (Tavakoli, 2018).

Most hydrocarbon wells, due to economic constraints, are uncored. Non the less, actual reservoir characteristics are often determined by core analysis tests. In the absence of core data, permeability distribution is assessed from porosity logs based on an empirical equation developed from the conventional cross-plot of porosity versus logarithmic permeability (Amaefule et al., 1993; Soto B. et al., 2001).

Figure 2-4 shows a traditional cross plot of K versus Φ ; only 14 % of the data fitted by the power function trendline, which means the variation in permeability isn't dependent only on porosity distribution. Lithology and pore geometry play an essential role in describing the variation in permeability. However, the classical cross plot doesn't consider the grain size distribution and lithological effect (Amaefule et al., 1993; Haikel et al., 2018).

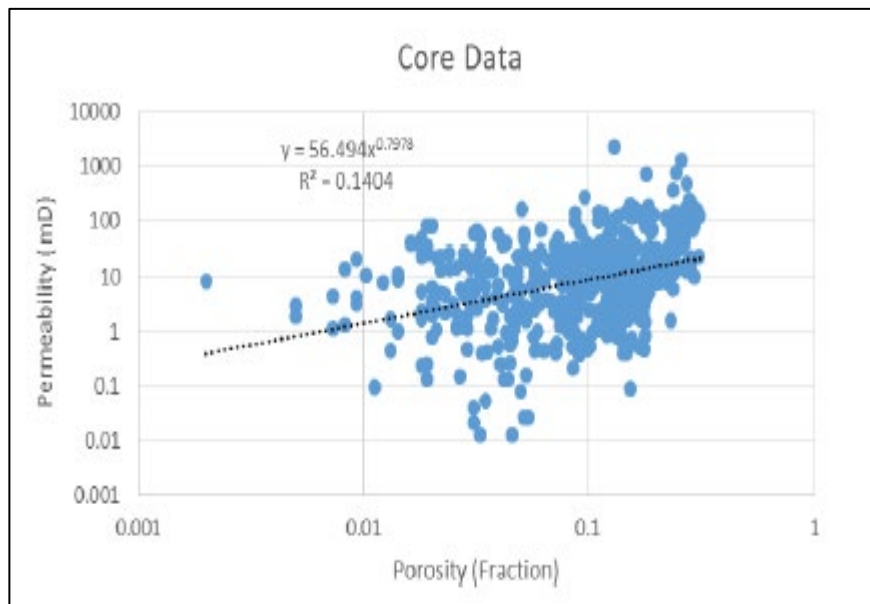


Figure 2-4 conventional K vs. PHI cross-plot

(source: (Haikel et al., 2018))

The generalized equation of the Kozeny-Carmen approach represents the pore throat as capillary tubes to consider the effect of the geological feature on permeability variation. The equation (2-10) (Amaefule et al., 1993) is described as follows:

$$K = \frac{\Phi_e^3}{(1 - \Phi_e)^2} \left[\frac{1}{F_s \tau^2 S_{gv}^2} \right] \quad (2-10)$$

where: K = permeability, μm^2

Φ_e = effective porosity

τ = tortuosity

F_s = shape factor

S_{gv} = surface area per unit grain volume, μm^2

The Kozeny-Carmen relationship describes the reservoir as a circular cylinder to measure the flow capacity through the entire domain. However, in reality, the reservoir is not a perfectly circular cylinder. Also, it is challenging to investigate and define the pore geometry to calculate the tortuosity and surface area. So this assumption is not applicable (Amaefule et al., 1993).

(Amaefule et al., 1993) manipulate the Kozeny-Carmen equation and reach the applicable equation in the porosity-permeability framework; the equation (2-11) as follows:

$$\sqrt{\frac{K}{\Phi_e}} = \left[\frac{\Phi_e}{1 - \Phi_e} \right] \left[\frac{1}{\sqrt{F_s \tau S_{gv}}} \right] \quad (2-11)$$

This equation (2-11) opens the door for one of the most crucial concepts for reservoir engineering and geoscientist, the flow zone indicator. The equation highlights three essential terms; the first one is the reservoir quality index (RQI) which represented as follows:

$$RQI = 0.0314 \sqrt{\frac{K}{\Phi_e}} \quad (2-12)$$

Where RQI is in μm

The second term is the ratio between the pore volume and the grain volume, which is known as Φ_z and characterized by the following equation:

$$\Phi_z = \frac{\Phi_e}{1 - \Phi_e} \quad (2-13)$$

The third and most important one is the flow zone indicator (FZI), which considers the pore geometry, grain distribution, and facies quality. The following equation estimates the FZI:

$$FZI = \frac{RQI}{\Phi_z} = \frac{1}{\sqrt{F_s \tau S_{gv}}} \quad (2-14)$$

Where FZI is in μm

By substituting the three terms into the equation (2-11) as logarithmic, the result will be as follows:

$$\log RQI = \log \Phi_z + \log FZI \quad (2-15)$$

RQI - Φ_z Cross-plot gives the number of the hydraulic units that have the same FZI values and represented by straight line has unit slop (see Figure 2-5).

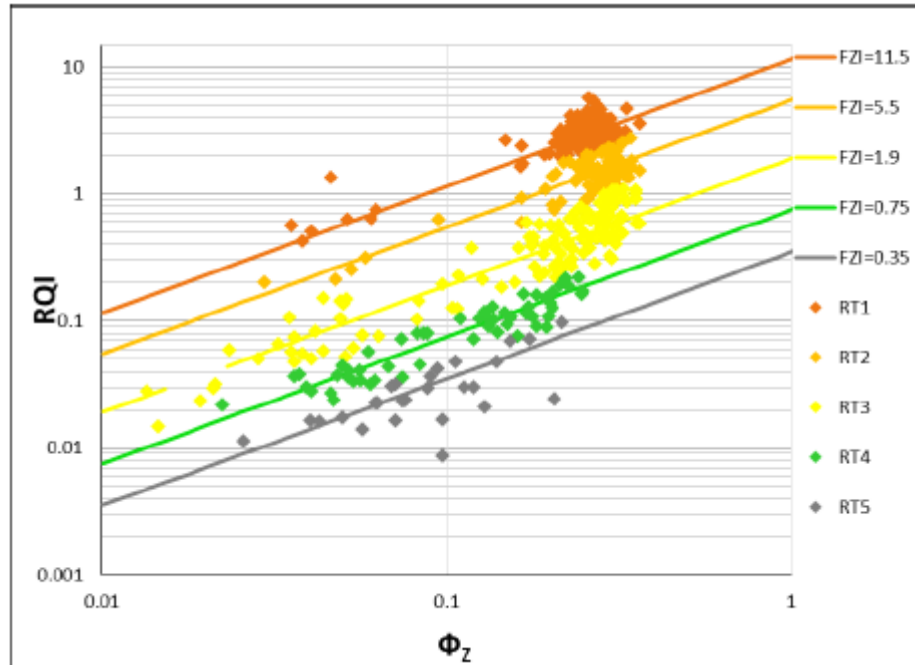


Figure 2-5 RQI – Φ_z Cross-plot

(source: (Sritongthae, 2016))

Once FZI has been detected and by substituting into the equation (2-10), it is feasible to appraise the permeability as follows:

$$K = 1014(FZI)^2 \frac{\Phi_e^3}{(1 - \Phi_e)^2} \quad (2-16)$$

Where K is in millidarcy, FZI is in μm .

2.3.1.1 FZI validation

(Abbas & Al Lawe, 2019; Biniwale, 2005; Dezfoolian, 2013; Hashim et al., 2017; Sritongthae, 2016; Uguru et al., 2005) tested the FZI method successfully for shale (Iraq), (Australian fields),(Thailand fields), carbonate study, laminated sandstone, and Nigr delta. All of them predicted the reservoir characteristics effectively.

2.4 Artificial neural networks (ANN)

ANN mimics the human brain function, which is composed of millions of neurons. Each group of neurons represents a layer where each layer has a specific job. Therefore, integrating the layers is essential to complete the required mission (Basheer & Hajmeer, 2000).

ANN receives input signals through the input layer; each neuron of the input layer retains one signal. Those signals transfer to other layers to be processed and produce final outputs transferred from the output layer; the processing layers are called hidden layers. The amount of neurons/units that make up the hidden sequence/ layer depends on the signal processing complexity (Kay, 2001).

Each neuron of the input sequence relates to the hidden unit (neurons) by so-called synapses, which allow the signal to transfer from the unit of the input sequence to the unit of the hidden sequence. The weights represent the synapses that control the signal transfer among the units; the weights behave as a filter for signals which permit free noise signal to transfer (Nielsen, 2006; Rodolfo et al., 2002). See Figure 2-6.

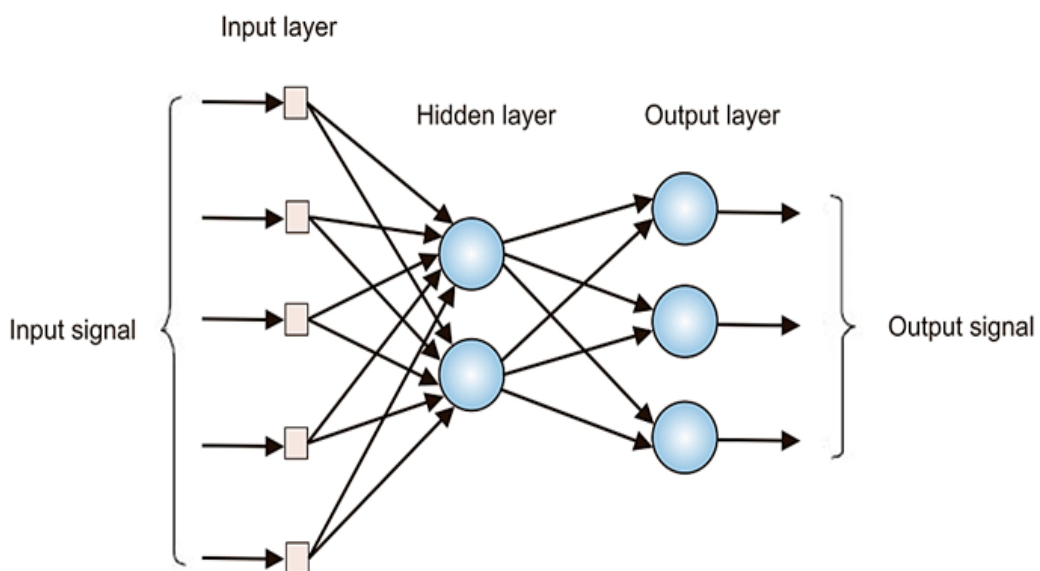


Figure 2-6 General ANN architecture

(source : (Al-Aboodi et al., 2017))

ANN aims to model the non-linearity between the inputs and outputs variables through learning the nature of variables dependency. So the starting point to build an artificial neural network model is splitting the dataset into:

1. The training set helps the ANN to model the non-linearity between dependent and independent variables.
2. The test set validates the ANN model.

One of the most important concepts is the misfit (cost function) between the predicted output & the observed outputs. The cost function decreases by updating the weights through adjusting the model parameters; these are:

1. The quantity of hidden stratification
2. The quantity of the hidden units
3. Trials number
4. Learning rate (η), which is the percentage of updated weights
5. The ratio between the test data to the total data set

The backpropagation process renovates the weights according to their share in the misfit; for each trial or optimization. Therefore, the cost function and the number of trials cross-plot control the ANN model's parameters. For instance, Figure 2-7 highlights the learning rate (η) effect on the misfit-number of epochs cross plot. The misfit decreases dramatically with diminishing the learning rate (Nielsen, 2006).

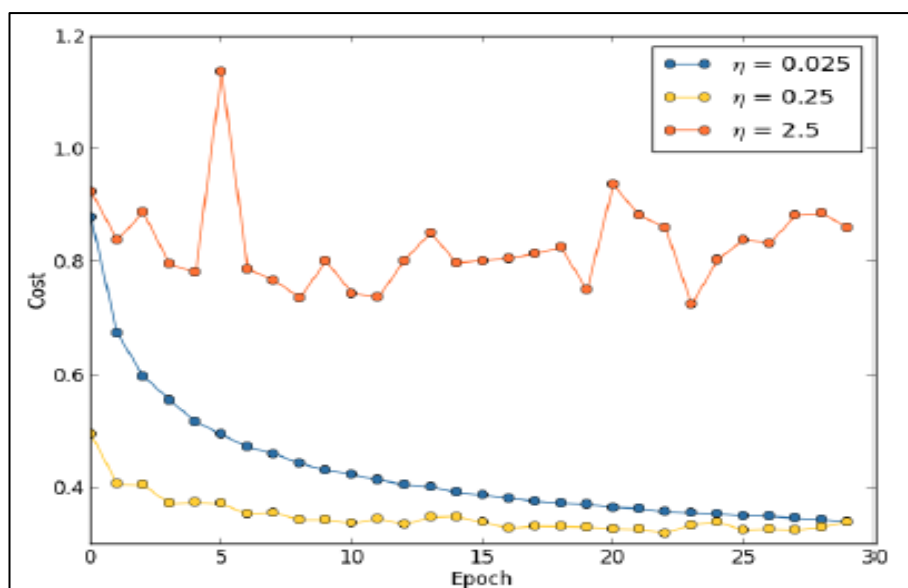


Figure 2-7 Cost function VS. NO of epochs

There are two backpropagation techniques to reach minimum misfit:

1. Batch-gradient descent (BGD)
2. Stochastic-gradient descent (SGD)

BGD, working on the complete matrix to research for the global error. It divides the dataset into groups; each group has a local error. BGD aims to decrease the significant misfit as a global error.

SGD reduces the local misfit for each element in the matrix domain, increasing the computational cost. However, it gives high accuracy.

2.4.1 ANN applications in the oil & gas industry

In the absence of the essential data to describe the reservoir properties, the ANN plays a vital role in estimating reservoir characteristics. The ANN method is tested successfully by (Rodolfo et al., 2002; Soto B. et al., 2001; Uguru et al., 2005).

3 METHODOLOGY

3.1 Activity workflow

Figure 3-1 shows the workflow to estimate the Tortonian reservoir properties.

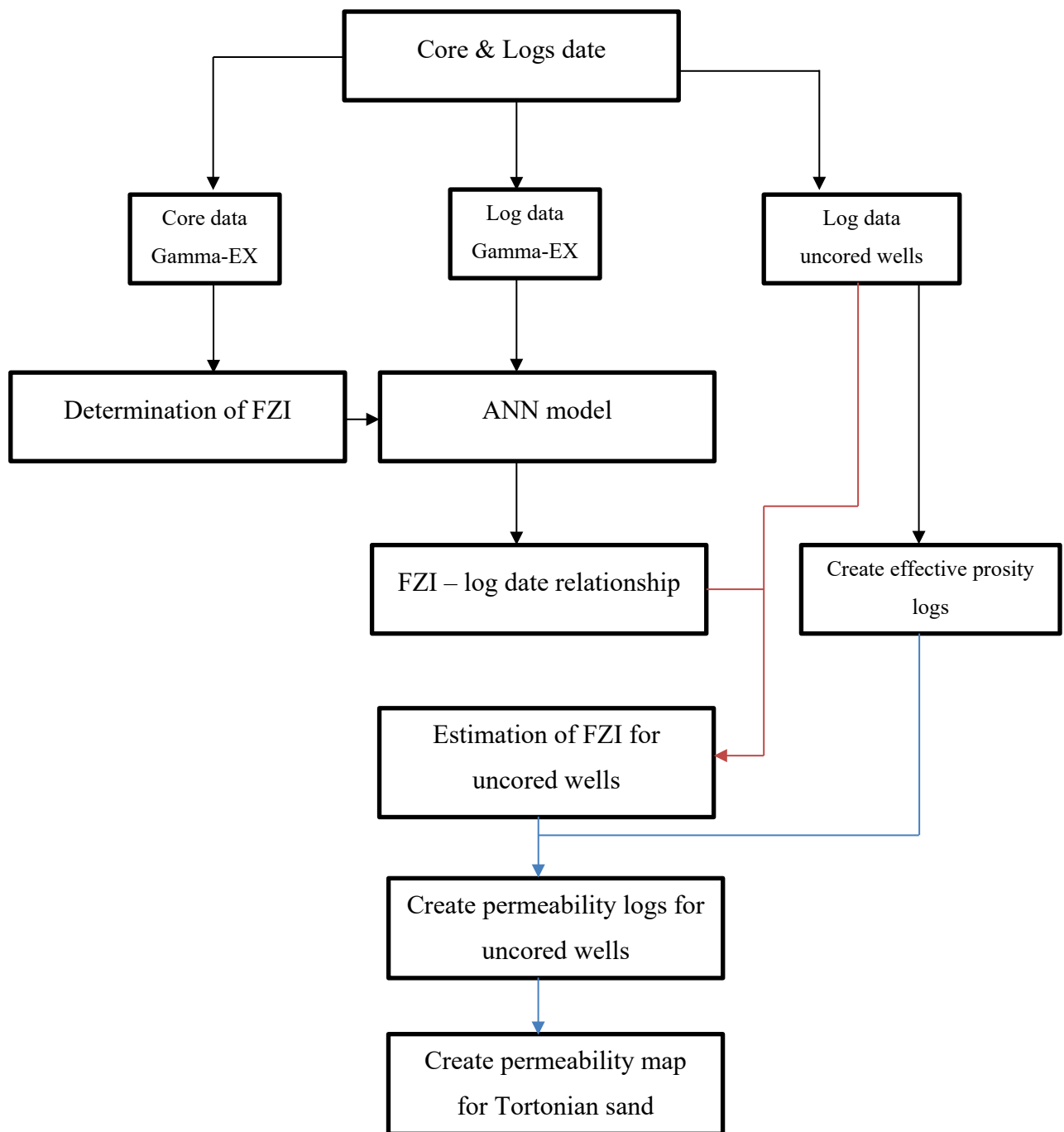


Figure 3-1 Methodology flow chart

3.2 Input description

3.2.1 Core data

The coring operation performed during the exploratory well Gamma-EX drilling activity shows two reservoir targets; these are

1. The upper target is Messenian sand
2. The lower target is Tortonian sand

The rock reservoir's unpreserved cores are acquired by the conventional coring bit. Tortonian sand is the reservoir of interest because its reservoir structure is more complex than the Messenian one.

3.2.1.1 *Messenian sand core*

The well Gamma-EX penetrates the Messenian reservoir and intersects the top of the formation at 6702 FT-MD till the bottom of the sand at 6725 FT-MD; the entire interval was cored and logged, the core has been cut, labeled, and packed in 1 feet boxes.

Thirteen plug samples were subjected to (RCA) test, where each sample represents a specific depth. The RCA test gives Messenian reservoir porosity and permeability (Table 1, appendix A).

The traditional K and Φ cross-plot graph shows that 33% of data fit the relationship developed from the classical plot, and the owner company accepts the ratio (as shown in Figure 3-2).

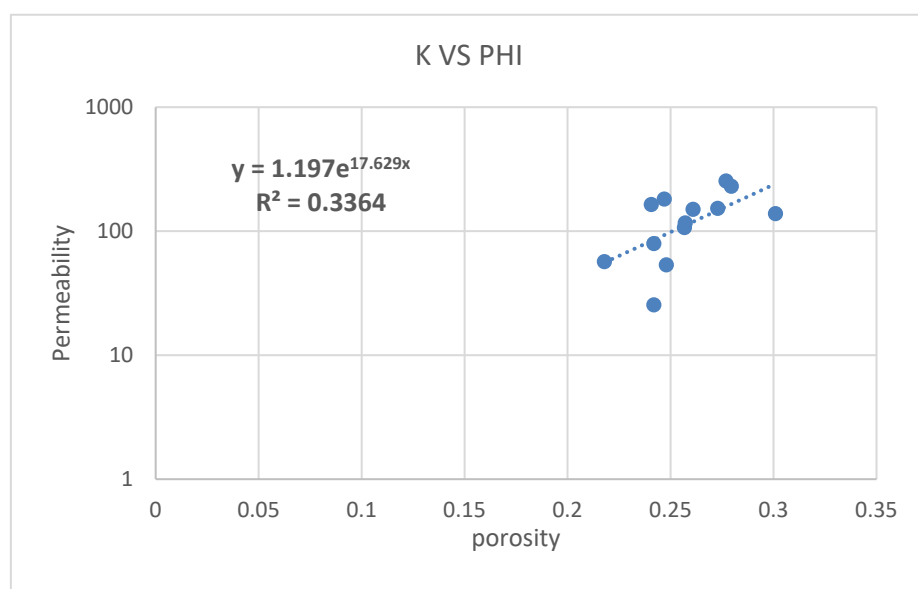


Figure 3-2 Traditional cross-plot for Messenian sand

3.2.1.2 Tortonian sand core

The well Gamma-EX penetrates the Tortonian reservoir and intersects the top of the formation at 7187 FT-MD till the bottom of the sand at 7229 FT-MD; the entire interval was cored and logged, the core has been cut, labeled, and packed in 1 feet boxes.

Twenty plug samples were subjected to (RCA) test, where each sample represents a specific depth. The RCA test gives Messenian reservoir Φ and K (Table 2, appendix A). The traditional K and Φ cross-plot graph shows that less than 1% of data fit the relationship developed from the classical plot due to the lithology effect. (see Figure 3-3).

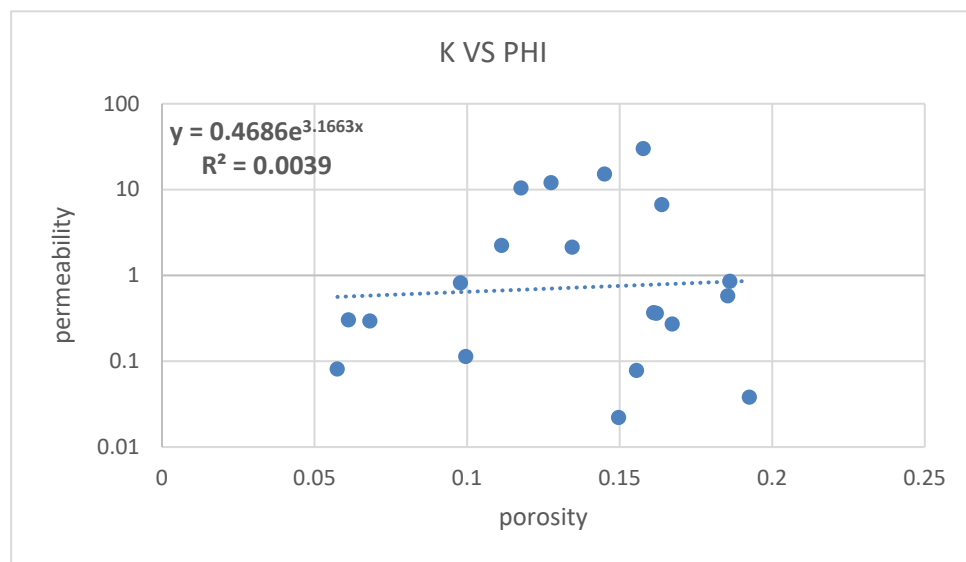


Figure 3-3 Traditional cross-plot for Tortonian sand

Tortoinian's porosity ranges from 0.05 to 0.2, and Tortoinian's permeability values from 0.02 to 30 millidarcy. The core data is reliable because it is measured directly through the lab. The company declares that the core data quality is high and efficient due to handle and preservation procedures.

3.2.2 Log data

The indirect method helps to investigate the geology and petrophysical parameters of the reservoir compared to the coring methodology as the direct method is well-logging.

The wireline logs that evaluate the Tortonian reservoir are:

1. Resistivity
2. Porosity
3. Gamma-ray

3.2.2.1 Gamma-EX open hole logs

Gamma-EX is the first well drilled in the Gamma oil field, which acted as the eye of the engineers in the subsurface formations after the interpretation of the seismic data. There was evidence of an amplitude anomaly that reflects the existence of hydrocarbons accumulation. The logging tool response is affected by formation lithology, petrophysical parameters, and clay minerals. Therefore, the change in the tool response gives information about reservoir characteristics.

The triple-combo (wireline tool) was used to investigate the Tortonian and Messenian reservoirs. The device is composed of three main parts:

1. Gamma source
2. Nuclear source
3. Electric source

Messenian reservoir

(Table 3, appendix B) shows the well-logs values for gamma-ray, neutron, and density logs acquired using a triple-combo tool for the cored interval of Messenian reservoir from 6702 FT-MD to 6725 FT-MD.

The gamma-ray recorded values in the range from 45.11 to 82.29 API; while the neutron porosity obtained is in a range from 0.24 to 0.40 FT³/FT³, and the density log readings among 2.1047 to 2.4491g/cm³, the values indicate different scale and units between the three mentioned logs.

Tortonian reservoir

The well-logs values for gamma-ray, neutron, and density logs acquired using a triple-combo tool for the cored interval of Tortonian reservoir from 7187 FT-MD to 7229 FT-MD (Table 4, appendix B).

The gamma-ray recorded values in the range from 45.54 to 83.09 API; while the neutron porosity obtained is in a range from 0.1642 to 0.272 FT³/FT³, and the density log readings among 2.368 to 2.5376 g/cm³, the values indicate different scale and units between the three mentioned logs.

Figure 3-4 indicates the absence of the balloon effect between density-neutron logs except at the depth 7206 FT-MD where the gamma-ray value tends to decrease, indicating sandy facies.

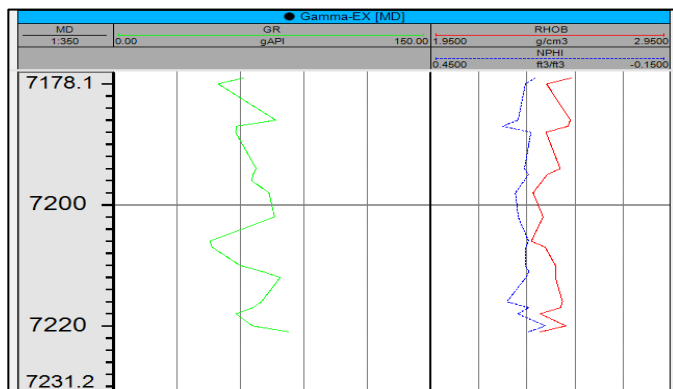


Figure 3-4 Tortonian reservoir (cored interval) log data

The frequency of changes in the gamma-ray values is around 10 API per feet as an average. It reaches 30 API per feet in some intervals, which gives an idea about the high degree of non-linearity from routine core analysis results illustrated by the classical porosity - permeability relationship.

Figure 3-5 shows the statistical distribution of gamma-ray values with formation depth; the values change continuously with the depth, reflecting the complex stratigraphic sequence and lamination effect.

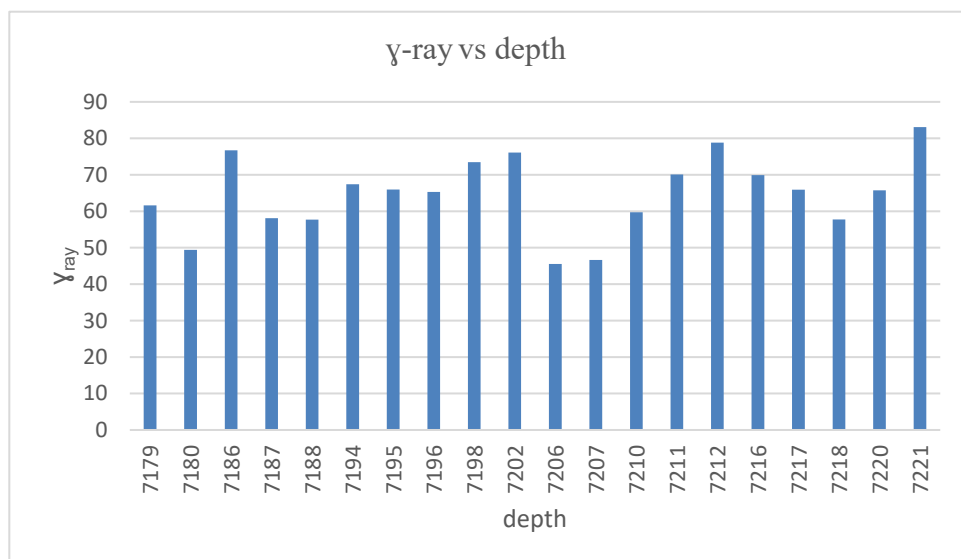


Figure 3-5 Statistical analysis of gamma-ray vs. depth

3.2.2.2 Gamma-1 open hole logs

Gamma-1 is an appraisal well. It investigated the southwest area of the Gamma field and the extension of the Tortonian reservoir in the lateral and vertical directions. Core samples for Gamma-1 are not available due to economic issues and the high cost of the coring operation. However, the logging data are available (Table 5, appendix B).

Figure 3-6 shows the log data for the entire reservoir from 7176 FT-MD until 7758 FT-MD. The well is vertical, so Tortonian thickness is 582 FT-SSTVD (177 M-SSTVD) as isopach depth, which is considered a high thickness. However, the facies are poor.

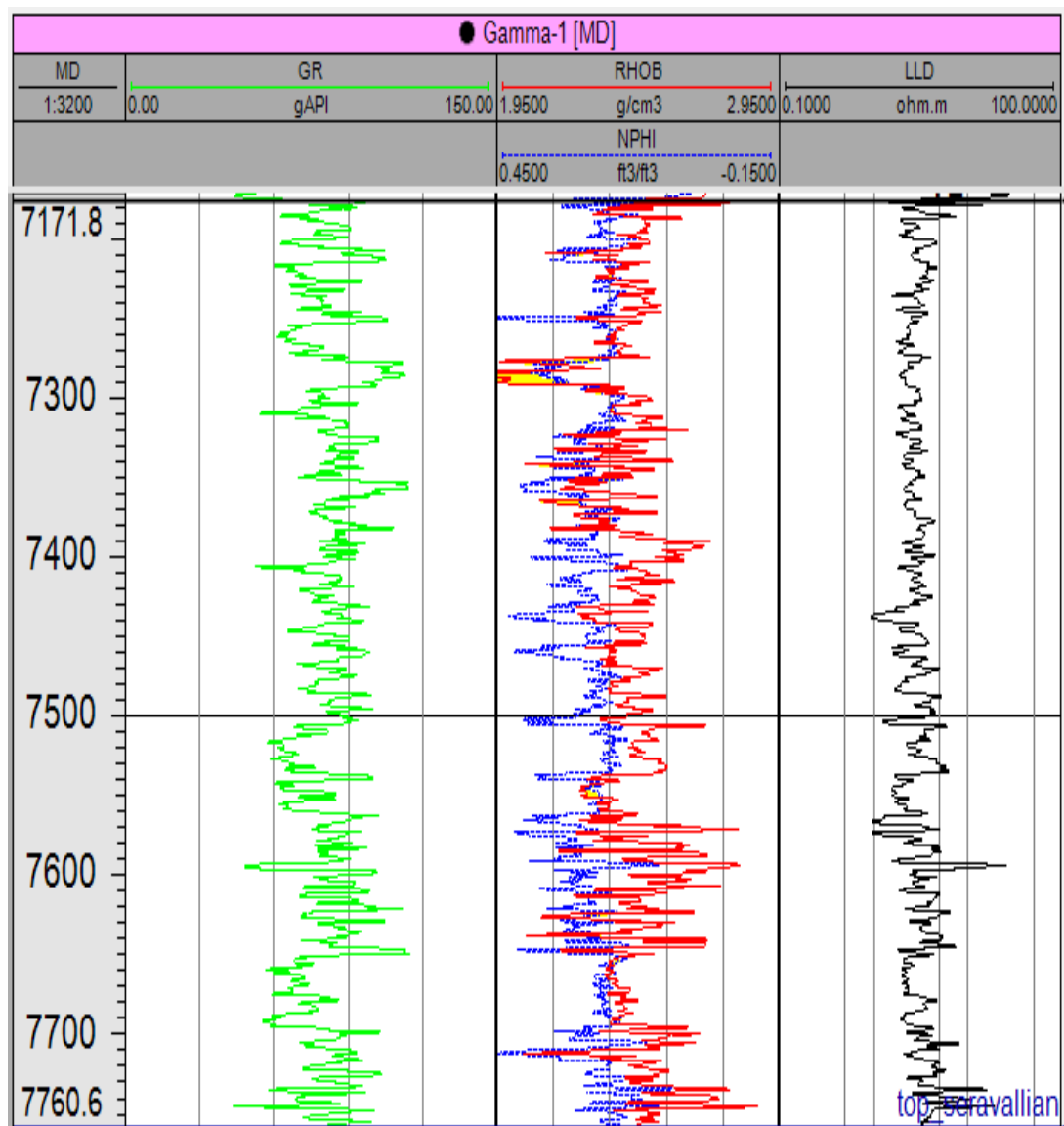


Figure 3-6 Gamma-1 log data for Tortonian reservoir

Neutron-density logs; highlight the poor quality of sand facies, which affect the resistivity readings. The resistivity log couldn't recognize the hydrocarbons bearing zone and fluid contacts due to low permeability and high water salinity (180,000 ppm NaCl). In addition, gamma-ray log response is affected by the lamination phenomena.

From the petrophysical evaluation, the net reservoir is 107 FT (33M), consisting of six interesting intervals:

1. The first interval is from 7214 to 7228 FT-MD with an average gamma-ray value of 69 API and resistivity value around 3.8 Ohm.M.
2. The second interval is from 7251 to 7273 FT-MD with an average Gamma-ray value of 70 API and resistivity value of about 3Ohm.m.
3. The third interval is from 7511 to 7561 FT-MD with an average Gamma-ray value of 69.6 API and resistivity value near 2.8 Ohm.M.
4. The fourth interval is from 7622 to 7627.83 FT-MD with an average Gamma-ray value of 81 API and the value of resistivity approximately 4.4 Ohm.M, there are two features regarding this interval, these are:
 - gamma-ray reaches the maximum value
 - resistivity response shows an increasing trend
5. The fifth interval is from 7635 to 7641 FT-MD with an average Gamma-ray value of 89 API and resistivity value around 4.6 Ohm.M.
6. The last one is from 7687 to 7695 FT-MD, with an average Gamma-ray value of 60 API and resistivity value around 2.2 Ohm.M.

There is a direct relationship between GR readings and resistivity readings; this relationship is unconventional. The effect of lithology and geological facies on logs tool response highlighted by two observations:

1. Gamma-ray readings decrease for the sand formation, and in the presence of HC, the resistivity values should increase, not decrease.
2. The difference between a low and high investigation resistivity response disappears.

The net pay after the final evaluation is 21 feet, the net to gross is around 20% with average porosity of 20%, and moderate water saturation is 50%.

3.2.2.3 Gamma-2 open hole logs

Gamma-2 is an appraisal well. It investigated the southeast area of the Gamma field and the extension of the Tortonian reservoir in the lateral and vertical directions. The well is uncored, but the logging data are available (Table 6, appendix B).

Gamma-2 penetrates the Tortonian reservoir and intersects the top of the formation at 7154 FT-MD until the bottom at 7407 FT-MD. Hence, the thickness of the formation is 253 FT (77m), so it is relatively small compared to Gamma-1, but still, the extension of the Tortonian reservoir exists in the southeast compartment of the Gamma field.

From the first look, the facies seemed to be improved. However, the complex reservoir structure limits the reliability of resistivity logs to identify the existence of the hydrocarbons and leads to mess interpretation. Concerning the balloon effect, some intervals display the balloon effect, but only for limited intervals w.r.t the entire thickness.

Once the lithology changes with the high frequency, the logging company adjusts the logging tool's resolution to distinguish the lamination phenomena and the interference between two laminae. The accuracy is adjusted for every 0.16 feet instead of 0.5 feet as Gamma-1 to enhance the acquired data interpretation, mainly in the absence of the coring operation and wireline formation tester.

The enhancement of the logging tool resolution enables a better petrophysical evaluation; in the interval from 7201.8 to 7203.5 FT-MD, which is less than 1M, the value of the gamma-ray decreases dramatically from 53.84 to 33.41 API as follows (see Figure 3-7).

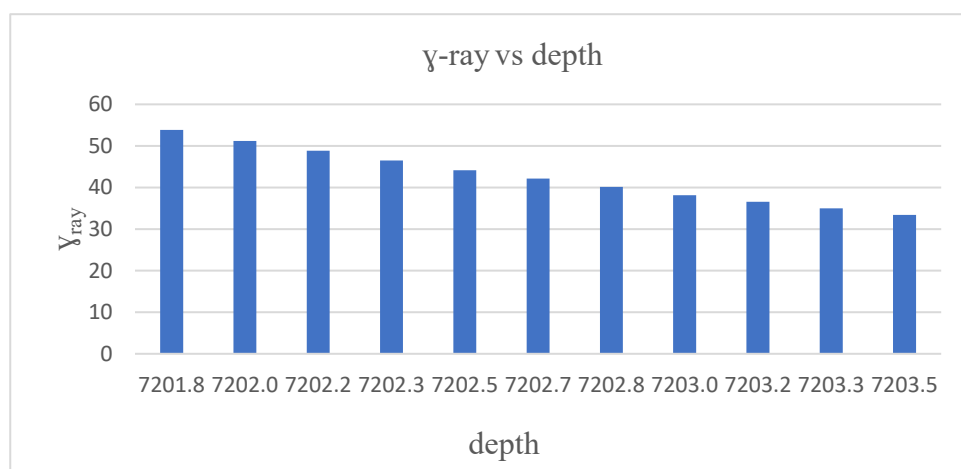


Figure 3-7 Statistical distribution of gamma-ray vs. depth

The petrophysical evaluation; shows that the net reservoir in the southeast area is around 100 FT, net-pay is approximately 15 FT, the net to gross is 15% with average porosity of 20 %, SW is 40%, and the average gamma-ray value of 42 API.

Figure 3-8 shows the logs data of Gamma-2

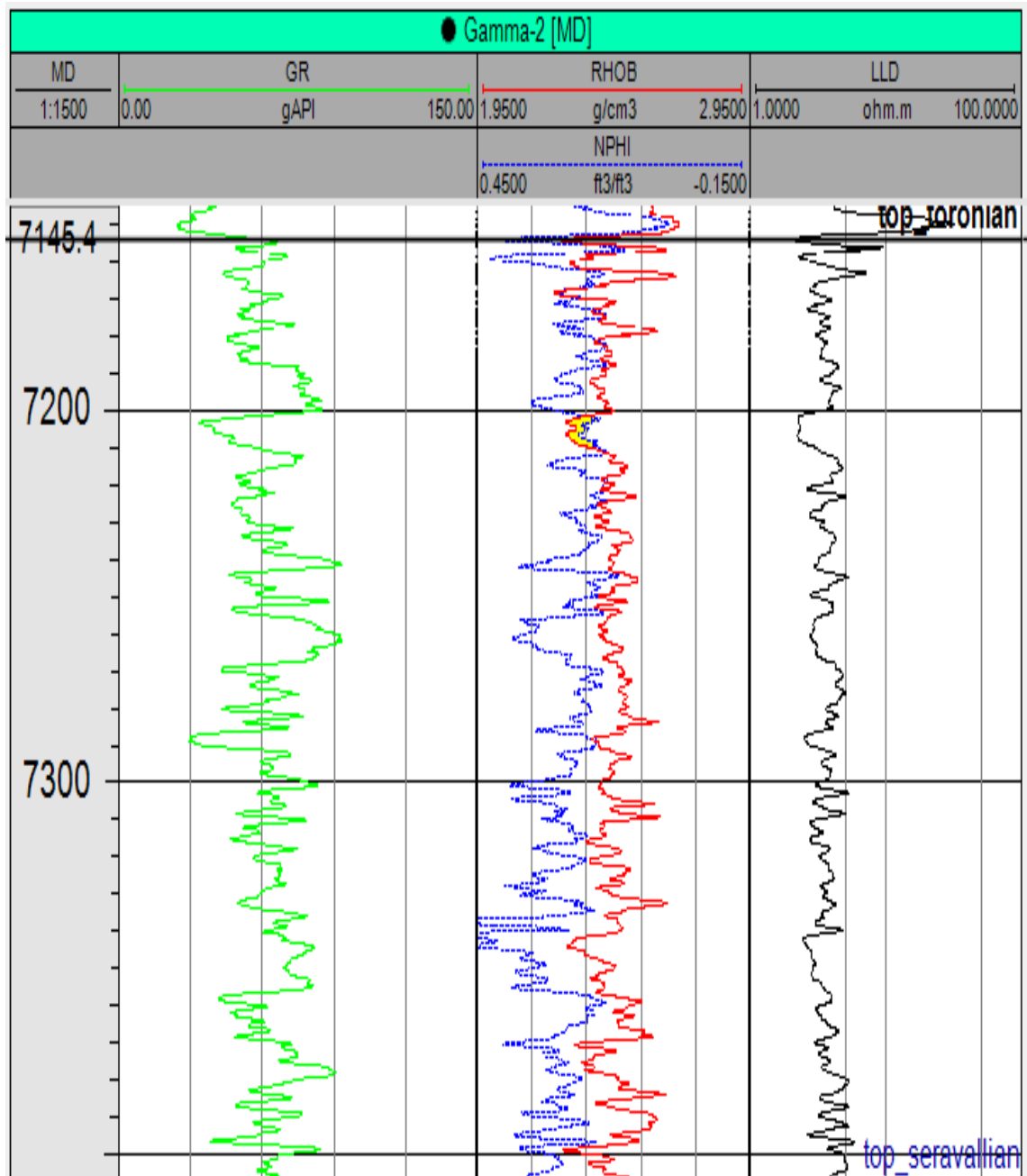


Figure 3-8 Gamma-2 log data for Tortonian formation

3.2.2.4 Gamma-3 open hole logs

Gamma-3 is an appraisal well. It investigated the northwest area of the Gamma field and the extension of the Tortonian reservoir in the lateral and vertical directions. The well is uncored, but the logging data are available (Table 7, appendix B).

Gamma-3 penetrates the Tortonian reservoir and intersects the top of the formation at 7041 FT-MD until the bottom at 7210 FT-MD. Hence, the thickness of the formation is 169 FT (52m), so it is relatively small compared to Gamma-1 and Gamma-2, but still, the extension of the Tortonian reservoir exists in the northwest compartment of the Gamma field.

There are improvements in geological facies, petrophysical parameters contoured by the porosity, and gamma-ray logs. This indicates the enhancement of the formation's storage capacity; subsequently, oil volume increases, and resistivity readings increase.

The sand body from 7046 until 7074 FT-MD did not appear in the previous appraisal wells, showing a different petrophysical parameter except for some interior intervals. Therefore, it seems as clean body-sand without lamination effect, the appearance of the clean-sand is due to the high structure of the well compared to the others. The statistical distribution of the gamma-ray through that interval also shows consistency and compatible values, most of the values between 27 to 34 API (see Figure 3-9).

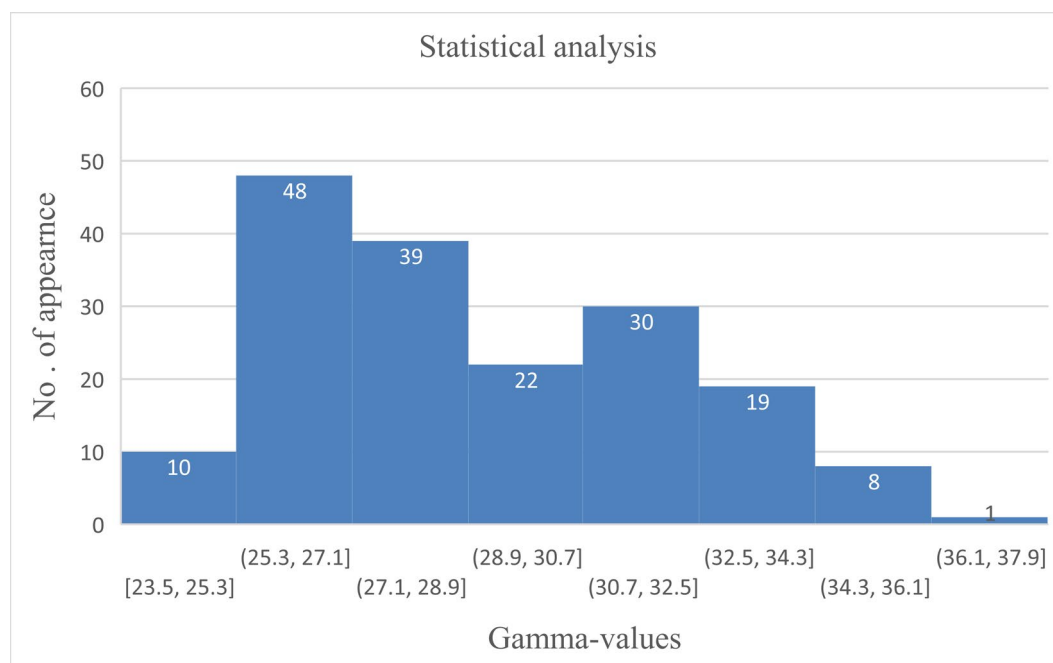


Figure 3-9 Statistical distribution of gamma-ray values for upper Tortonian body sand for well Gamma-3

There are other intervals, but they mimic the petrophysical evaluation for the previous appraisal wells. The net reservoir is around 116 FT with average porosity of 22 %. Some tight layers embedded into the upper clean sand are affecting the porosity and resistivity readings. Figure 3-10 displays the log data.

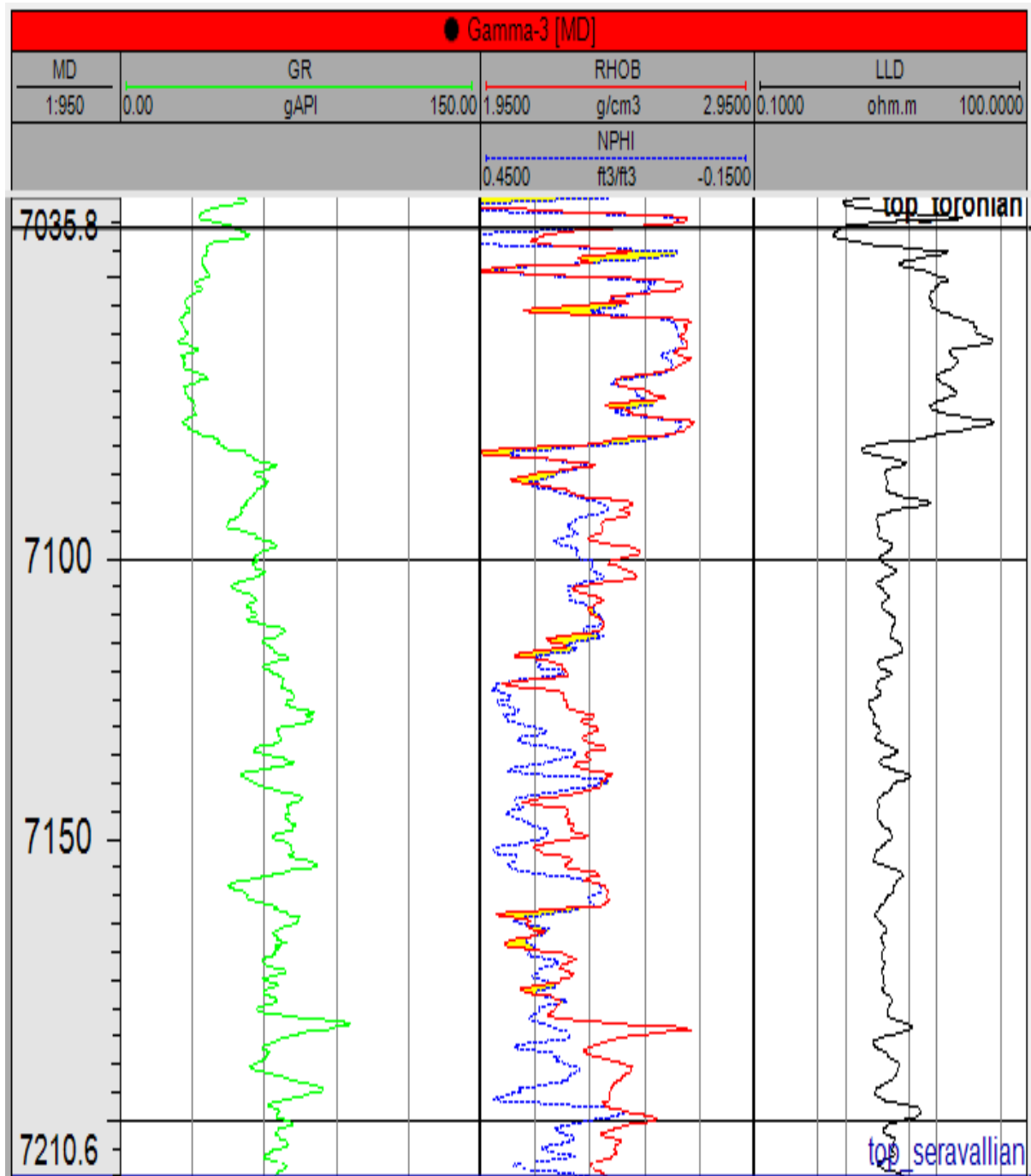


Figure 3-10 Gamma-3 logs data for Tortonian formation

3.2.2.5 Gamma-4 open hole logs

Gamma-4 is an appraisal well. It investigated the northeast area of the Gamma field and the extension of the Tortonian reservoir in the lateral and vertical directions. The well is uncored, but the logging data are available (Table 8, appendix B).

Gamma-4 penetrates the Tortonian reservoir and intersects the top of the formation at 7168 FT-MD until the bottom at 7323 FT-MD. Hence, the formation's thickness is 155 FT (47m), so it is relatively small compared to previous appraisal wells. However, the extension of the Tortonian reservoir still exists in the northwest compartment of the Gamma field.

The northeast region petrophysical parameters are identical to the south area except the thickness, which is less than the south compartment, which contains Gamma-1 and Gamma-2. Also, it matches with the central region of Gamma-EX, the average gamma-values nearby 56 API and resistivity values approximately 2 Ohm.M. Figure 3-11 displays the log data.

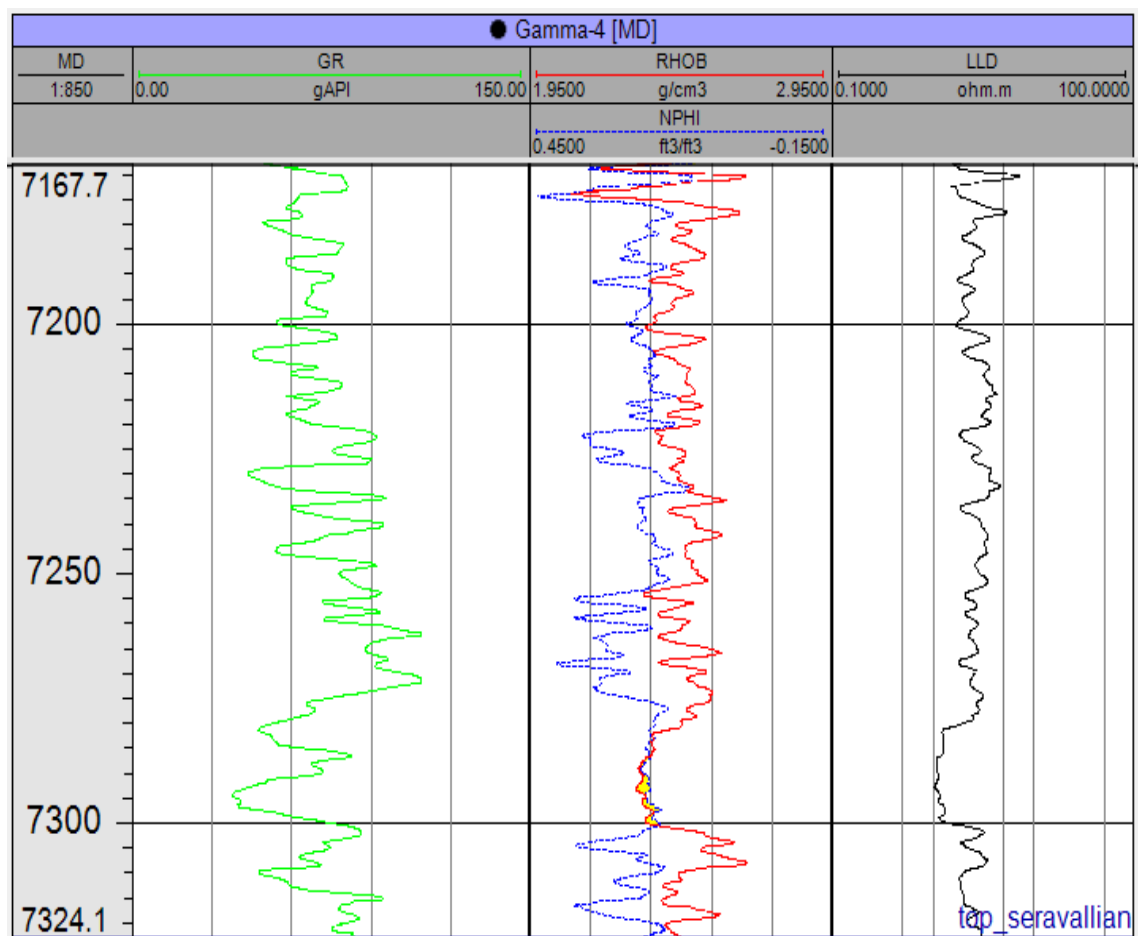


Figure 3-11Gamma-4 logs data for Tortonian formation

3.2.2.6 Well logs correlation

Figure 3-12 gives information about the evolution of the Tortonian's thickness.

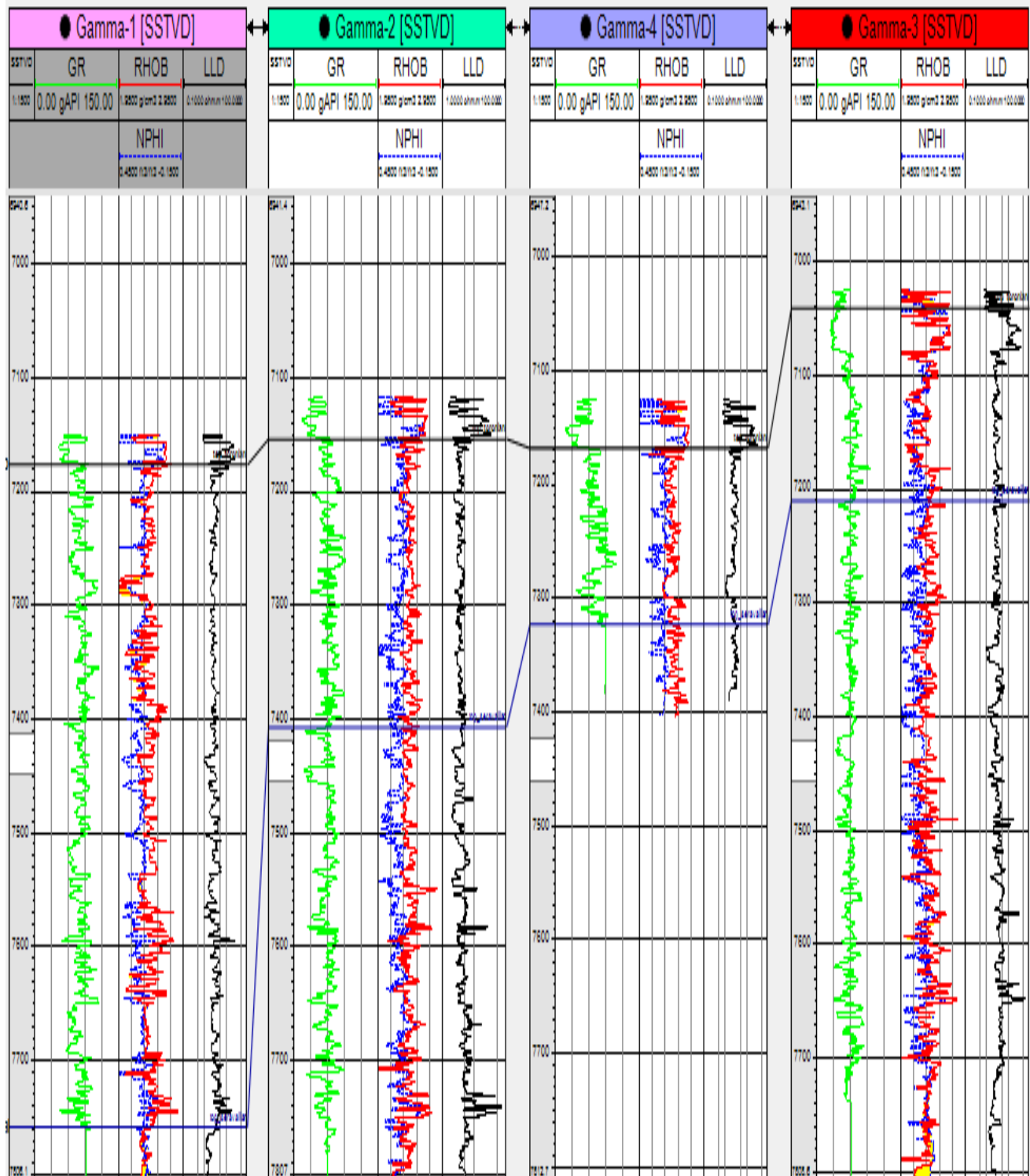


Figure 3-12 Well logs correlation

3.3 Estimation of FZI

3.3.1 Estimation of FZI flowchart

Figure 3-13 Flowchart for FZI estimation highlights the main steps to identify the flow units within the Tortonian reservoir.

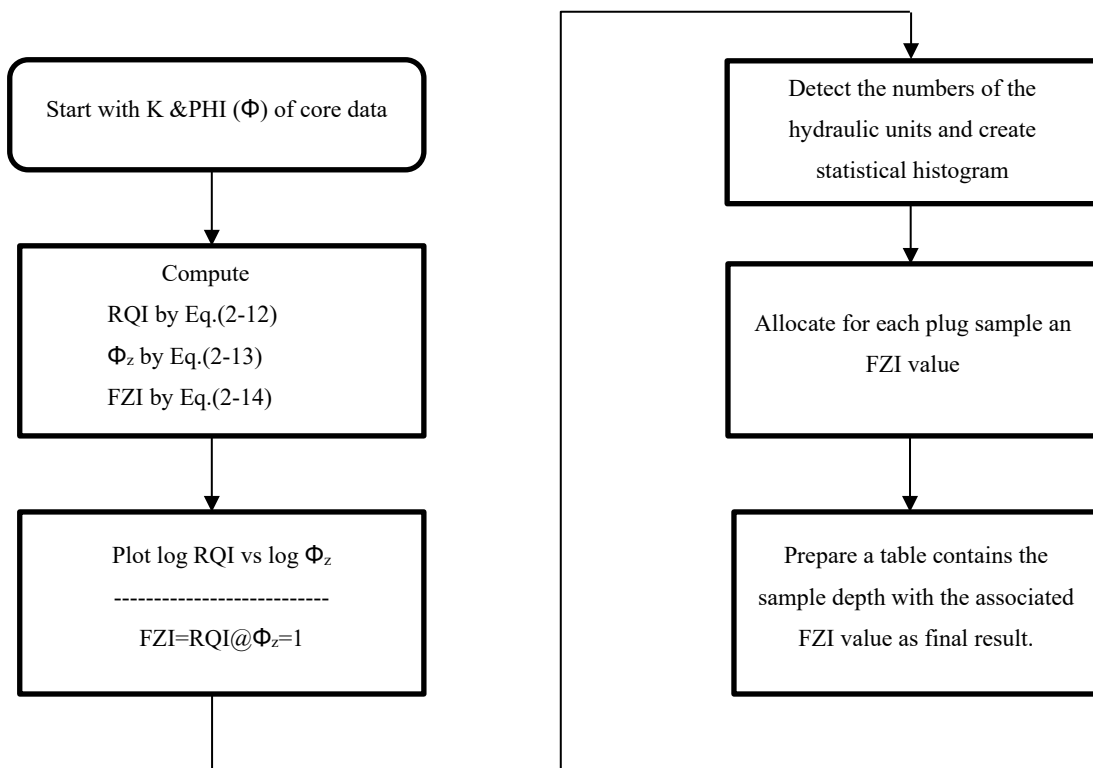


Figure 3-13 Flowchart for FZI estimation

The main steps to estimate the FZI within the Tortonian reservoir are:

1. Calculate Φ_z from core porosity (Gamma-EX) for both:
 - Tortonian reservoir
 - Messenian reservoir
2. Calculate RQI from core permeability and porosity (Gamma-EX) for both:
 - Tortonian reservoir
 - Messenian reservoir
3. Plot RQI versus Φ_z on a log-log plot for Tortonian reservoir
4. Identify the flow unit within Tortonian reservoir
5. Register the results of Tortonian and Messenian reservoirs for future use.

3.4 Effective porosity estimation

3.4.1 Effective porosity estimation flow chart for Tortonian reservoir

Figure 3-14 shows the main steps to calculate Tortonian's effective porosity

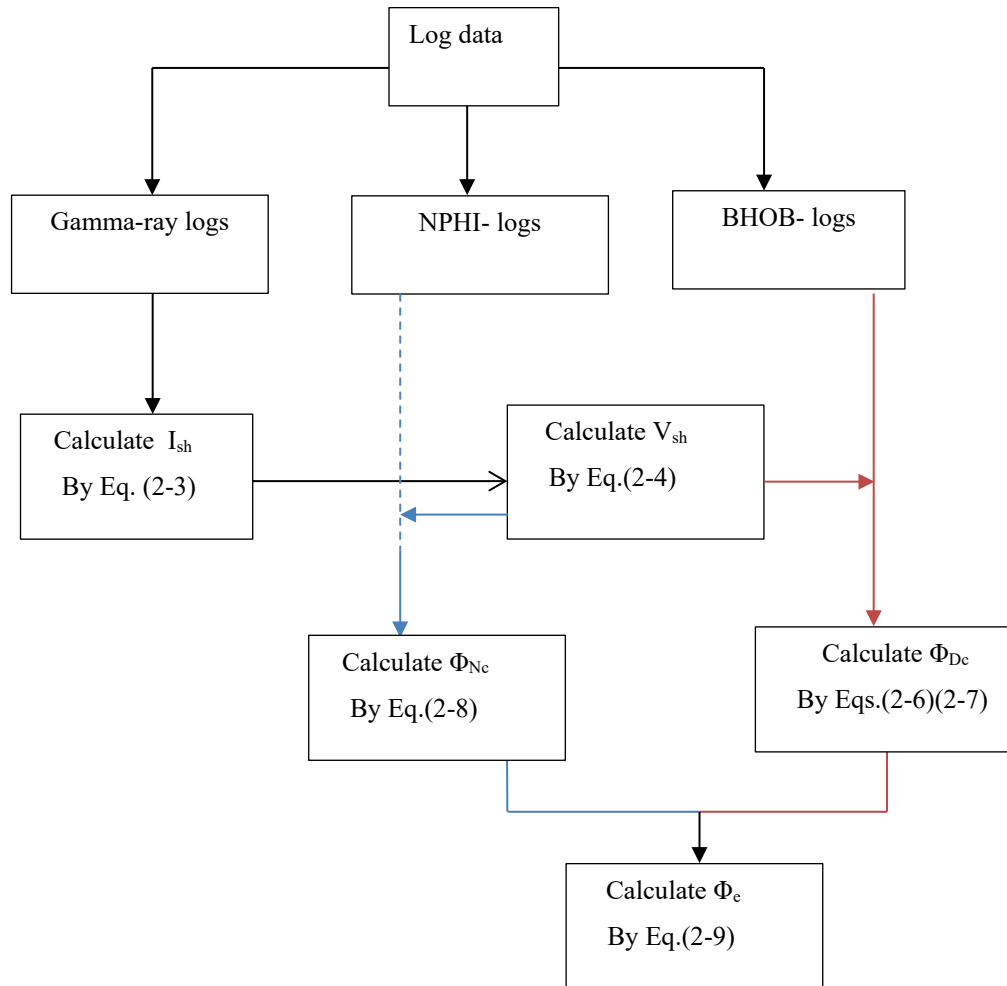


Figure 3-14 Effective porosity estimation flow chart

Gamma-ray and Φ logs are the most crucial tools to calculate Tortonian's effective porosity, through:

1. Evaluating Tortonian's shale volume
2. Calibrating Tortonian's porosity readings by removing the shale effect

3.5 Estimation permeability logs for uncored appraisal wells

3.5.1 Activity flow chart to assess the permeability for the appraisal wells

Figure 3-15 shows the essential steps to evaluate the permeability in the absence of core data for the Gamma oil field.

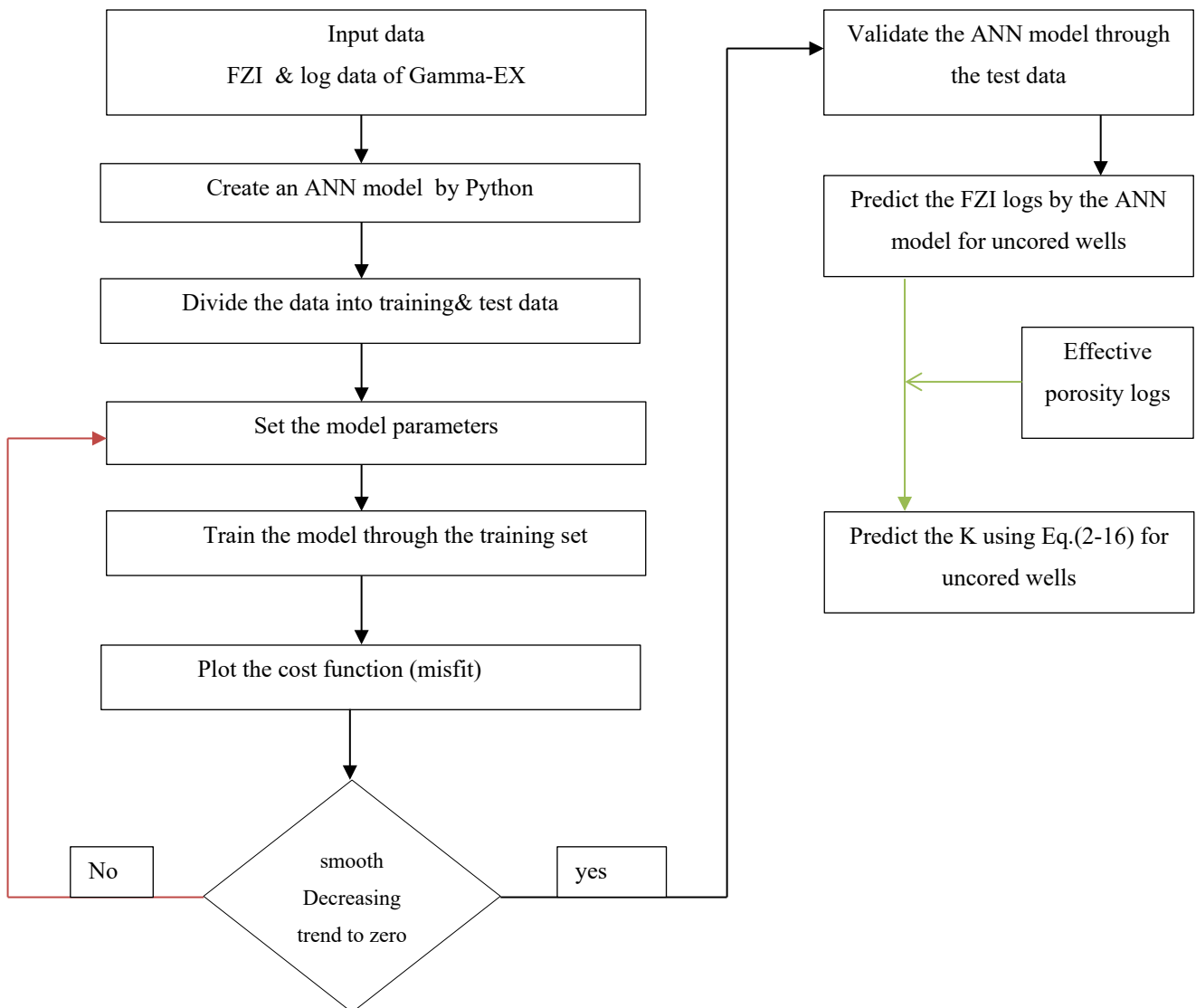


Figure 3-15 Permeability estimation flow chart

3.5.2 ANN model for Gamma oil field

Python is used to create the ANN for the Gamma oil field to manage the relationship between the dependent and independent variables for two reasons:

1. FZI is dependent on the core data and independent from well logs data.
2. The core data is not available for the appraisal wells.

The model is composed of the following sections:

1. Data processing of Gamma-EX dataset
2. Building the ANN model
3. Training the ANN on the training set of Gamma-EX
4. Predicting the FZI for the test set of Gamma-EX
5. Predicting the FZI for the appraisal wells

3.5.2.1 Data processing of Gamma-EX dataset

Deep learning needs a sufficient amount of data to train the model; the estimated FZI from the Messenian core data is used in addition to Tortonian FZI to train the model. The data set (Table 9, appendix C) is composed of:

1. FZI from the Gamma-EX core date
2. GR, NPHI, and RHOB well logs.

The data organized in a matrix, which consists of :

- 33 rows (equal to the number of the core samples)
- Four columns represent the dependent (log data) and independent (FZI) variables.

The normalization feature scaling is essential for the log data to have an equal effect on the FZI values. After the normalization process for the input data, Python divides the data into a test set and a training set. The ratio between the test set and the total data is one of the model parameters. In Gamma field application, it is 30%.

3.5.2.2 Building the ANN model

The ANN for Gamma field consists of :

1. The input layer, which hosts the GR, NPHI, and RHOB
2. Two hidden layers, each one composed of 500 neurons (units)
3. The output layer, which produces the FZI value.

Figure 3-16 shows the ANN architecture for the Gamma oil field.

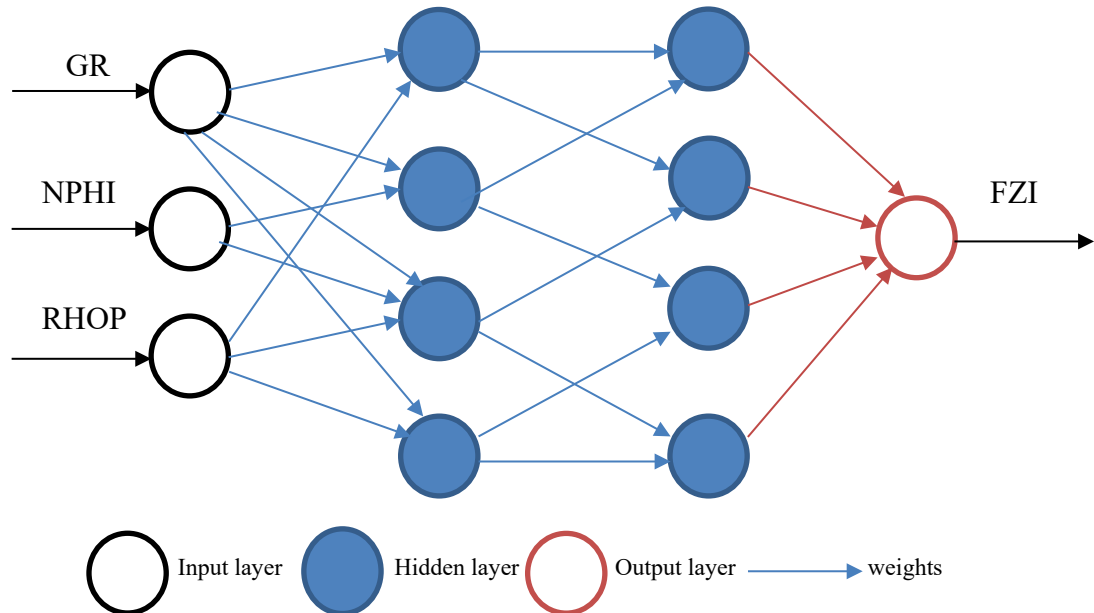


Figure 3-16 ANN architecture for Gamma oil field

The rectifier activation function forced the model to respect the non-linear relation for the entire domain. Figure 3-17 shows the python code to build the ANN model.

Initializing the ANN

```
[ ] ann = tf.keras.models.Sequential()
```

Adding the input layer and the first hidden layer

```
[ ] ann.add(tf.keras.layers.Dense(units=500, activation='relu'))
```

Adding the second hidden layer

```
[ ] ann.add(tf.keras.layers.Dense(units=500, activation='relu'))
```

Adding the output layer

```
[ ] ann.add(tf.keras.layers.Dense(units=1))
```

Figure 3-17 Python code to build ANN model

3.5.2.3 Training the ANN on the training set of Gamma-EX

Training the ANN is the most crucial section. The section functions are:

1. Identify the backpropagation technique
2. Identify the misfit (loss equation)
3. Train the ANN model
4. Identify the trials number

The ANN for the Gamma oil field uses the SGD (Adam optimizer) backpropagation method, MSE, and the number of trials is 400 (as shown in Figure 3-18).

- ▼ Compiling the ANN

```
[ ] ann.compile(optimizer = 'adam', loss = 'mean_squared_error')
```

- ▼ Training the ANN model on the Training set

```
[ ] history=ann.fit(log_data_train, FZI_train, batch_size = 32, epochs = 400)
```

Figure 3-18 Training the ANN code

the loss function shows a decreasing trend to zero (see Figure 3-19).

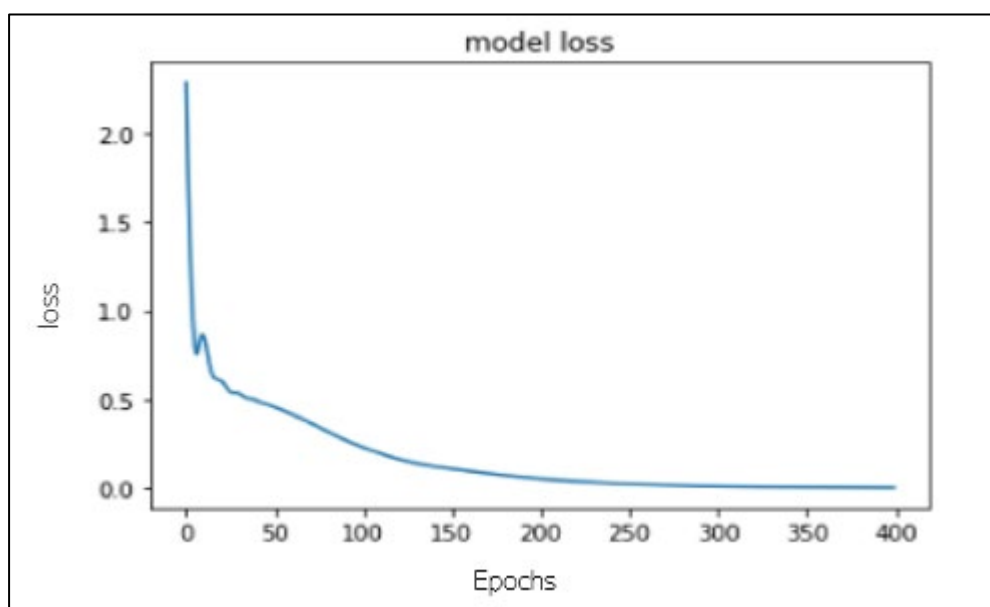


Figure 3-19 Gamma-field ANN cost function plot

3.5.2.4 Predicting the FZI for the test set of Gamma-EX

The tasks of this section are:

1. Predict the FZI for test data
2. Validate the ANN for further use

Figure 3-20 shows that around 90 of the test set predicted correctly from the model

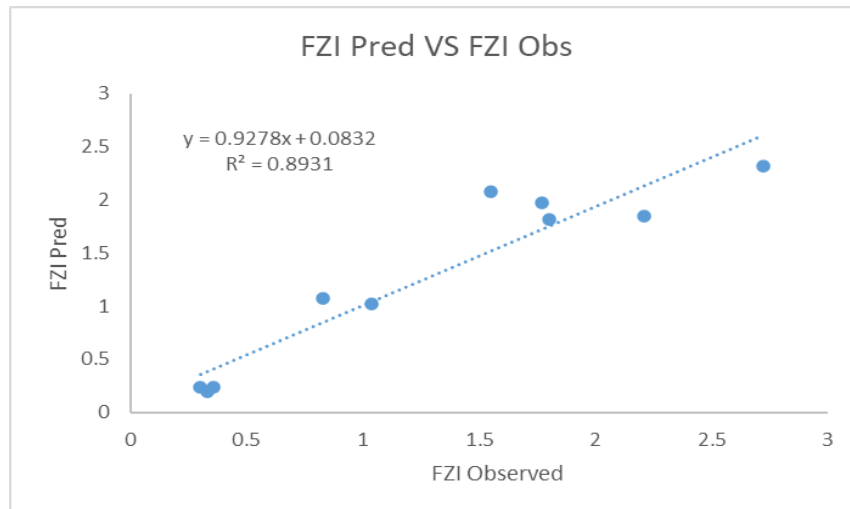


Figure 3-20 FZI Pred VS FZI Obs

3.5.2.5 Predicting the FZI for the appraisal wells

This section aims to predict the FZI for uncored wells for further use, for instance, FZI of Gamma-1 (see Figure 3-21).

```
[ ] dataset1 = pd.read_excel('Gamma-1.xlsx')
logs1 = dataset1.iloc[:, :].values
print(logs1)
```

```
[ ] from sklearn.preprocessing import MinMaxScaler
sc = MinMaxScaler()
logs1 = sc.fit_transform(logs1)
print(logs1)
```

```
[ ] FZI1_pred = ann.predict(logs1)
print(FZI1_pred)
```

Figure 3-21 FZI prediction code

3.6 Creating the permeability map of the Tortonian reservoir

Figure 3-22 shows the main steps to develop Toronian's permeability map.

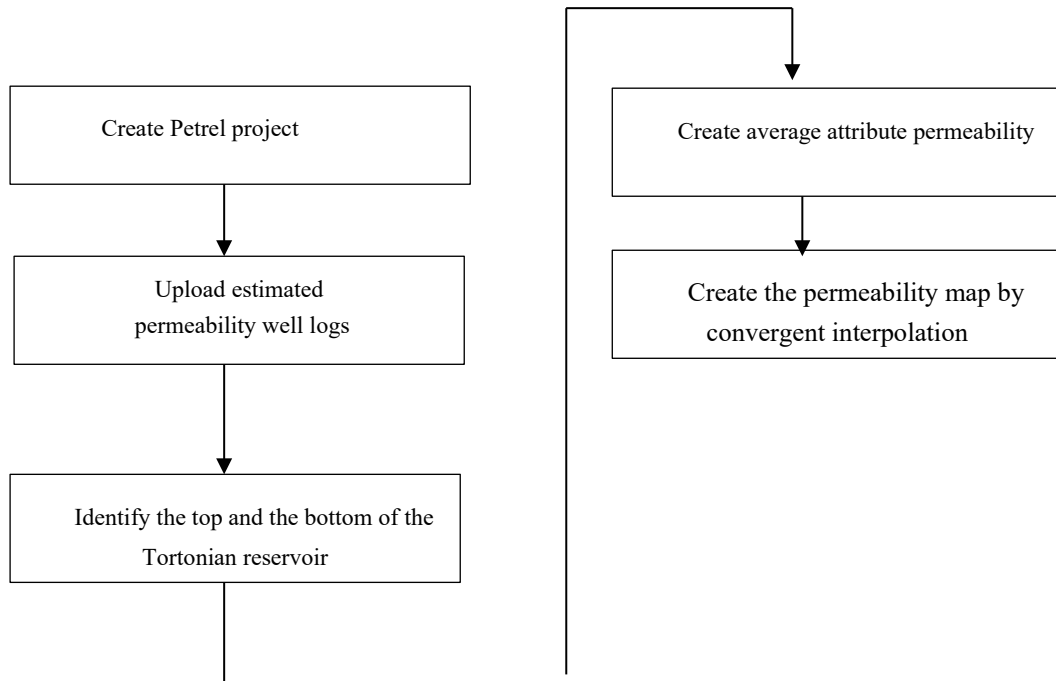


Figure 3-22 Permeability map creation workflow

4 RESULTS

4.1 Tortonian's rock types

Tortonian's rock types are three based on the FZI technique (as shown in Figure 4-1)

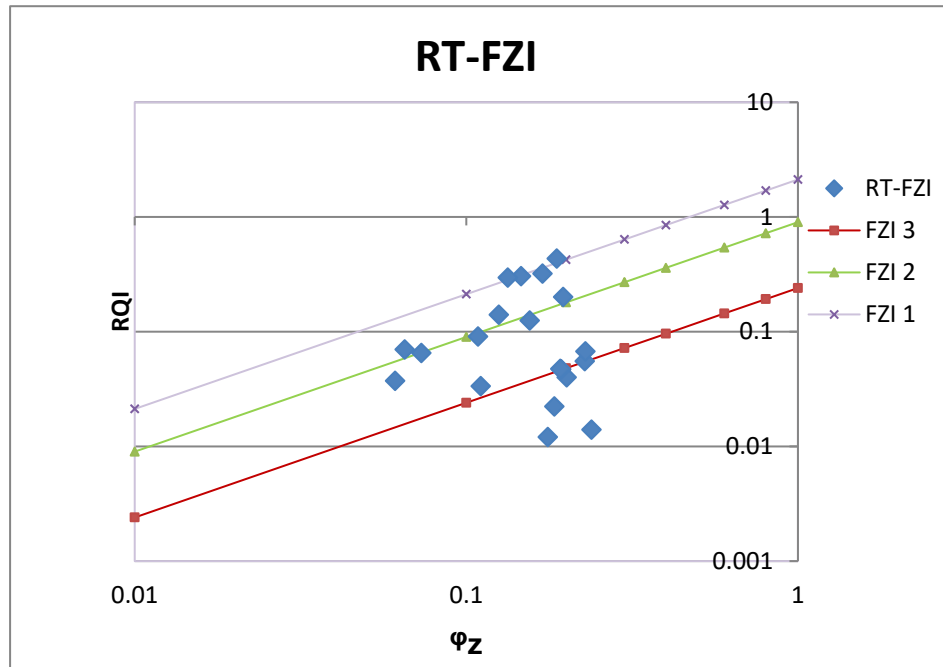


Figure 4-1 Tortonian's rock types

4.1.1 FZI statistical analysis

Flow zone indicators show range from $0.06 \mu\text{m}$ to $2.31 \mu\text{m}$ (as shown in Figure 4-2)

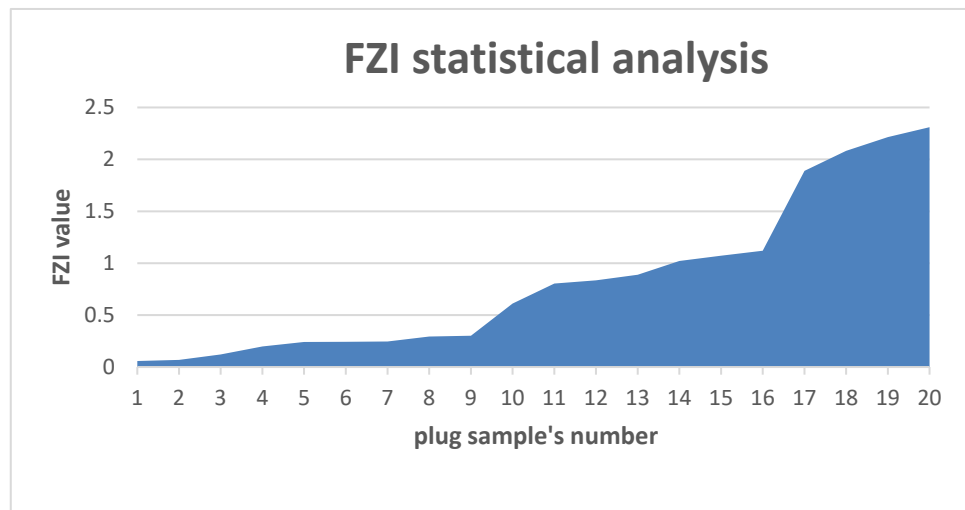


Figure 4-2 FZI statistical analysis

4.2 FZI, effective porosity, and permeability logs for uncored wells

4.2.1 Gamma-1

Figure 4-3 shows two sets of logs of the well (Gamma-1). These are:

1. Created logs (FZI, K, and Φ_e)
2. Quality check logs (GR, NPHI, and RHOB)

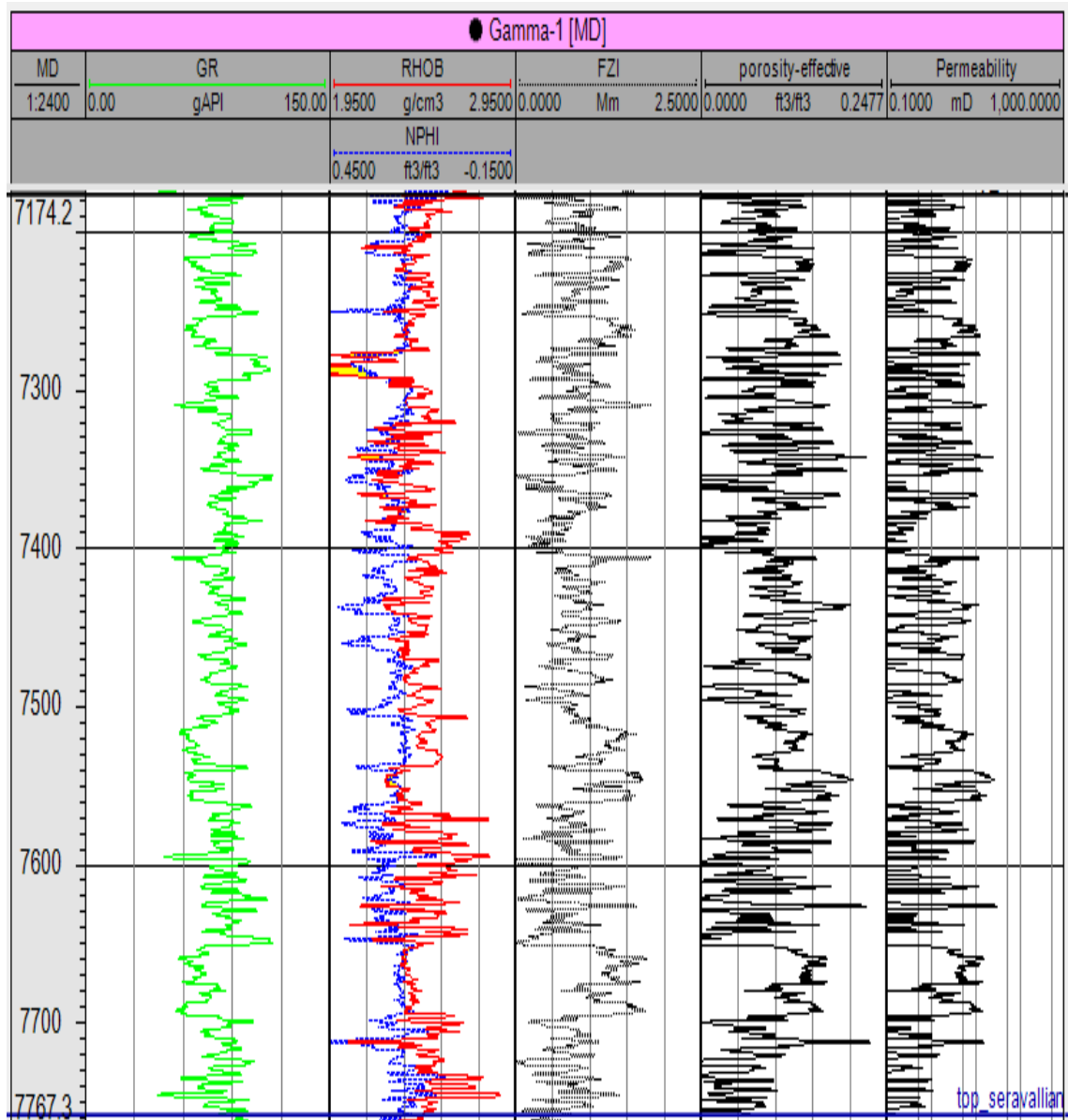


Figure 4-3 Created logs vs. quality check logs for Gamma-1

The comparison between created and quality check logs reflects the high model quality.

(Table 10, appendix C) shows the created log readings for curious intervals.

4.2.2 Gamma-2

Figure 4-4 shows two sets of logs of the well (Gamma-2). These are:

1. Created logs (FZI, K, and Φ_e)
2. Quality check logs (GR, NPHI, and RHOB)

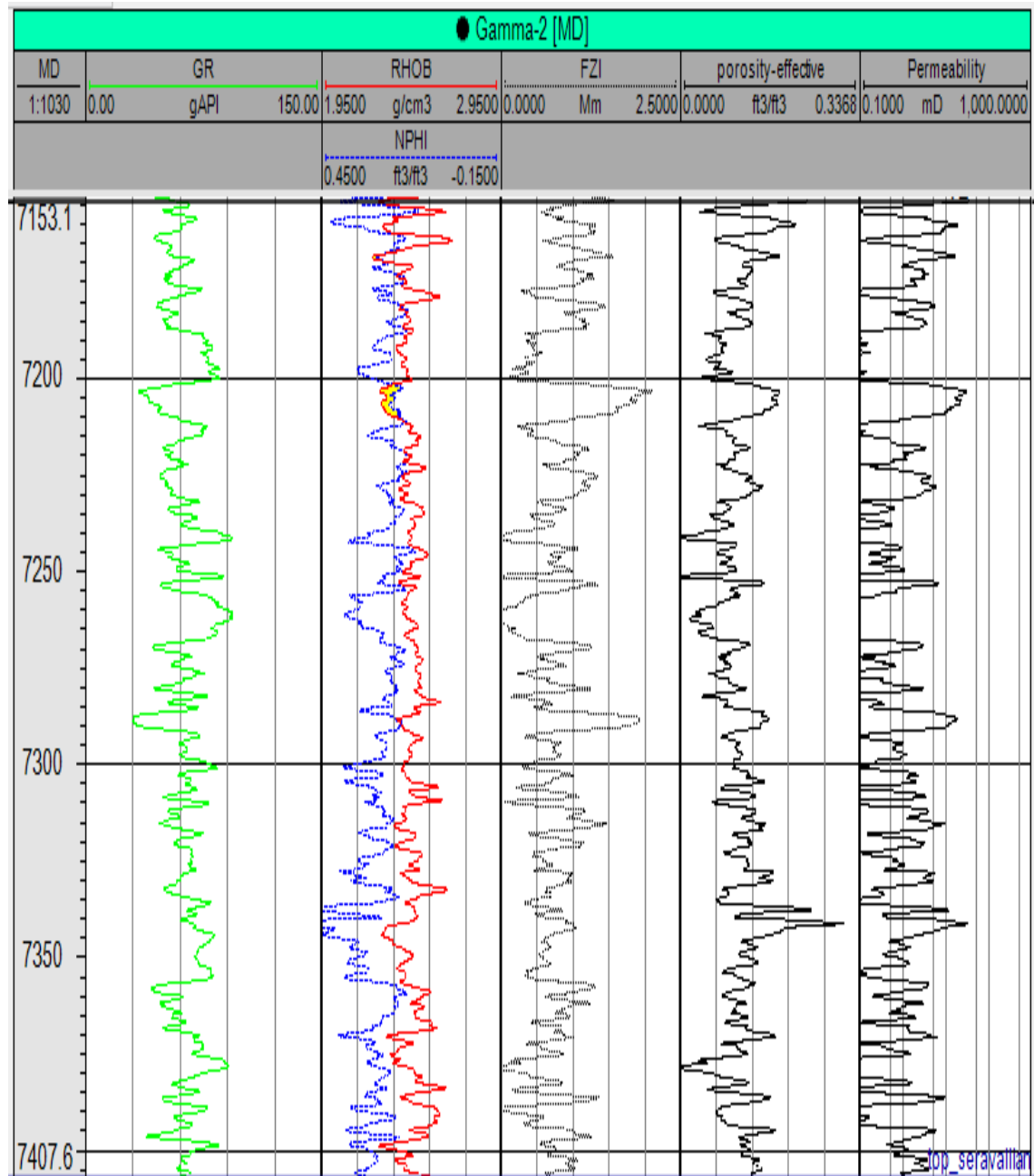


Figure 4-4 Created logs vs. quality check logs for Gamma-2

The comparison between created and quality check logs reflects the high model quality.

(Table 11, appendix C) shows the created log readings for curious intervals.

4.2.3 Gamma-3

Figure 4-5 shows two sets of logs of the well (Gamma-3). These are:

1. Created logs (FZI, K, and Φ_e)
2. Quality check logs (GR, NPHI, and RHOB)

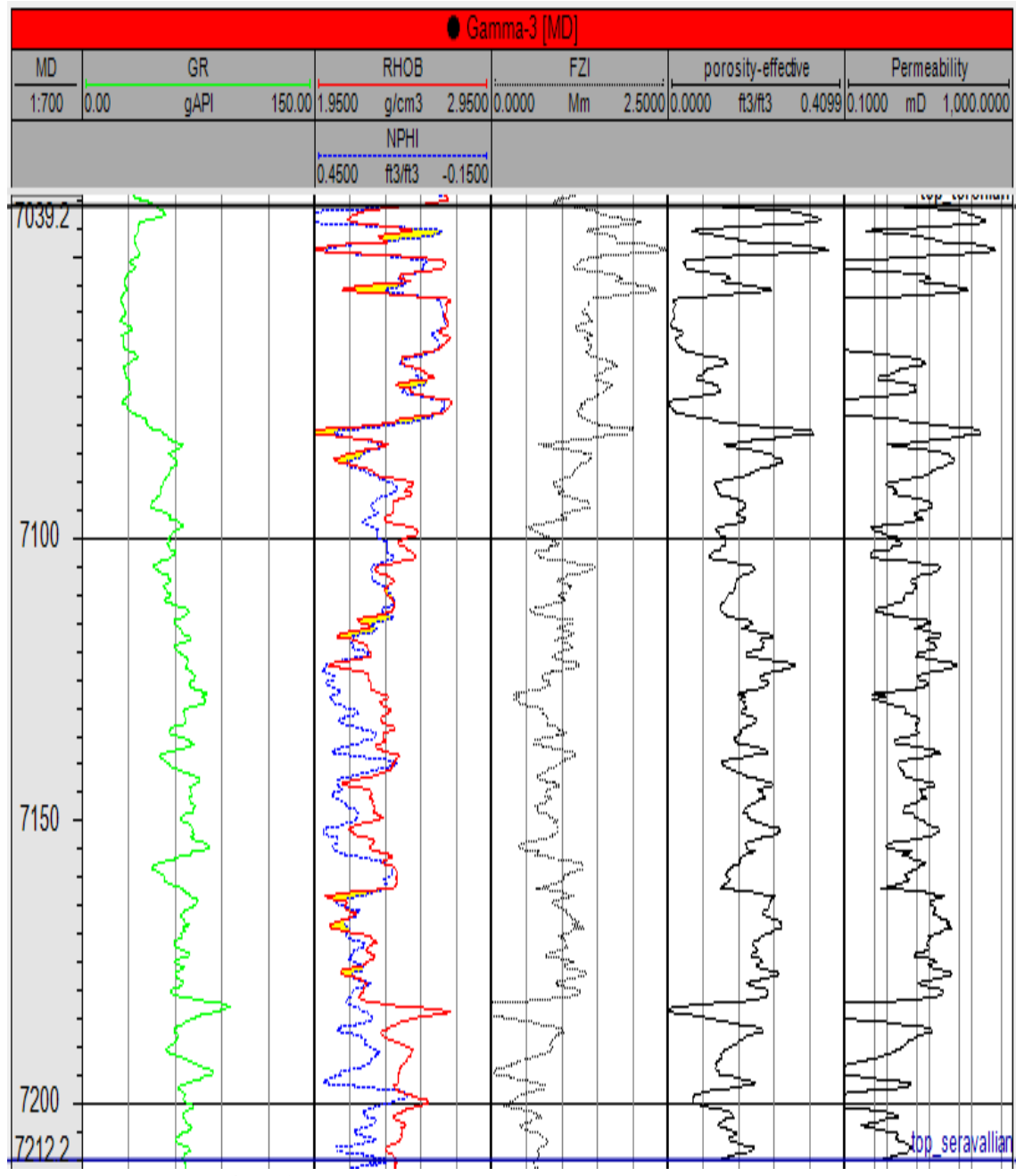


Figure 4-5 Created logs vs. quality check logs for Gamma-3

The comparison between created and quality check logs reflects the high model quality.

(Table 12, appendix C) shows the created log readings for curious intervals.

4.2.4 Gamma-4

Figure 4-6 shows two sets of logs of the well (Gamma-4). These are:

1. Created logs (FZI, K, and Φ_e)
2. Quality check logs (GR, NPHI, and RHOB)

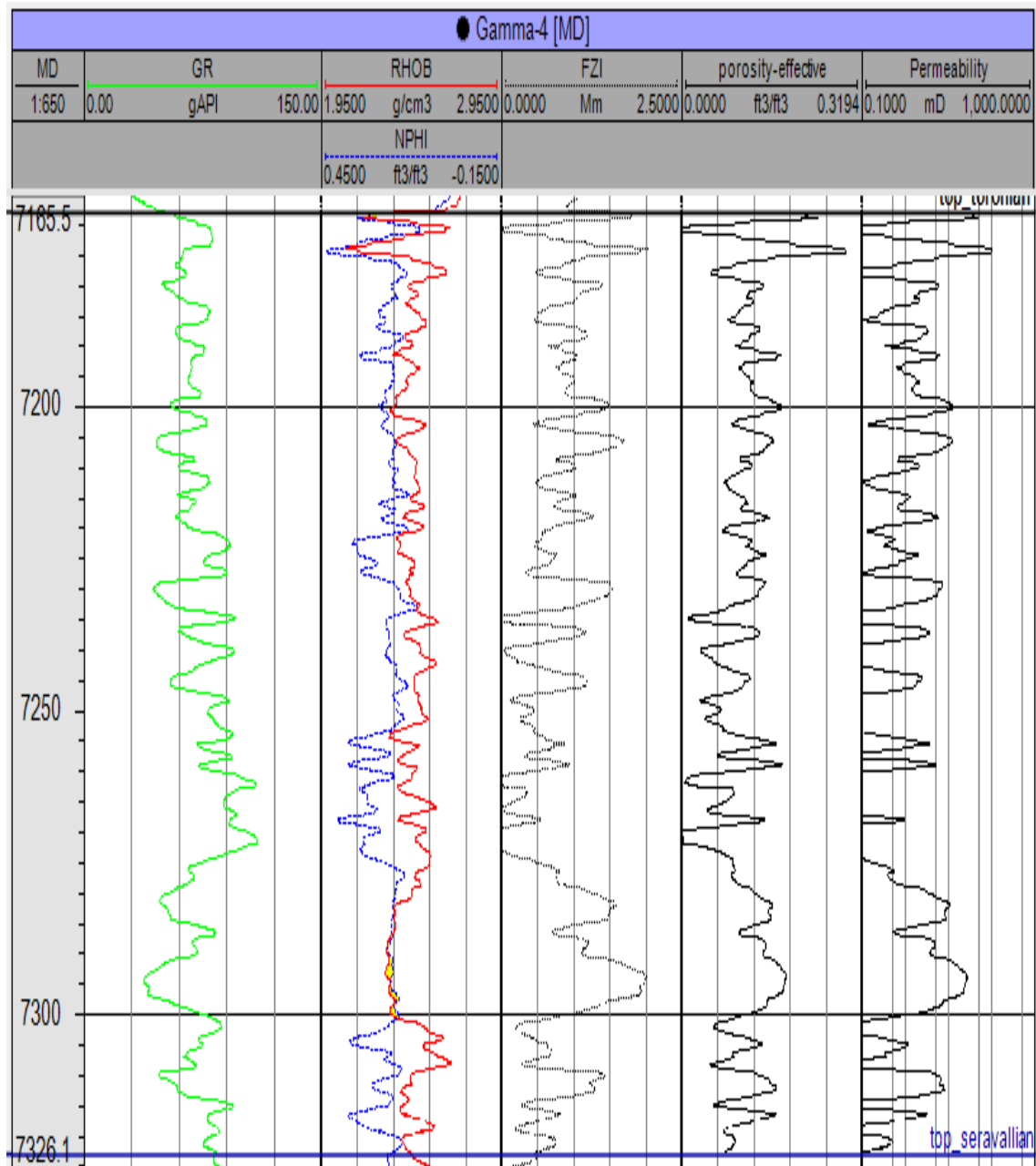


Figure 4-6 Created logs vs. quality check logs for Gamma-4

The comparison between created and quality check logs reflects the high model quality.

(Table 13, appendix C) shows the created log readings for curious intervals.

4.3 Developed Tortonian's porosity and permeability relationship for the three rock types

- For RT-1, the porosity and permeability relationship has a determination coefficient value of 0.95. The porosity ranges from 15 to 37 %, and the permeability ranges from 15 to 374 millidarcy (as shown in Figure 4-7).

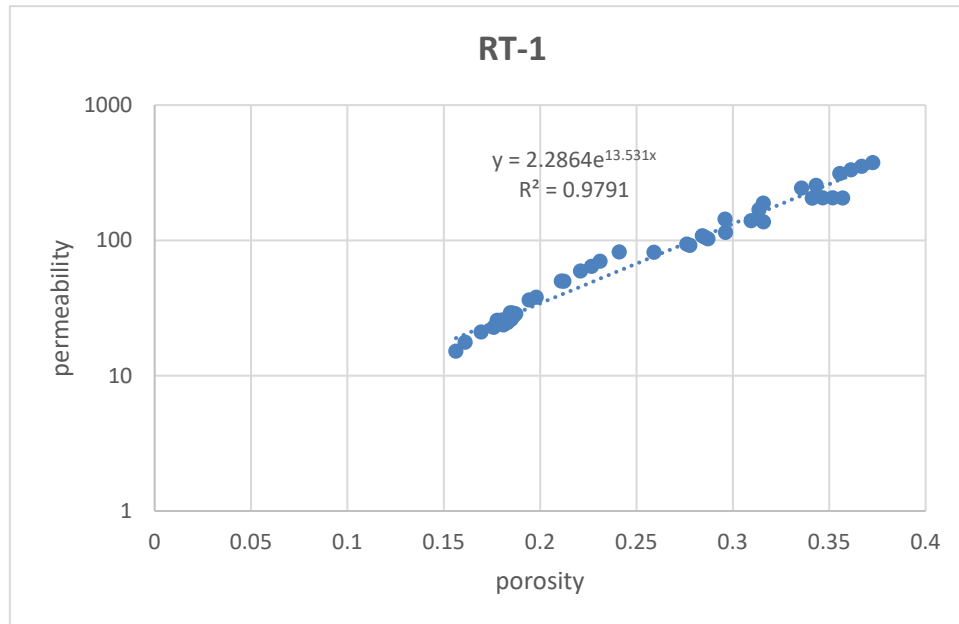


Figure 4-7 Porosity-permeability relationship of RT-1

- For RT-2, the porosity and permeability relationship has a determination coefficient value of 0.92. The porosity ranges from 9 to 30 %, and the permeability ranges from 1 to 33 millidarcy (as shown in Figure 4-8).

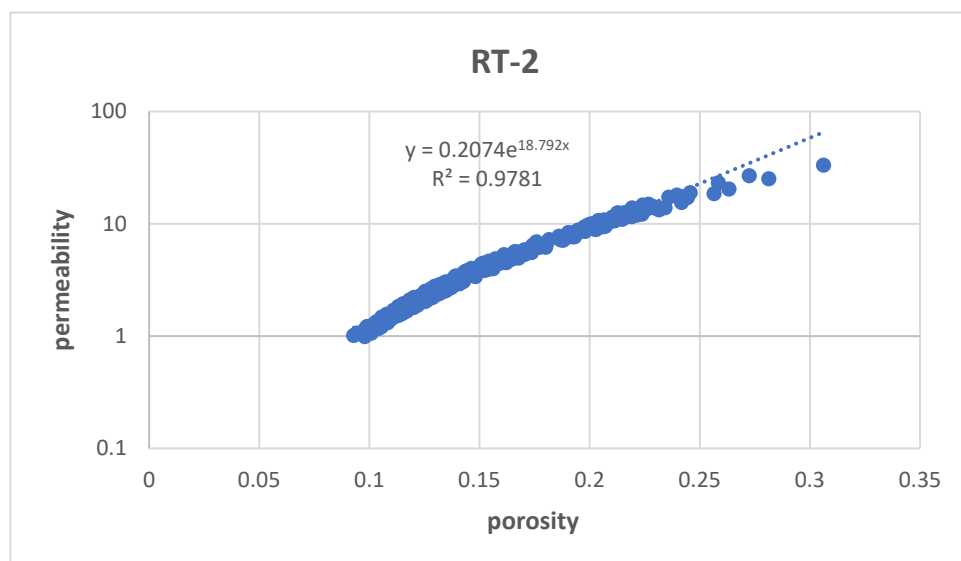


Figure 4-8 Porosity-permeability relationship of RT-2

3. For RT-3, the porosity and permeability relationship has a determination coefficient value of 0.93. The porosity ranges from 4 to 20 %, and the permeability ranges from 0.025 to 4.5 millidarcy (as shown in Figure-4-9).

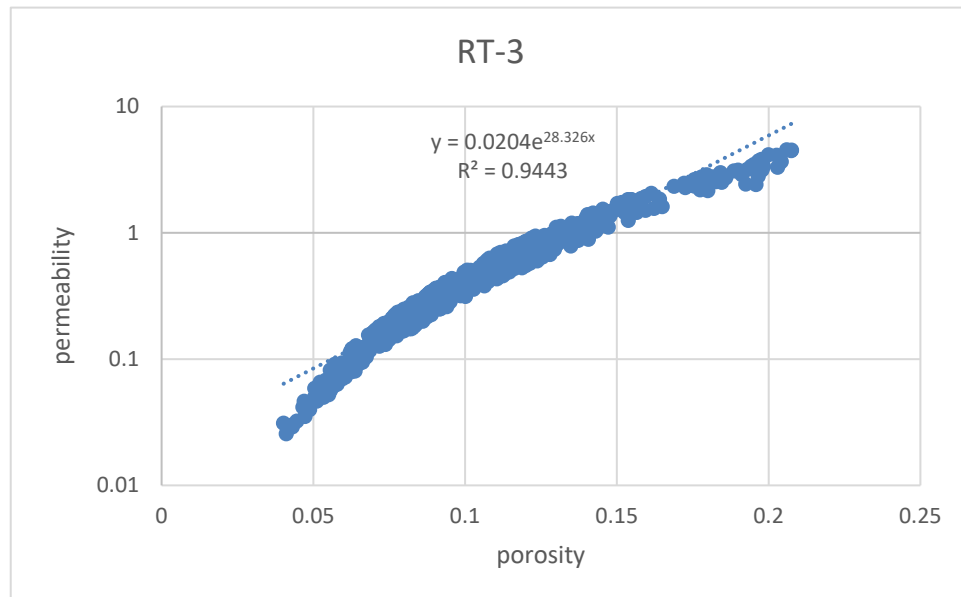


Figure 4-9 Porosity-permeability relationship of RT-3

4.4 Permeability & effective porosity maps of the Tortonian reservoir

4.4.1 Tortonian's permeability map

Figure 4-10 shows Tortonian's permeability map created by Petrel software.

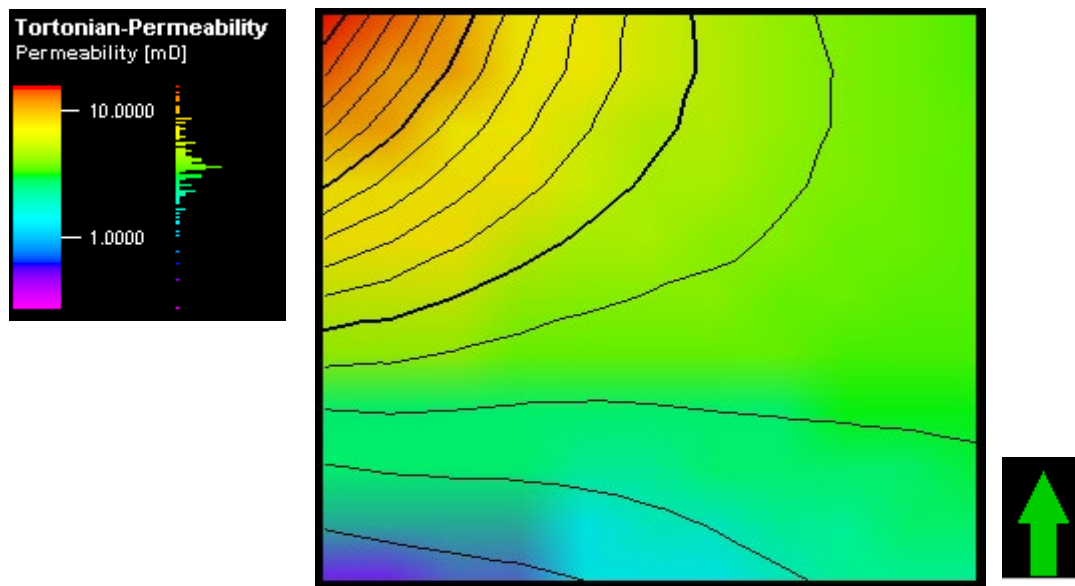


Figure 4-10 Tortonian's permeability map

4.4.2 Tortonian's effective porosity map

Figure 4-11 shows Torontonian's effective porosity map created by Petrel software and used to check the quality of the permeability map.

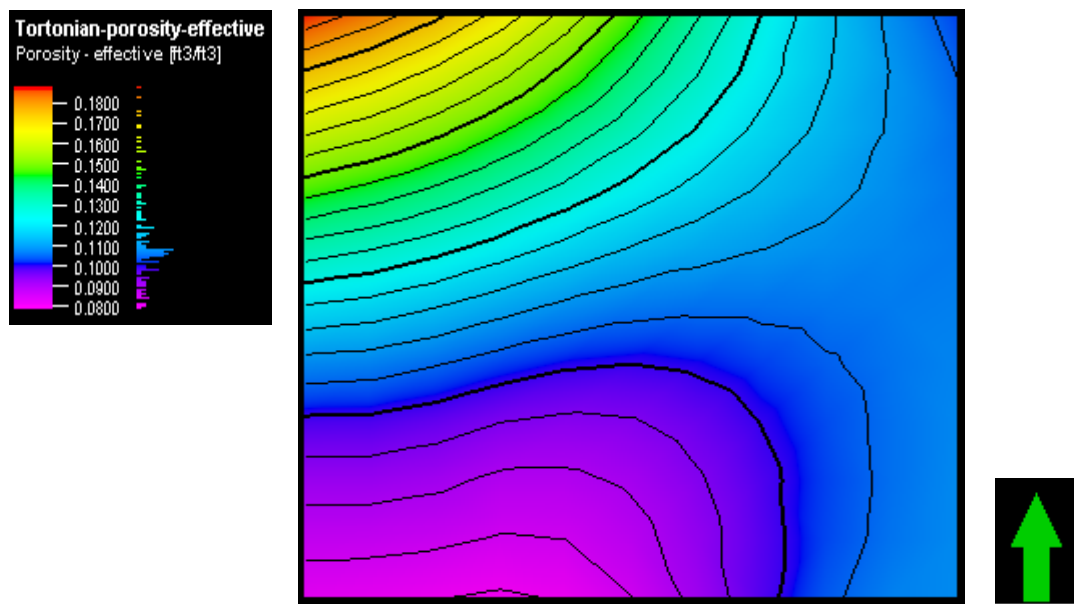


Figure 4-11 Tortonian's effective porosity map

5 CONCLUSION

The integration between flow zone indicator, artificial neural networks, and convergent interpolation techniques has been successfully tested through developing the permeability map of the complex Tortonian reservoir structure. Based on the results of this study, the following conclusions have been drawn:

1. The techniques used in this study successfully modeled the porosity and permeability relationship and increased the model reliability up to 90% (the developed relationships have fitted more than 90% of the data).
2. The FZI technique showed the presence of three different rock types within the Tortonian reservoir.
3. The reliability of the porosity log readings has increased after removing the effect of shale and improved the effective porosity estimation from the well-logs.
4. The integration between FZI, ANN, and calibrating the porosity logs readings has successfully allowed the estimation of reservoir permeability for uncored wells.
5. The permeability map shows that the well Gamma-3 penetrates the northwest area that has the highest reservoir quality.
6. The reservoir quality increases from south to north, which is inversely proportional to the reservoir thickness.
7. The reservoir thickness decreases in the upper reservoir structure. Therefore, the overburden pressure declines, and the pore space compaction diminishes, and the effective porosity increases.
8. Finally, the developed relationship showed that there is a direct relationship between the effective porosity and permeability, which validates the petro-physical evaluation presented in the study.

REFERENCES

- Abbas, M. A., & Al Lawe, E. M. (2019). Clustering analysis and flow zone indicator for electrofacies characterization in the upper shale member in Luhais oil field, southern Iraq. *Society of Petroleum Engineers - Abu Dhabi International Petroleum Exhibition and Conference 2019, ADIP 2019*.
<https://doi.org/10.2118/197906-ms>
- Ahmed, T. (2001). Reservoir Engineering handbook. In *Reservoir Engineering Handbook*.
- Al-Aboodi, A. H., Al-Abadi, A. M., & T. Ibrahim, H. (2017). A Committee Machine with Intelligent Systems for Estimating Monthly Mean Reference Evapotranspiration in an Arid Region. *Research Journal of Applied Sciences, Engineering, and Technology*, 14(10), 386–398.
<https://doi.org/10.19026/rjaset.14.5131>
- Alyafei, N. (2019). Fundamentals of reservoir rock properties. In *Fundamentals of Reservoir Rock Properties* (Issue January). <https://doi.org/10.1007/978-3-030-28140-3>
- Amaefule, J. O., Altunbay, M., Tiab, D., Kersey, D. G., & Keelan, D. K. (1993). Enhanced reservoir description: using core and log data to identify hydraulic (flow) units and predict permeability in uncored intervals/ wells. *Proceedings - SPE Annual Technical Conference and Exhibition, Omega(c)*, 205–220.
<https://doi.org/10.2523/26436-ms>
- Amyx, J. W., Jr, D. ; B., & Whiting, R. L. (1960). *Petroleum Reservoir Engineering.pdf*.
- Asquith, G., & Krygowski, D. (2014). Basic Well Log Analysis Second Edition for Geologists. In *Dictionary Geotechnical Engineering/Wörterbuch GeoTechnik*.
- Baker, R. O., Yarranton, H. W., & Jensen, J. L. (2015a). Openhole Well Logs—Log Interpretation Basics. In *Practical Reservoir Engineering and Characterization*.
<https://doi.org/10.1016/b978-0-12-801811-8.00009-2>
- Baker, R. O., Yarranton, H. W., & Jensen, J. L. (2015b). Special Core Analysis—Rock–Fluid Interactions. In *Practical Reservoir Engineering and Characterization*.
<https://doi.org/10.1016/b978-0-12-801811-8.00008-0>

- Basheer, I. A., & Hajmeer, M. (2000). Artificial neural networks: fundamentals, computing, design, and application. *Journal of Microbiological Methods*, 43(1), 3–31. [https://doi.org/10.1016/S0167-7012\(00\)00201-3](https://doi.org/10.1016/S0167-7012(00)00201-3)
- Bassiouni, Z. (1994). Theory, measurements, and interpretation of well-logs. In *Journal of Petroleum Science and Engineering* (Vol. 13, Issues 3–4). [https://doi.org/10.1016/0920-4105\(95\)90010-1](https://doi.org/10.1016/0920-4105(95)90010-1)
- Biniwale, S. (2005). An integrated method for modeling fluid saturation profiles and characterizing geological environments using a modified FZI approach: Australian fields case study. *Proceedings - SPE Annual Technical Conference and Exhibition, Student 4*, 4847–4864. <https://doi.org/10.2118/99285-stu>
- Bjorlykkee, K., Faleide, J. I., Roy H. Gabrielsen, Nils-Martin Hanken, Kaare Høeg, J. J., Martin Landrø, Nazmul Haque Mondol, J. N., & Nielsen, and J. K. (2011). *Petroleum Geoscience: From Sedimentary Environments to Rock Physics*.
- Clark, N. (1960). *Elements of petroleum reservoir.pdf*.
- Dandekar, A. (2015). Petroleum reservoir rock and fluid properties. In *Methods of Soil Analysis, Part 1: Physical and Mineralogical Properties, Including Statistics of Measurement and Sampling*. <https://doi.org/10.2134/agronmonogr9.1.c21>
- Dezfoolian, M. A. (2013). Flow zone indicator estimation based on petrophysical studies using an artificial neural network in a southern Iran reservoir. *Petroleum Science and Technology*, 31(12), 1294–1305. <https://doi.org/10.1080/10916466.2010.542421>
- Haikel, S., Rosid, M. S., & Haidar, M. W. (2018). Study comparative rock typing methods to classify rock type carbonate reservoir Field “s” East Java. *Journal of Physics: Conference Series*, 1120(1), 0–10. <https://doi.org/10.1088/1742-6596/1120/1/012047>
- Hashim, N. S., Zakaria, A. F., & Ishak, N. A. (2017). An innovative approach towards improving the relationship between flow zone indicators with lithofacies: A case study in carbonate oil field, middle east. *Society of Petroleum Engineers - SPE Reservoir Characterisation and Simulation Conference and Exhibition, RCSC 2017*, 799–825. <https://doi.org/10.2118/186005-ms>
- HLS, A. (2007). Basic logic interpretation. In *Classical and Nonclassical Logics* (Issue May). <https://doi.org/10.2307/j.ctv15r582q.16>

- Kamel, M. H., & Mohamed, M. M. (2006). Effective porosity determination in clean/shaly formations from acoustic logs with applications. *Journal of Petroleum Science and Engineering*, 51(3–4), 267–274.
<https://doi.org/10.1016/j.petrol.2006.01.007>
- Kay, A. (2001). *Artificial Neural Networks | Computerworld*. Computer World.
<https://www.computerworld.com/article/2591759/artificial-neural-networks.html>
- Killeen, P. G. (1982). Gamma-ray logging and interpretation. *Developments in Geophysical Exploration Methods - 3*, 95–150. https://doi.org/10.1007/978-94-009-7349-7_4
- Miah, M. I. (2014). Porosity assessment of gas reservoir using wireline log data: A case study of Bokabil formation, Bangladesh. *Procedia Engineering*, 90, 663–668.
<https://doi.org/10.1016/j.proeng.2014.11.789>
- MK, G. A. (2017). Determination of Shale Types using Well Logs. *International Journal Of Petrochemical Science & Engineering*, 2(5), 274–280.
<https://doi.org/10.15406/ipcse.2017.02.00051>
- Nielsen, M. (2006). Neural Networks and Deep Learning. In *The Machine Age of Customer Insight*. <https://doi.org/10.1108/978-1-83909-694-520211010>
- Rodolfo, S. B., Torres, F., Arango, S., Cobaleda, G., Holditch, S., & Wu, C. (2002). *How to Improve Reservoir Characterization Models Using Intelligent Systems*. 2, 387–417. https://doi.org/10.1007/978-3-7908-1807-9_16
- Skopec, R. A. (1994). proper coring and well-site core handling procedures: the first step toward reliable core analysis. *Journal of Petroleum Technology*, 2815.
- Soto B., R., Torres, F., Arango, S., & Cobaleda, G. (2001). *Improved Reservoir Permeability Models From Flow Units And Soft Computing Techniques: A Case Study, Suria And Reforma-Libertad Fields, Colombia*. 1–10.
<https://doi.org/10.2118/69625-ms>
- Sritongthae, W. (2016). Petrophysical Rock Typing : Enhanced Permeability Prediction and Reservoir Descriptions. *AAPG Asia Pacific Region Geosciences Technology Workshops 2016*, 51265(March 2016).
- Tavakoli, V. (2018). *Geological Core Analysis: Application to Reservoir Characterization*.

Ubani, C., & Adeboye, Y. (2013). *ADVANCES IN CORING AND CORE ANALYSIS FOR RESERVOIR FORMATION EVALUATION*. 3(1), 240–246.

Uguru, C. I., Onyeagoro, U. O., Lin, J., Okkerman, J., & Sikiru, I. O. (2005).

Permeability prediction using genetic unit averages of flow zone indicators (FZIs) and neural networks. *Society of Petroleum Engineers - Nigeria Annual International Conference and Exhibition 2005, NAICE 2005, i.*

<https://doi.org/10.2523/98828-ms>

APPENDICES

Appendix A tables of core data

Table 1 Messenian sand core data

Sample	Depth (MD) in FT	NPHI Helium	K h (M. Darcy)
1	6702	0.247	181
2	6703	0.2407	163.54
3	6704	0.2796	229.46
4	6705	0.242	25.39
5	6707	0.242	79.32
6	6708	0.273	152.15
7	6709	0.261	149.69
8	6710	0.2572	116.1
9	6711	0.277	253.4
10	6712	0.301	138.3
11	6717	0.2568	106.7
12	6718	0.218	56.7
13	6725	0.248	53.37

Table 2 Tortonian reservoir core data

Sample	Depth (MD) in FT	NPHI Helium	K h (M. Darcy)
1	7187	0.1497	0.022
2	7188	0.1556	0.078
3	7194	0.1855	0.576
4	7195	0.1177	10.42
5	7196	0.1345	2.128
6	7202	0.1612	0.367
7	7203	0.0979	0.815
8	7204	0.0612	0.303
9	7206	0.1114	2.225
10	7210	0.0575	0.081
11	7214	0.1276	12.01
12	7215	0.1578	29.98

Sample	Depth (MD) in FT	NPHI Helium	K h (M. Darcy)
13	7218	0.1621	0.361
14	7219	0.1926	0.038
15	7220	0.1862	0.853
16	7224	0.0996	0.113
17	7225	0.1639	6.658
18	7226	0.1673	0.27
19	7228	0.1451	15.138
20	7229	0.0682	0.293

Appendix B tables of well-logs

Table 3 Messenian sand (cored interval) log data.

Depth (FT)	Gamma-ray (API)	NPHI (neutron) (FT3/FT3)	RHOB (density) (g/cm3)
6702	73.03	0.2563	2.3665
6703	73.66	0.2698	2.4053
6704	69.62	0.2563	2.3873
6705	66.84	0.2654	2.3522
6707	58.75	0.4064	2.1047
6708	59.59	0.3134	2.2312
6709	62.06	0.2669	2.2711
6710	63.86	0.279	2.2946
6711	57.58	0.2724	2.3038
6712	45.11	0.2586	2.2635
6717	62.5	0.247	2.3321
6718	51.81	0.2607	2.2716
6725	82.29	0.2464	2.4491

Table 4 Tortonian sand (cored interval) log data.

Depth (FT)	Gamma-ray (API)	NPHI (neutron) (FT3/FT3)	RHOB (density) (g/cm3)
7179	61.6	0.1886	2.5376
7180	49.41	0.214	2.4314
7186	76.72	0.2322	2.5304

Depth (FT)	Gamma-ray (API)	NPHI (neutron) (FT3/FT3)	RHOB (density) (g/cm3)
7187	58.1	0.272	2.5203
7188	57.71	0.2004	2.429
7194	67.39	0.2161	2.4885
7195	65.96	0.2069	2.4334
7196	65.3	0.2171	2.4148
7198	73.45	0.2388	2.3754
7202	76.11	0.2319	2.417
7206	45.54	0.206	2.368
7207	46.62	0.213	2.4259
7210	59.72	0.2148	2.4682
7211	70.09	0.2049	2.4683
7212	78.8	0.2128	2.468
7216	69.9	0.2603	2.4982
7217	65.9	0.2053	2.4897
7218	57.75	0.2333	2.4046
7220	65.74	0.1642	2.5118
7221	83.09	0.2069	2.404

Table 5 Gamma-1 logs data for interesting intervals of Tortonian FM

Depth FT-MD	Gamma-ray API	Neutron FT/FT	Density G/cm3	Resistivity Ohm. m
7214	102.13	0.301	2.385	3.1195
7214.5	98	0.252	2.492	3.4083
7215	84.5	0.2	2.479	3.7986
7215.5	73.44	0.184	2.448	3.9894
7216	65.13	0.171	2.431	3.881
7216.5	61.91	0.173	2.408	3.7493
7217	60	0.187	2.388	3.6168
7217.5	59.81	0.199	2.384	3.7487
7218	61.81	0.22	2.399	4.2842
7218.5	64.19	0.223	2.417	4.6341
7219	68.19	0.212	2.42	4.7212
7219.5	67.56	0.203	2.404	4.3908

Depth FT-MD	Gamma-ray API	Neutron FT/FT	Density G/cm3	Resistivity Ohm. m
7220	65.88	0.198	2.361	3.7821
7220.5	65.44	0.207	2.337	3.6161
7221	64.94	0.212	2.355	3.5605
7221.5	66.5	0.211	2.364	3.5898
7222	69.44	0.203	2.361	3.7357
7222.5	72.31	0.203	2.341	3.6896
7223	73.19	0.203	2.339	3.4729
7223.5	68.25	0.206	2.317	3.3864
7224	70.75	0.207	2.299	3.2386
7224.5	70.94	0.205	2.312	3.0908
7225	76.75	0.193	2.336	3.3961
7225.5	76.75	0.182	2.379	3.8386
7226	81.44	0.18	2.423	4.1349
7226.5	87.13	0.201	2.483	4.4101
7227	94.38	0.217	2.487	4.3561
7227.5	96.06	0.243	2.485	4.0901
7228	89.69	0.245	2.477	3.8605
7251	106.31	0.384	2.312	2.5123
7251.5	104.5	0.286	2.415	2.8212
7252	97.5	0.217	2.464	2.9704
7252.5	92.19	0.218	2.459	2.882
7253	89.06	0.231	2.461	2.6921
7253.5	83.38	0.237	2.421	2.46
7254	73.38	0.223	2.411	2.3148
7254.5	65.25	0.213	2.406	2.327
7255	66.19	0.214	2.41	2.3278
7255.5	70.19	0.242	2.39	2.2617
7256	71.06	0.239	2.394	2.2489
7256.5	71.31	0.246	2.38	2.2474
7257	68.94	0.221	2.369	2.2638
7257.5	68.56	0.214	2.378	2.3535
7258	68	0.198	2.403	2.4343
7258.5	69.13	0.2	2.398	2.4857

Depth FT-MD	Gamma-ray API	Neutron FT/FT	Density G/cm3	Resistivity Ohm. m
7259	66.44	0.201	2.376	2.4759
7259.5	62.03	0.205	2.363	2.4337
7260	61.69	0.21	2.35	2.3814
7260.5	66.19	0.215	2.361	2.3193
7261	63.41	0.218	2.37	2.2283
7261.5	61.72	0.217	2.352	2.2136
7262	60.47	0.206	2.338	2.2567
7262.5	65.88	0.198	2.35	2.3231
7263	68.81	0.19	2.362	2.351
7263.5	65.19	0.206	2.372	2.2007
7264	67.25	0.22	2.365	1.971
7264.5	65.19	0.237	2.347	1.8411
7265	66.88	0.232	2.319	1.7242
7265.5	64.5	0.23	2.301	1.6842
7266	66.44	0.218	2.292	1.8184
7266.5	71.56	0.21	2.307	2.0991
7267	73.38	0.196	2.351	2.4076
7267.5	73.94	0.195	2.407	2.6402
7268	75.75	0.194	2.426	2.6337
7268.5	80.25	0.205	2.423	2.4373
7269	80.19	0.201	2.399	2.1779
7269.5	77.75	0.208	2.388	2.0295
7270	71.5	0.21	2.374	1.9284
7270.5	76.38	0.214	2.376	1.8661
7271	71.56	0.209	2.38	1.8447
7271.5	73.75	0.198	2.389	1.7682
7272	66.31	0.186	2.388	1.7656
7272.5	68.63	0.202	2.38	2.1124
7273	74.88	0.213	2.387	2.3897
7511	75.94	0.255	2.472	3.4998
7511.5	69.38	0.228	2.479	3.6025
7512	69.06	0.214	2.493	3.5821
7512.5	74.94	0.2	2.483	3.2241

Depth FT-MD	Gamma-ray API	Neutron FT/FT	Density G/cm3	Resistivity Ohm. m
7513	72.63	0.216	2.482	3.0736
7513.5	67.94	0.21	2.492	3.1141
7514	64.88	0.189	2.496	3.2713
7514.5	64.81	0.174	2.502	3.6888
7515	63.25	0.172	2.521	4.0371
7515.5	57.44	0.197	2.515	4.0889
7516	59.91	0.216	2.476	3.938
7516.5	60.19	0.215	2.448	3.4113
7517	61.09	0.224	2.436	2.9049
7517.5	57.31	0.216	2.425	2.6126
7518	62.72	0.221	2.43	2.3308
7518.5	63.5	0.2	2.43	2.2177
7519	64.13	0.207	2.428	2.2801
7519.5	61.59	0.207	2.413	2.4261
7520	62	0.211	2.428	2.7189
7520.5	64	0.208	2.454	2.8435
7521	62.31	0.205	2.458	2.8655
7521.5	63.53	0.205	2.433	3.1894
7522	64.56	0.197	2.445	3.1399
7522.5	67.31	0.203	2.476	2.9841
7523	68.5	0.22	2.472	3.0751
7523.5	68.06	0.225	2.441	2.7771
7524	68.19	0.215	2.423	2.4438
7524.5	67.31	0.213	2.42	2.3294
7525	70.31	0.214	2.417	2.3265
7525.5	67.69	0.217	2.421	2.5888
7526	67.88	0.192	2.428	2.8219
7526.5	61.97	0.189	2.452	3.1303
7527	62.34	0.207	2.465	3.7895
7527.5	58.59	0.233	2.5	4.3381
7528	61.78	0.235	2.525	4.6753
7528.5	62.88	0.227	2.532	4.6315
7529	66.44	0.223	2.517	4.5075

Depth FT-MD	Gamma-ray API	Neutron FT/FT	Density G/cm3	Resistivity Ohm. m
7529.5	68.44	0.212	2.526	4.5397
7530	67.06	0.197	2.53	4.6486
7530.5	66.06	0.186	2.545	5.1023
7531	68.5	0.19	2.547	5.4297
7531.5	74.13	0.193	2.555	5.5579
7532	76.5	0.208	2.548	5.9196
7532.5	71.31	0.209	2.555	5.5409
7533	66.44	0.216	2.555	5.1335
7533.5	64.38	0.205	2.545	5.1673
7534	65.81	0.214	2.536	5.0675
7534.5	68.19	0.203	2.52	5.1482
7535	67.5	0.207	2.534	5.9096
7535.5	66.56	0.206	2.531	6.3249
7536	67.13	0.218	2.535	6.1143
7536.5	71.69	0.227	2.525	4.8239
7537	81.31	0.303	2.506	3.2765
7537.5	91.19	0.344	2.427	2.3126
7538	98.38	0.37	2.36	1.8094
7538.5	97.75	0.346	2.318	1.664
7539	99.94	0.365	2.281	1.7628
7539.5	94.81	0.344	2.266	2.0725
7540	91.13	0.307	2.349	2.4773
7540.5	79.13	0.254	2.385	2.66
7541	71.63	0.237	2.357	2.631
7541.5	63.59	0.231	2.331	2.4231
7542	60.31	0.232	2.328	2.1451
7542.5	64.75	0.241	2.319	2.0244
7543	66.25	0.246	2.303	2.0268
7543.5	68.13	0.243	2.268	1.9885
7544	62.5	0.24	2.251	1.86
7544.5	66.13	0.23	2.249	1.7379
7545	62.63	0.24	2.258	1.6802
7545.5	64	0.26	2.258	1.5862

Depth FT-MD	Gamma-ray API	Neutron FT/FT	Density G/cm3	Resistivity Ohm. m
7546	62.53	0.267	2.257	1.5316
7546.5	63.44	0.255	2.252	1.5237
7547	63.5	0.247	2.246	1.5327
7547.5	67.25	0.24	2.24	1.5734
7548	72.5	0.242	2.255	1.6727
7548.5	80.63	0.234	2.269	1.725
7549	85.19	0.235	2.271	1.6677
7549.5	82.44	0.234	2.259	1.5978
7550	75.31	0.226	2.248	1.571
7550.5	69.69	0.225	2.258	1.6548
7551	76.31	0.219	2.289	1.8907
7551.5	80.06	0.222	2.332	2.2372
7552	85.19	0.225	2.366	2.369
7552.5	82.06	0.231	2.383	2.1342
7553	80.13	0.229	2.367	1.9108
7553.5	69.25	0.227	2.353	1.7391
7554	63.66	0.227	2.343	1.6438
7554.5	64.5	0.239	2.334	1.6602
7555	64.88	0.232	2.31	1.6996
7555.5	65.94	0.247	2.304	1.795
7556	62.06	0.256	2.319	1.9496
7556.5	66.13	0.254	2.339	2.0958
7557	66	0.222	2.349	2.2257
7557.5	64.88	0.221	2.343	2.2638
7558	63.66	0.219	2.327	2.1379
7558.5	64.19	0.238	2.312	2.0524
7559	67.5	0.229	2.314	2.1517
7559.5	69.13	0.237	2.344	2.3759
7560	73.63	0.23	2.376	2.7688
7560.5	79.44	0.232	2.403	3.3674
7561	84.44	0.247	2.43	3.7583
7622	112	0.33	2.41	2.23
7622.5	102.81	0.28	2.463	2.4907

Depth FT-MD	Gamma-ray API	Neutron FT/FT	Density G/cm3	Resistivity Ohm. m
7623	86.38	0.231	2.572	3.2675
7623.5	78.69	0.222	2.627	4.8386
7624	75.31	0.193	2.651	6.4746
7624.5	73.5	0.2	2.566	6.3526
7625	71.38	0.207	2.303	5.4904
7625.5	73.06	0.232	2.21	5.0269
7626	70.88	0.269	2.105	4.6378
7626.5	71.44	0.267	2.106	4.2862
7627	75.31	0.293	2.137	4.1801
7627.5	85.69	0.278	2.302	3.7922
7635.5	95.5	0.295	2.408	3.2712
7636	91.44	0.247	2.431	3.5166
7636.5	94.31	0.222	2.428	4.0257
7637	92.38	0.221	2.262	4.7101
7637.5	89.63	0.229	2.107	4.9284
7638	86.06	0.228	2.053	5.0941
7638.5	85.38	0.227	2.166	5.2167
7639	88.06	0.228	2.343	5.3358
7639.5	86.06	0.252	2.467	5.4354
7640	88.75	0.261	2.57	5.0017
7640.5	89.63	0.246	2.635	5.1106
7641	82.13	0.227	2.689	5.2309
7687	69	0.221	2.427	2.2862
7687.5	63.69	0.213	2.395	2.1389
7688	60.97	0.218	2.396	2.0913
7688.5	59.72	0.206	2.399	2.1463
7689	62.25	0.221	2.404	2.1399
7689.5	58.78	0.216	2.384	2.0918
7690	62.94	0.213	2.369	2.0409
7690.5	58.69	0.186	2.355	1.9323
7691	61	0.184	2.368	1.9423
7691.5	56.75	0.193	2.388	2.0328
7692	56.03	0.207	2.368	2.079

Depth FT-MD	Gamma-ray API	Neutron FT/FT	Density G/cm3	Resistivity Ohm. m
7692.5	55.31	0.203	2.357	2.1338
7693	58.44	0.187	2.35	2.1817
7693.5	60.34	0.176	2.352	2.2759
7694	60.38	0.181	2.403	2.3619
7694.5	58.56	0.209	2.49	2.6213
7695	62.44	0.243	2.592	3.2123

Table 6 Gamma-2 logs data for interesting intervals of Tortonian FM

Depth FT-MD	Gamma-ray API	Neutron FT3/FT3	Density G/cm3	Resistivity Ohm. m
7201.8	53.84	0.2036	2.3372	2.2756
7202.0	51.19	0.1958	2.3263	2.2446
7202.2	48.84	0.1909	2.319	2.2524
7202.3	46.5	0.186	2.3116	2.2602
7202.5	44.16	0.1811	2.3043	2.268
7202.7	42.16	0.1818	2.2934	2.2669
7202.8	40.16	0.1825	2.2826	2.2658
7203.0	38.16	0.1832	2.2717	2.2647
7203.2	36.57	0.1892	2.2726	2.2734
7203.3	34.99	0.1952	2.2734	2.282
7203.5	33.41	0.2012	2.2742	2.2907
7203.7	33.95	0.2062	2.2772	2.299
7205.0	40.25	0.2049	2.3085	2.3185
7205.2	40.22	0.2058	2.3087	2.3116
7205.3	40.19	0.2066	2.309	2.3048
7205.5	40.16	0.2075	2.3093	2.2979
7205.7	39.93	0.2096	2.3012	2.2832
7208.2	46.67	0.2049	2.2953	2.2799
7208.3	46.11	0.1951	2.2983	2.3124
7208.5	45.56	0.1853	2.3014	2.3449
7208.7	45.75	0.1895	2.3043	2.3863
7208.8	45.94	0.1937	2.3073	2.4276
7209.0	46.13	0.198	2.3102	2.469

Depth FT-MD	Gamma-ray API	Neutron FT3/FT3	Density G/cm3	Resistivity Ohm. m
7209.2	47.49	0.1942	2.3142	2.5354
7209.3	48.85	0.1904	2.3182	2.6018
7209.5	50.22	0.1867	2.3222	2.6681
7209.7	51.91	0.1903	2.3309	2.7576
7209.8	53.59	0.194	2.3396	2.8472
7210.0	55.28	0.1976	2.3482	2.9367
7210.2	56.61	0.1935	2.3579	2.9904
7210.3	57.95	0.1894	2.3676	3.0442
7210.5	59.28	0.1853	2.3773	3.0979
7210.7	59.52	0.1815	2.3853	3.132
7210.8	59.76	0.1778	2.3933	3.1661
7211.0	60	0.1741	2.4013	3.2002
7211.2	61.79	0.1697	2.4039	3.2343
7211.3	63.58	0.1653	2.4065	3.2684
7211.5	65.38	0.1609	2.4091	3.3025
7211.7	67.27	0.1646	2.4154	3.3877
7211.8	69.17	0.1682	2.4216	3.4729
7212.0	71.06	0.1719	2.4279	3.5581
7218.0	48.84	0.2158	2.4303	3.915
7218.2	49.27	0.2089	2.4221	3.9197
7218.3	49.7	0.2019	2.4139	3.9244
7218.5	50.13	0.1949	2.4057	3.9291
7218.7	51.31	0.1864	2.4049	3.9488
7218.8	52.5	0.1778	2.4042	3.9686
7219.0	53.69	0.1693	2.4034	3.9883
7219.2	54.24	0.1675	2.408	4.0259
7219.3	54.79	0.1658	2.4126	4.0635
7219.5	55.34	0.164	2.4173	4.101
7219.7	53.53	0.166	2.4295	3.9196
7219.8	51.72	0.168	2.4417	3.7382
7220.0	49.91	0.1699	2.4539	3.5568
7223.0	57.91	0.2022	2.5251	4.7745
7223.2	57.7	0.1989	2.528	4.8709
7223.3	57.49	0.1955	2.5309	4.9673

Depth FT-MD	Gamma-ray API	Neutron FT3/FT3	Density G/cm3	Resistivity Ohm. m
7223.5	57.28	0.1921	2.5338	5.0637
7223.7	54.67	0.1895	2.5233	4.8735
7223.8	52.05	0.1869	2.5127	4.6832
7224.0	49.44	0.1844	2.5022	4.493
7224.2	49.56	0.1783	2.4815	4.2812
7224.3	49.69	0.1723	2.4608	4.0693
7224.5	49.81	0.1662	2.44	3.8575
7224.7	48.95	0.1723	2.4306	3.771
7224.8	48.08	0.1785	2.4211	3.6844
7225.0	47.22	0.1846	2.4116	3.5979
7225.2	47.31	0.186	2.4039	3.5536
7225.3	47.41	0.1874	2.3962	3.5093
7225.5	47.5	0.1887	2.3884	3.4651
7225.7	47.6	0.193	2.3935	3.421
7225.8	47.71	0.1972	2.3987	3.3769
7226.0	47.81	0.2015	2.4038	3.3328
7226.2	48.8	0.1971	2.4065	3.3716
7226.3	49.79	0.1927	2.4093	3.4104
7226.5	50.78	0.1882	2.4121	3.4492
7226.7	51.18	0.2011	2.4196	3.3938
7226.8	51.57	0.214	2.4271	3.3384
7288.2	30.18	0.2084	2.3801	2.5151
7288.3	30.55	0.2064	2.3727	2.5047
7288.5	30.92	0.2045	2.3653	2.4942
7288.7	30.3	0.1981	2.3698	2.5088
7288.8	29.68	0.1916	2.3744	2.5234
7289.0	29.06	0.1851	2.3789	2.5379
7289.2	29.9	0.1852	2.3837	2.559
7289.3	30.73	0.1853	2.3885	2.5801
7289.5	31.56	0.1854	2.3933	2.6012
7289.7	31.73	0.1845	2.3934	2.6091
7289.8	31.9	0.1835	2.3934	2.617
7290.0	32.06	0.1826	2.3935	2.6249
7290.2	33.76	0.1884	2.3961	2.6915

Depth FT-MD	Gamma-ray API	Neutron FT3/FT3	Density G/cm3	Resistivity Ohm. m
7290.3	35.46	0.1942	2.3987	2.7582
7290.5	37.16	0.1999	2.4013	2.8249
7290.7	40.39	0.1972	2.4016	2.9418
7290.8	43.61	0.1945	2.402	3.0587
7291.0	46.84	0.1917	2.4023	3.1756
7291.2	50.93	0.1997	2.4128	3.2879
7291.3	55.01	0.2077	2.4233	3.4003
7314.0	59.59	0.2177	2.4188	3.3718
7314.2	56.97	0.2137	2.419	3.2559
7314.3	54.34	0.2097	2.4193	3.14
7314.5	51.72	0.2056	2.4195	3.0241
7314.7	51.29	0.2084	2.4154	2.9407
7314.8	50.86	0.2112	2.4114	2.8574
7315.0	50.44	0.2141	2.4074	2.774
7315.2	49.07	0.2219	2.3937	2.7566
7315.3	47.71	0.2298	2.3801	2.7393
7315.5	46.34	0.2377	2.3664	2.7219
7315.7	48.14	0.2355	2.3595	2.727
7315.8	49.93	0.2333	2.3525	2.7321
7316.0	51.72	0.2311	2.3456	2.7372
7316.2	52.64	0.2319	2.3508	2.7901
7316.3	53.55	0.2328	2.3559	2.8431
7316.5	54.47	0.2336	2.3611	2.896
7316.7	57.03	0.258	2.3685	3.0472
7316.8	59.59	0.2823	2.376	3.1984
7317.0	62.16	0.3067	2.3835	3.3496

Table 7 Gamma-3 log data for interesting intervals of Tortonian FM

Depth FT-MD	Gamma-ray API	Neutron FT3/FT3	Density G/cm3	Resistivity Ohm. m
7046.0	36.0	0.022	2.385	10.5
7046.2	35.3	0.036	2.358	9.3
7046.3	34.6	0.050	2.331	8.0
7046.5	33.9	0.064	2.303	6.8

Depth FT-MD	Gamma-ray API	Neutron FT3/FT3	Density G/cm3	Resistivity Ohm. m
7046.7	34.0	0.091	2.312	6.1
7046.8	34.1	0.118	2.320	5.4
7047.0	34.2	0.145	2.328	4.7
7047.2	34.1	0.174	2.339	4.4
7047.3	33.9	0.202	2.349	4.1
7050.2	35.4	0.184	2.471	12.2
7050.3	34.0	0.149	2.541	12.8
7050.5	32.7	0.114	2.612	13.5
7050.7	32.1	0.098	2.636	12.6
7050.8	31.4	0.083	2.661	11.8
7051.0	30.8	0.067	2.685	11.0
7051.2	31.1	0.073	2.687	10.7
7051.3	31.5	0.079	2.689	10.3
7051.5	31.8	0.086	2.692	10.0
7051.7	32.6	0.083	2.687	9.9
7051.8	33.4	0.081	2.683	9.7
7052.0	34.3	0.079	2.679	9.5
7052.2	33.9	0.082	2.667	9.3
7052.3	33.5	0.085	2.656	9.1
7052.5	33.2	0.088	2.644	8.9
7052.7	32.0	0.095	2.595	8.7
7052.8	30.9	0.103	2.545	8.5
7053.0	29.7	0.110	2.495	8.3
7053.2	29.4	0.125	2.472	8.3
7053.3	29.0	0.139	2.449	8.2
7053.5	28.7	0.154	2.427	8.2
7053.7	28.1	0.158	2.425	8.4
7053.8	27.6	0.163	2.423	8.6
7054.0	27.0	0.168	2.421	8.8
7054.2	27.1	0.163	2.445	8.8
7054.3	27.1	0.158	2.469	8.8
7054.5	27.2	0.153	2.493	8.8
7054.7	27.2	0.149	2.432	8.7
7054.8	27.3	0.145	2.372	8.6

Depth FT-MD	Gamma-ray API	Neutron FT3/FT3	Density G/cm3	Resistivity Ohm. m
7055.0	27.3	0.141	2.311	8.6
7055.2	27.6	0.151	2.261	8.7
7055.3	28.0	0.161	2.210	8.8
7055.5	28.3	0.171	2.160	8.9
7055.7	28.5	0.184	2.141	9.4
7055.8	28.7	0.197	2.123	9.9
7056.0	28.9	0.210	2.105	10.3
7056.2	28.3	0.203	2.153	11.3
7056.3	27.7	0.196	2.201	12.3
7056.5	27.1	0.189	2.249	13.3
7056.7	26.7	0.164	2.322	14.0
7056.8	26.3	0.139	2.395	14.7
7057.0	25.9	0.114	2.467	15.5
7057.2	25.5	0.090	2.544	16.7
7057.3	25.1	0.066	2.620	17.9
7057.5	24.7	0.041	2.696	19.2
7057.7	24.8	0.035	2.705	21.3
7057.8	24.9	0.029	2.714	23.5
7058.0	25.1	0.023	2.722	25.6
7058.2	25.4	0.023	2.711	25.2
7058.3	25.7	0.023	2.700	24.8
7058.5	26.1	0.023	2.689	24.5
7058.7	26.2	0.022	2.694	25.3
7058.8	26.4	0.021	2.698	26.2
7059.0	26.5	0.020	2.702	27.1
7059.2	26.7	0.019	2.701	26.8
7059.3	26.9	0.018	2.700	26.6
7059.5	27.1	0.017	2.699	26.3
7059.7	27.5	0.017	2.697	26.5
7059.8	28.0	0.017	2.696	26.8
7060.0	28.4	0.017	2.695	27.0
7060.2	27.9	0.017	2.689	28.7
7060.3	27.5	0.016	2.684	30.4
7060.5	27.0	0.016	2.678	32.1

Depth FT-MD	Gamma-ray API	Neutron FT3/FT3	Density G/cm3	Resistivity Ohm. m
7060.7	26.6	0.015	2.682	34.5
7060.8	26.1	0.014	2.685	37.0
7061.0	25.7	0.013	2.689	39.4
7061.2	25.0	0.011	2.693	39.8
7061.3	24.2	0.010	2.698	40.2
7061.5	23.5	0.008	2.703	40.6
7061.7	25.0	0.008	2.705	37.8
7061.8	26.4	0.008	2.707	35.0
7062.0	27.8	0.008	2.708	32.1
7062.2	28.9	0.009	2.706	27.8
7062.3	29.9	0.010	2.705	23.5
7062.5	30.9	0.010	2.703	19.1
7062.7	31.4	0.016	2.691	17.3
7062.8	31.9	0.022	2.679	15.5
7063.0	32.4	0.028	2.667	13.6
7063.2	31.4	0.034	2.662	13.6
7063.3	30.4	0.040	2.657	13.5
7063.5	29.4	0.045	2.653	13.4
7063.7	28.0	0.049	2.664	13.9
7063.8	26.6	0.053	2.675	14.4
7064.0	25.1	0.057	2.687	14.8
7064.2	25.6	0.051	2.699	15.4
7064.3	26.2	0.046	2.711	16.0
7064.5	26.7	0.041	2.722	16.6
7064.7	26.4	0.038	2.715	16.8
7064.8	26.2	0.035	2.707	17.0
7065.0	25.9	0.031	2.699	17.2
7065.2	26.3	0.031	2.694	16.8
7065.3	26.6	0.030	2.689	16.4
7065.5	27.0	0.030	2.684	16.0
7065.7	26.7	0.029	2.678	15.8
7065.8	26.4	0.029	2.672	15.6
7066.0	26.1	0.029	2.665	15.4
7066.2	26.5	0.032	2.661	14.8

Depth FT-MD	Gamma-ray API	Neutron FT3/FT3	Density G/cm3	Resistivity Ohm. m
7066.3	26.9	0.036	2.658	14.1
7066.5	27.3	0.039	2.654	13.5
7066.7	29.1	0.041	2.633	12.7
7066.8	30.8	0.044	2.612	11.9
7067.0	32.5	0.046	2.591	11.0
7067.2	33.1	0.057	2.570	10.7
7067.3	33.8	0.067	2.548	10.4
7067.5	34.5	0.078	2.526	10.0
7067.7	35.2	0.092	2.499	10.0
7067.8	35.9	0.106	2.473	10.0
7068.0	36.6	0.120	2.446	10.0
7068.2	35.1	0.134	2.446	10.2
7068.3	33.6	0.149	2.446	10.4
7068.5	32.0	0.163	2.445	10.7
7068.7	31.6	0.163	2.443	11.0
7068.8	31.1	0.163	2.441	11.4
7069.0	30.6	0.163	2.439	11.8
7069.2	29.2	0.154	2.451	12.5
7069.3	27.8	0.146	2.462	13.2
7069.5	26.3	0.137	2.474	13.9
7069.7	26.6	0.128	2.498	14.3
7069.8	26.9	0.119	2.522	14.7
7070.0	27.1	0.110	2.546	15.1
7070.2	26.9	0.110	2.552	15.6
7070.3	26.7	0.109	2.558	16.0
7070.5	26.5	0.109	2.564	16.4
7070.7	27.1	0.108	2.572	16.3
7070.8	27.7	0.107	2.580	16.1
7071.0	28.2	0.106	2.588	15.9
7071.2	28.2	0.104	2.601	14.9
7071.3	28.2	0.102	2.615	13.9
7071.5	28.2	0.100	2.629	12.9
7071.7	29.0	0.090	2.606	12.1
7071.8	29.8	0.080	2.584	11.3

Depth FT-MD	Gamma-ray API	Neutron FT3/FT3	Density G/cm3	Resistivity Ohm. m
7072.0	30.5	0.070	2.561	10.5
7072.2	30.6	0.070	2.514	10.0
7072.3	30.7	0.069	2.467	9.6
7072.5	30.8	0.069	2.421	9.1
7072.7	30.8	0.077	2.415	8.8
7072.8	30.8	0.085	2.410	8.6
7073.0	30.8	0.094	2.404	8.3
7073.2	30.7	0.111	2.434	8.5
7073.3	30.6	0.129	2.463	8.6
7073.5	30.5	0.146	2.492	8.8
7073.7	30.7	0.150	2.492	9.4
7073.8	30.9	0.153	2.491	9.9
7074.0	31.1	0.157	2.490	10.5
7074.2	31.4	0.147	2.500	11.8
7074.3	31.6	0.137	2.510	13.0
7074.5	31.9	0.127	2.520	14.2
7074.7	30.7	0.109	2.546	16.6
7074.8	29.6	0.091	2.572	18.9
7075.0	28.4	0.072	2.598	21.3
7075.2	27.9	0.057	2.636	26.9
7075.3	27.4	0.041	2.673	32.5
7075.5	26.9	0.026	2.710	38.1
7075.7	26.5	0.020	2.717	39.5
7075.8	26.0	0.015	2.723	41.0
7076.0	25.6	0.010	2.730	42.4
7076.2	26.6	0.009	2.724	38.8
7076.3	27.6	0.009	2.719	35.2
7076.5	28.6	0.008	2.713	31.7
7076.7	28.5	0.010	2.708	28.5
7076.8	28.3	0.012	2.703	25.4
7077.0	28.2	0.014	2.698	22.3
7077.2	29.2	0.016	2.695	20.0
7077.3	30.3	0.019	2.692	17.7
7077.5	31.3	0.021	2.690	15.4

Depth FT-MD	Gamma-ray API	Neutron FT3/FT3	Density G/cm3	Resistivity Ohm. m
7077.7	31.9	0.026	2.674	13.5
7077.8	32.5	0.030	2.658	11.6
7078.0	33.1	0.034	2.642	9.7
7108.8	53.4	0.207	2.349	2.5
7109.0	54.1	0.201	2.343	2.6
7109.2	54.2	0.201	2.344	2.6
7109.3	54.2	0.202	2.346	2.7
7109.5	54.2	0.202	2.347	2.8
7109.7	55.2	0.198	2.350	2.9
7109.8	56.2	0.194	2.353	3.0
7110.0	57.2	0.190	2.355	3.1
7110.2	56.5	0.189	2.363	3.2
7110.3	55.9	0.187	2.371	3.3
7110.5	55.3	0.186	2.379	3.4
7110.7	54.4	0.184	2.383	3.4
7110.8	53.5	0.183	2.387	3.4
7111.0	52.5	0.181	2.392	3.4
7111.2	53.9	0.180	2.395	3.4
7111.3	55.2	0.179	2.398	3.4
7111.5	56.6	0.178	2.401	3.4
7111.7	58.2	0.183	2.401	3.4
7111.8	59.8	0.188	2.400	3.4
7112.0	61.4	0.193	2.400	3.3
7112.2	63.5	0.203	2.397	3.3
7113.5	66.4	0.204	2.329	3.1
7113.7	66.1	0.196	2.297	3.1
7113.8	65.8	0.187	2.265	3.1
7114.0	65.4	0.179	2.232	3.1
7114.2	63.5	0.189	2.219	3.2
7114.3	61.6	0.199	2.205	3.3
7114.5	59.7	0.209	2.192	3.4
7157.7	48.4	0.208	2.345	3.6
7157.8	47.2	0.202	2.365	3.5
7158.0	46.1	0.196	2.385	3.5

Depth FT-MD	Gamma-ray API	Neutron FT3/FT3	Density G/cm3	Resistivity Ohm. m
7158.2	45.7	0.193	2.391	3.4
7158.3	45.3	0.190	2.397	3.4
7158.5	44.8	0.187	2.404	3.3
7158.7	45.8	0.187	2.407	3.3
7158.8	46.8	0.187	2.410	3.3
7159.0	47.8	0.186	2.413	3.3
7159.2	49.1	0.186	2.414	3.3
7159.3	50.4	0.187	2.416	3.3
7159.5	51.7	0.187	2.417	3.3
7159.7	52.1	0.192	2.414	3.2
7159.8	52.6	0.196	2.412	3.1
7160.0	53.0	0.201	2.409	3.0
7160.2	52.8	0.206	2.410	3.0
7161.2	56.3	0.210	2.417	2.7
7161.3	57.3	0.206	2.412	2.6
7161.5	58.4	0.202	2.408	2.6
7161.7	60.7	0.203	2.402	2.5
7161.8	63.0	0.204	2.396	2.4
7162.0	65.4	0.204	2.390	2.3

Table 8 Gamma-4 logs data for interesting intervals of Tortonian FM

Depth FT-MD	Gamma-ray API	Neutron FT3/FT3	Density G/cm3	Resistivity Ohm. m
7173.0	80.59	0.3259	2.2774	1.7224
7173.2	80	0.3299	2.237	1.7298
7173.3	79.41	0.3339	2.1967	1.7371
7173.5	78.82	0.3379	2.1564	1.7445
7173.7	73.73	0.3535	2.1313	1.7431
7173.8	68.63	0.3691	2.1062	1.7417
7174.0	63.54	0.3847	2.0812	1.7402
7174.2	63.21	0.402	2.1089	1.7812
7174.3	62.87	0.4192	2.1366	1.8222
7174.5	62.54	0.4364	2.1643	1.8632
7174.7	62.29	0.4211	2.2188	1.9611

Depth FT-MD	Gamma-ray API	Neutron FT3/FT3	Density G/cm3	Resistivity Ohm. m
7174.8	62.05	0.4059	2.2733	2.0589
7175.0	61.8	0.3906	2.3278	2.1567
7175.2	61.63	0.3616	2.3634	2.2766
7175.3	61.45	0.3327	2.3989	2.3965
7175.5	61.28	0.3037	2.4345	2.5163
7175.7	61.01	0.2783	2.4511	2.6284
7175.8	60.75	0.2529	2.4678	2.7405
7176.0	60.48	0.2275	2.4844	2.8526
7176.2	59.61	0.2185	2.4991	3.0071
7176.3	58.75	0.2094	2.5138	3.1615
7176.5	57.88	0.2004	2.5286	3.316
7176.7	57.81	0.1968	2.5517	3.63
7176.8	57.73	0.1932	2.5749	3.944
7177.0	57.66	0.1897	2.5981	4.258
7177.2	59.28	0.1871	2.6126	4.6332
7177.3	60.89	0.1845	2.6271	5.0083
7177.5	62.51	0.182	2.6416	5.3834
7177.7	62.99	0.1764	2.6411	5.2806
7177.8	63.47	0.1709	2.6406	5.1777
7178.0	63.95	0.1653	2.6401	5.0748
7178.2	63.95	0.1675	2.6277	4.6049
7178.3	63.94	0.1696	2.6152	4.1349
7178.5	63.94	0.1718	2.6028	3.6649
7178.7	63.16	0.1774	2.581	3.2957
7178.8	62.38	0.183	2.5593	2.9266
7179.0	61.6	0.1886	2.5376	2.5574
7179.2	57.46	0.1965	2.5151	2.5374
7179.3	53.32	0.2045	2.4926	2.5174
7179.5	49.18	0.2124	2.4701	2.4975
7179.7	49.26	0.2129	2.4572	2.5202
7179.8	49.33	0.2135	2.4443	2.543
7180.0	49.41	0.214	2.4314	2.5657
7180.2	50.39	0.2166	2.432	2.6148
7180.3	51.37	0.2192	2.4326	2.6639

Depth FT-MD	Gamma-ray API	Neutron FT3/FT3	Density G/cm3	Resistivity Ohm. m
7180.5	52.35	0.2218	2.4332	2.713
7180.7	53.16	0.2173	2.4435	2.6824
7180.8	53.98	0.2128	2.4538	2.6518
7181.0	54.79	0.2083	2.4641	2.6212
7181.2	55.54	0.2073	2.4715	2.5477
7181.3	56.29	0.2062	2.479	2.4742
7181.5	57.04	0.2052	2.4865	2.4007
7181.7	57.79	0.2014	2.4814	2.335
7181.8	58.53	0.1975	2.4764	2.2694
7182.0	59.28	0.1937	2.4713	2.2038
7182.2	60.41	0.2012	2.4607	2.1267
7182.3	61.55	0.2086	2.4501	2.0496
7182.5	62.68	0.2161	2.4395	1.9725
7182.7	64.86	0.2215	2.4302	1.9534
7182.8	67.03	0.2268	2.421	1.9343
7183.0	69.21	0.2321	2.4117	1.9153
7203.0	77.13	0.2504	2.5324	3.6405
7203.2	75.89	0.2499	2.5262	3.6008
7203.3	74.65	0.2494	2.5199	3.5611
7203.5	73.41	0.2489	2.5137	3.5215
7203.7	70.53	0.2453	2.5049	3.3232
7203.8	67.66	0.2417	2.4962	3.1249
7204.0	64.78	0.238	2.4874	2.9267
7204.2	61.8	0.2314	2.4694	2.7856
7204.3	58.82	0.2249	2.4515	2.6445
7204.5	55.84	0.2183	2.4335	2.5034
7204.7	53.2	0.2164	2.4192	2.4016
7204.8	50.55	0.2146	2.4049	2.2999
7205.0	47.91	0.2128	2.3906	2.1981
7205.2	47.12	0.2105	2.3801	2.1149
7205.3	46.33	0.2083	2.3696	2.0318
7205.5	45.54	0.206	2.3591	1.9486
7205.7	45.54	0.206	2.3621	1.9539
7205.8	45.54	0.206	2.365	1.9592

Depth FT-MD	Gamma-ray API	Neutron FT3/FT3	Density G/cm3	Resistivity Ohm. m
7206.0	45.54	0.206	2.368	1.9646
7206.2	45.57	0.204	2.377	2.0226
7206.3	45.61	0.202	2.386	2.0807
7206.5	45.64	0.2	2.395	2.1388
7206.7	45.97	0.2043	2.4053	2.256
7206.8	46.29	0.2087	2.4156	2.3733
7207.0	46.62	0.213	2.4259	2.4905
7207.2	48.21	0.2138	2.4286	2.6665
7207.3	49.8	0.2146	2.4312	2.8425
7207.5	51.39	0.2154	2.4339	3.0184
7207.7	54.08	0.2155	2.435	3.1497
7207.8	56.77	0.2157	2.436	3.281
7208.0	59.46	0.2159	2.4371	3.4123
7297.0	40.52	0.2	2.3351	1.2881
7297.2	42.97	0.1961	2.3411	1.2942
7297.3	45.41	0.1922	2.347	1.3004
7297.5	47.86	0.1883	2.3529	1.3065
7297.7	49.74	0.1928	2.3555	1.3103
7297.8	51.63	0.1974	2.3582	1.314
7298.0	53.51	0.2019	2.3608	1.3177
7298.2	54.86	0.2028	2.3565	1.289
7298.3	56.22	0.2038	2.3521	1.2603
7298.5	57.57	0.2047	2.3478	1.2316
7298.7	59.37	0.2065	2.3422	1.2014
7298.8	61.16	0.2083	2.3367	1.1712
7299.0	62.96	0.2101	2.3311	1.141
7299.2	64.76	0.2077	2.3312	1.15
7299.3	66.55	0.2052	2.3312	1.159
7299.5	68.35	0.2028	2.3313	1.1681
7299.7	70.15	0.1997	2.3315	1.2242
7299.8	71.94	0.1965	2.3317	1.2803
7300.0	73.74	0.1934	2.3319	1.3365
7300.2	75.54	0.1923	2.3391	1.4726
7300.3	77.33	0.1912	2.3464	1.6087

Depth FT-MD	Gamma-ray API	Neutron FT3/FT3	Density G/cm3	Resistivity Ohm. m
7300.5	79.13	0.1901	2.3536	1.7448
7300.7	80.55	0.1959	2.3701	1.9556

Appendix C tables of results

Table 9 FZI and its relevant log data of Gamma-EX

Gamma-ray API	Neutron FT3/FT3	Density G/cm3	FZI (original) μm
73.03	0.2563	2.3665	2.591304694
73.66	0.2698	2.4053	2.581908868
69.62	0.2563	2.3873	2.317667315
66.84	0.2654	2.3522	1.007412082
58.75	0.4064	2.1047	1.780603233
59.59	0.3134	2.2312	1.974040537
62.06	0.2669	2.2711	2.129166967
63.86	0.279	2.2946	1.926687176
57.58	0.2724	2.3038	2.478857703
45.11	0.2586	2.2635	1.563033083
62.5	0.247	2.3321	1.852358445
51.81	0.2607	2.2716	1.816532575
82.29	0.2464	2.4491	1.396749642
61.6	0.1886	2.5376	0.068372344
49.41	0.214	2.4314	0.120645405
76.72	0.2322	2.5304	0.242949555
58.1	0.272	2.5203	2.214700953
57.71	0.2004	2.429	0.803709507
67.39	0.2161	2.4885	0.24653214
65.96	0.2069	2.4334	0.834812796
65.3	0.2171	2.4148	1.071758435
73.45	0.2388	2.3754	1.11936875
76.11	0.2319	2.417	0.610874152
45.54	0.206	2.368	2.082767523
46.62	0.213	2.4259	2.30993735

Gamma-ray API	Neutron FT3/FT3	Density G/cm3	FZI (original) μm
59.72	0.2148	2.4682	0.242214934
70.09	0.2049	2.4683	0.058469014
78.8	0.2128	2.468	0.293732725
69.9	0.2603	2.4982	0.302353742
65.9	0.2053	2.4897	1.020919118
57.75	0.2333	2.4046	0.198543733
65.74	0.1642	2.5118	1.889635751
83.09	0.2069	2.404	0.889220779

Table 10 FZI, effective porosity, and permeability logs of Gamma-1

Depth FT-MD	FZI μm	Effective Porosity FT^3/FT^3	Permeability mD
7254	1.1012	0.1179	2.0457
7254.5	1.3768	0.1363	4.9565
7255	1.3402	0.1336	4.4185
7255.5	1.2532	0.1408	4.5346
7256	1.2156	0.136	3.8442
7256.5	1.2316	0.1419	4.483
7257	1.3078	0.1398	4.8311
7257.5	1.3029	0.1354	4.355
7258	1.2756	0.1236	3.1644
7258.5	1.2456	0.1228	2.9591
7259	1.3678	0.1353	4.7915
7259.5	1.5386	0.1501	8.3026
7260	1.5719	0.1562	9.784
7260.5	1.4076	0.1459	6.373
7261	1.4925	0.1513	8.0138
7261.5	1.5736	0.1588	10.3123
7262	1.6266	0.1597	11.2153
7262.5	1.4199	0.1416	5.9276
7263	1.2973	0.1279	3.626
7263.5	1.4197	0.1415	5.9085
7264	1.37	0.1446	5.8753
7264.5	1.4779	0.1615	9.5803

Depth FT-MD	FZI μm	Effective Porosity FT ³ /FT ³	Permeability mD
7265	1.4546	0.162	9.3765
7265.5	1.5584	0.1711	12.6971
7266	1.4953	0.1633	10.1514
7266.5	1.2941	0.1426	5.0316
7267	1.1617	0.1203	2.4184
7270	1.2052	0.1266	3.0372
7270.5	1.0396	0.1127	1.5882
7271	1.1941	0.1245	2.8353
7271.5	1.0988	0.1109	1.6888
7272	1.344	0.126	3.7223
7272.5	1.2887	0.1294	3.709
7275.5	0.7694	0.0889	0.4254
7276	1.0171	0.1283	2.2538
7276.5	1.2385	0.1552	5.9622
7277	1.3705	0.1863	12.7682
7290	1.0698	0.1668	5.5359
7290.5	0.9921	0.1569	3.9524
7294.5	1.119	0.1525	4.6139
7295	1.1098	0.1463	3.9984
7295.5	1.0008	0.1055	1.2043
7296	1.0655	0.1065	1.405
7296.5	1.2586	0.1363	4.1435
7297	1.2726	0.1511	5.7934
7307	1.1066	0.1185	2.0971
7307.5	1.2402	0.1286	3.3758
7308	1.2952	0.1323	4.0093
7308.5	1.5746	0.151	8.8576
7309	1.6612	0.1583	11.3749
7309.5	1.8296	0.1723	17.8914
7310	1.6654	0.1645	12.8667
7310.5	1.4469	0.1523	7.6735
7315	0.4989	0.0251	0.004
7511	0.9561	0.1094	1.2268
7511.5	1.1489	0.1151	2.0703

Depth FT-MD	FZI μm	Effective Porosity FT ³ /FT ³	Permeability mD
7515.5	1.4821	0.1184	3.7478
7516	1.466	0.1319	5.0859
7516.5	1.4937	0.1377	6.0159
7517	1.4862	0.1428	6.6642
7517.5	1.6236	0.1489	9.0326
7518	1.4366	0.1396	5.8105
7518.5	1.3936	0.1285	4.2502
7519	1.3805	0.1308	4.3981
7519.5	1.4871	0.1398	6.2445
7520	1.456	0.1371	5.6466
7520.5	1.3502	0.1252	3.6867
7521	1.3999	0.1265	4.0875
7521.5	1.3924	0.13	4.3903
7522	1.3347	0.1212	3.263
7522.5	1.2036	0.1099	1.9737
7523	1.182	0.1155	2.2134
7523.5	1.2429	0.1264	3.2145
7524	1.2553	0.1259	3.2429
7524.5	1.2876	0.128	3.581
7525	1.1903	0.1213	2.6034
7525.5	1.2766	0.1286	3.5724
7526	1.2411	0.1152	2.4183
7526.5	1.4072	0.1215	3.6517
7527	1.3909	0.1256	3.9525
7527.5	1.4913	0.1362	5.7994
7528	1.3504	0.1249	3.6565
7528.5	1.2974	0.1173	2.7928
7529	1.1933	0.1111	2.0049
7530	1.134	0.0947	1.1188
7541	1.2452	0.1425	4.6445
7541.5	1.5492	0.1662	11.4983
7542	1.6658	0.1741	15.3223
7542.5	1.534	0.1711	12.3093
7543	1.5086	0.1737	12.4774

Depth FT-MD	FZI μm	Effective Porosity FT ³ /FT ³	Permeability mD
7543.5	1.49	0.1762	12.7183
7544	1.7023	0.192	21.5899
7544.5	1.5738	0.1799	15.1123
7545	1.6885	0.19	20.5831
7545.5	1.6573	0.1961	21.8369
7546	1.7142	0.2026	25.8481
7546.5	1.6807	0.1965	22.6085
7547	1.6805	0.1942	21.8046
7547.5	1.5555	0.1839	15.7836
7548	1.3579	0.1669	8.9431
7548.5	1.056	0.132	2.6474
7550	1.2592	0.1526	5.8524
7550.5	1.4363	0.1665	9.926
7551	1.1639	0.1362	3.5373
7551.5	0.9801	0.1135	1.4447
7553.5	1.3236	0.1455	5.5946
7554	1.5277	0.1614	10.2153
7554.5	1.5206	0.1671	11.2562
7555	1.535	0.1689	11.8559
7555.5	1.5187	0.1747	12.8564
7556	1.6372	0.1836	17.4168
7556.5	1.4702	0.1689	10.8719
7557	1.4358	0.1524	7.5724
7557.5	1.4815	0.156	8.6579
7558	1.5432	0.1617	10.4779
7558.5	1.5603	0.1727	13.1037
7559	1.4378	0.1604	8.8743
7559.5	1.348	0.1525	6.6958
7564	0.6332	0.1126	0.5872
7652	1.114	0.1005	1.29
7652.5	1.2155	0.1148	2.2991
7653	1.1294	0.1064	1.5767
7653.5	1.2407	0.1186	2.6414
7654	1.3159	0.1268	3.6377

Depth FT-MD	FZI μm	Effective Porosity FT ³ /FT ³	Permeability mD
7654.5	1.3414	0.135	4.5703
7655	1.1927	0.1251	2.8665
7655.5	1.0922	0.1204	2.1396
7656	1.1087	0.1254	2.4951
7656.5	1.2271	0.1391	4.1878
7657	1.3108	0.1419	5.0809
7657.5	1.2481	0.133	3.7842
7658	1.3995	0.1449	6.1778
7658.5	1.5271	0.1535	8.7579
7659	1.7626	0.1675	15.2251
7659.5	1.7484	0.1666	14.742
7660	1.6341	0.1593	11.2359
7660.5	1.535	0.1562	9.3358
7661	1.4275	0.1449	6.4253
7661.5	1.3958	0.1401	5.5411
7662	1.4762	0.1436	6.6863
7662.5	1.6273	0.1533	9.9016
7663	1.6598	0.1639	12.6489
7663.5	1.5443	0.1661	11.4058
7664	1.302	0.1524	6.228
7664.5	1.241	0.1451	4.8697
7665	1.2079	0.1346	3.6734
7665.5	1.2308	0.1329	3.6667
7666	1.3708	0.1408	5.4308
7666.5	1.3492	0.1418	5.3733
7667	1.3694	0.147	6.1742
7667.5	1.2478	0.1389	4.3123
7668	1.283	0.1428	4.9623
7668.5	1.1523	0.1337	3.2736
7669	1.2607	0.1473	5.2625
7669.5	1.1465	0.1362	3.4339
7670	1.2594	0.1406	4.5559
7670.5	1.2159	0.1308	3.4146
7671	1.3224	0.1339	4.3308

Depth FT-MD	FZI μm	Effective Porosity FT ³ /FT ³	Permeability mD
7671.5	1.396	0.1387	5.3762
7672	1.3763	0.1473	6.2725
7672.5	1.3135	0.1386	4.7489
7673	1.2767	0.134	4.0472
7673.5	1.3377	0.131	4.1479
7674	1.6039	0.1581	10.5825
7674.5	1.68	0.1683	14.0367
7675	1.5428	0.164	10.932
7675.5	1.1614	0.1322	3.2191
7681	1.2504	0.1357	4.0401
7681.5	1.2957	0.1391	4.6731
7682	1.1922	0.1272	3.0136
7687.5	1.445	0.1424	6.2443
7688	1.5401	0.1501	8.3181
7688.5	1.5692	0.1464	8.002
7689	1.488	0.1469	7.2744
7689.5	1.6293	0.1563	10.5268
7690	1.5058	0.1503	7.9938
7690.5	1.6484	0.1499	9.5037
7691	1.5505	0.1415	7.048
7691.5	1.675	0.1485	9.5321
7692	1.7377	0.1609	13.0879
7692.5	1.7739	0.1629	14.1758
7693	1.6645	0.1521	10.1127
7693.5	1.5883	0.1431	7.6467
7694	1.5219	0.1329	5.6118
7694.5	1.4872	0.1278	4.7624
7695	1.2432	0.1109	2.1631

Table 11 FZI, effective porosity, and permeability logs of Gamma-2

Depth FT-MD	FZI μm	Effective Porosity FT ³ /FT ³	Permeability mD
7159.167	0.8258	0.1784	4.0551
7159.334	0.8799	0.1878	5.3935

Depth FT-MD	FZI μm	Effective Porosity FT ³ /FT ³	Permeability mD
7159.5	0.934	0.197	7.0357
7159.667	1.03	0.2039	9.516
7159.834	1.1259	0.2106	12.571
7160	1.2219	0.2172	16.2777
7160.167	1.2597	0.2159	16.992
7160.334	1.2973	0.2146	17.6785
7160.5	1.3353	0.2132	18.3605
7160.667	1.3038	0.2022	14.8492
7160.834	1.2725	0.1911	11.8975
7161	1.2413	0.18	9.4254
7161.167	1.2331	0.1779	8.9693
7161.334	1.2251	0.1758	8.5377
7161.5	1.2171	0.1737	8.1223
7161.667	1.2506	0.173	8.4574
7161.834	1.2844	0.1721	8.7922
7162	1.3181	0.1712	9.1024
7162.167	1.3072	0.166	8.1541
7162.334	1.2963	0.1607	7.2625
7162.5	1.2853	0.1553	6.4289
7162.667	1.2521	0.1419	4.6385
7167.667	1.4139	0.1635	9.096
7167.834	1.4473	0.1709	10.9151
7168	1.4809	0.1782	12.9996
7168.167	1.5056	0.1811	14.1224
7168.334	1.5303	0.184	15.3159
7168.5	1.555	0.1869	16.5829
7168.667	1.4515	0.1807	13.0388
7168.834	1.3477	0.1737	9.9542
7175	1.1554	0.1074	1.6944
7201.667	1.1824	0.1339	3.4689
7201.834	1.2903	0.1389	4.6161
7202	1.3983	0.1434	5.9721
7202.167	1.4886	0.1474	7.3487
7202.334	1.5792	0.151	8.9068

Depth FT-MD	FZI μm	Effective Porosity FT ³ /FT ³	Permeability mD
7202.5	1.6695	0.1543	10.6348
7202.667	1.7618	0.1602	13.2871
7202.834	1.8538	0.1659	16.3745
7203	1.946	0.1715	19.9612
7203.167	1.9973	0.1759	22.7366
7203.334	2.0489	0.1803	25.7898
7203.5	2.1005	0.1846	29.1207
7203.667	2.0785	0.1855	28.9584
7203.834	2.0568	0.1864	28.8023
7204	2.0348	0.1874	28.6148
7204.167	1.9803	0.185	26.056
7204.334	1.9261	0.1826	23.6985
7204.5	1.8717	0.1802	21.4799
7204.667	1.8466	0.1767	19.6929
7204.834	1.8214	0.1732	18.0048
7205	1.7963	0.1696	16.4424
7205.167	1.7973	0.17	16.5794
7205.334	1.798	0.1704	16.6906
7205.5	1.7988	0.1707	16.8171
7205.667	1.8285	0.1739	18.3991
7205.834	1.8583	0.1772	20.1154
7206	1.8884	0.1805	21.9729
7206.167	1.8607	0.181	21.5276
7206.334	1.8332	0.1815	21.0795
7206.5	1.8056	0.182	20.6112
7206.667	1.7967	0.1826	20.6133
7206.834	1.7877	0.1831	20.5928
7207	1.7788	0.1837	20.5836
7207.167	1.7134	0.1783	17.4311
7207.334	1.6483	0.1728	14.6607
7207.5	1.5829	0.1672	12.2202
7207.667	1.5967	0.1673	12.4486
7207.834	1.6105	0.1673	12.6764
7208	1.6243	0.1674	12.9035

Depth FT-MD	FZI μm	Effective Porosity FT ³ /FT ³	Permeability mD
7208.167	1.628	0.1632	11.9924
7208.334	1.6317	0.1589	11.1202
7208.5	1.6352	0.1547	10.2783
7208.667	1.6241	0.1556	10.3183
7208.834	1.6129	0.1564	10.3478
7209	1.6019	0.1573	10.3932
7209.167	1.546	0.1524	8.7782
7209.334	1.4901	0.1473	7.3557
7209.5	1.4342	0.1422	6.1169
7209.667	1.3602	0.1384	5.0736
7209.834	1.2862	0.1346	4.1615
7210	1.2124	0.1305	3.3668
7288	1.9223	0.1649	17.2603
7288.167	1.9291	0.1655	17.5783
7288.334	1.9356	0.166	17.8709
7288.5	1.9422	0.1666	18.182
7288.667	1.9462	0.1632	17.1548
7288.834	1.9498	0.1598	16.135
7289	1.9537	0.1563	15.1626
7289.167	1.9148	0.1544	14.029
7289.334	1.876	0.1525	12.9579
7289.5	1.8371	0.1505	11.9473
7289.667	1.831	0.1499	11.725
7289.834	1.8251	0.1493	11.5036
7290	1.8191	0.1487	11.2876

Table 12 FZI, effective porosity, and permeability logs of Gamma-3

Depth FT-MD	FZI μm	Effective Porosity FT ³ /FT ³	Permeability mD
7041	0.9806	0.075	0.4133
7041.167	1.0858	0.1088	1.5593
7041.334	1.1908	0.1426	4.2556
7041.5	1.2961	0.1764	9.653
7041.667	1.3523	0.2095	17.8231

Depth FT-MD	FZI μm	Effective Porosity FT ³ /FT ³	Permeability mD
7041.834	1.4083	0.2424	30.445
7042	1.4645	0.2754	49.138
7042.167	1.4841	0.2882	58.3243
7042.334	1.5039	0.3011	68.8349
7042.5	1.5236	0.3139	80.7453
7042.667	1.5718	0.3213	92.6752
7042.834	1.62	0.3288	106.0322
7043	1.6681	0.3362	120.8399
7043.167	1.7692	0.3434	145.7218
7043.334	1.8704	0.3504	173.9647
7043.5	1.9714	0.357	205.5467
7043.667	2.021	0.3519	206.0759
7043.834	2.0704	0.3466	205.737
7044	2.12	0.3412	204.9087
7044.167	2.0475	0.3095	139.3663
7044.334	1.975	0.2777	91.7846
7044.5	1.9025	0.246	58.1245
7044.667	1.7674	0.2038	27.964
7044.834	1.6322	0.1615	11.6882
7045	1.4971	0.1193	3.9184
7045.167	1.4486	0.0977	2.0044
7045.334	1.4	0.0761	0.8808
7045.5	1.3515	0.0545	0.3002
7045.667	1.4085	0.0641	0.5315
7045.834	1.4654	0.0737	0.8751
7046	1.5225	0.0833	1.3666
7046.167	1.5993	0.0968	2.3763
7046.334	1.6763	0.1104	3.8808
7046.5	1.7533	0.1239	6.0269
7046.667	1.7534	0.134	7.6351
7046.834	1.7534	0.144	9.5123
7047	1.7534	0.1541	11.6811
7047.167	1.76	0.1645	14.3713
7047.334	1.7664	0.1749	17.4767

Depth FT-MD	FZI μm	Effective Porosity FT ³ /FT ³	Permeability mD
7047.5	1.7729	0.1854	21.0311
7047.667	1.9257	0.2222	43.4177
7047.834	2.0785	0.2591	81.6776
7048	2.2314	0.296	143.4853
7048.167	2.3025	0.3158	188.041
7048.334	2.3737	0.3357	243.534
7048.5	2.445	0.3555	311.8744
7048.667	2.4569	0.3613	331.8619
7048.834	2.4685	0.3669	352.7561
7049	2.4802	0.3726	374.713
7049.167	2.342	0.3432	254.7215
7049.334	2.2037	0.3136	168.5039
7049.5	2.0655	0.2842	107.9931
7049.667	1.9111	0.2454	58.2723
7049.834	1.7566	0.2067	28.8621
7050	1.6021	0.1679	12.6822
7050.167	1.5126	0.1362	5.9697
7050.334	1.423	0.1043	2.3579
7050.5	1.3334	0.0724	0.6891
7050.667	1.3066	0.06	0.3749
7050.834	1.2796	0.0475	0.1782
7051	1.2528	0.035	0.0683
7051.167	1.2415	0.037	0.0793
7051.334	1.2304	0.039	0.0915
7051.5	1.219	0.041	0.1043
7051.667	1.1966	0.0405	0.0967
7051.834	1.1742	0.04	0.0898
7052	1.1519	0.0395	0.0831
7052.167	1.1839	0.0438	0.1198
7052.334	1.2162	0.0482	0.1682
7052.5	1.2483	0.0525	0.2297
7052.667	1.3721	0.0688	0.6256
7052.834	1.496	0.0851	1.4101
7053	1.6198	0.1013	2.7977

Depth FT-MD	FZI μm	Effective Porosity FT ³ /FT ³	Permeability mD
7053.167	1.6767	0.1136	4.2334
7053.334	1.7337	0.1258	6.1696
7053.5	1.7906	0.1381	8.7253
7053.667	1.8156	0.141	9.5595
7053.834	1.8405	0.1439	10.4582
7054	1.8655	0.1468	11.4178
7054.167	1.8231	0.1389	9.2158
7054.334	1.7806	0.131	7.3459
7054.5	1.738	0.123	5.7846
7054.667	1.8301	0.1357	8.6395
7054.834	1.9221	0.1484	12.5085
7055	2.0144	0.1611	17.6676
7055.167	2.0898	0.1777	25.6689
7055.334	2.1652	0.1943	36.2515
7055.5	2.2407	0.211	50.0278
7055.667	2.2712	0.221	59.3816
7055.834	2.3016	0.2311	70.0048
7056	2.332	0.2411	81.9999
7056.167	2.2722	0.2267	64.2887
7056.334	2.2125	0.2124	49.7827
7056.5	2.1527	0.198	37.9543
7056.667	2.0343	0.1694	21.007
7056.834	1.9161	0.1409	10.6273
7057	1.7978	0.1124	4.7086
7113.5	0.688	0.1315	1.1112
7113.667	0.7455	0.1364	1.4577
7113.834	0.803	0.1413	1.8818
7114	0.8606	0.1462	2.3979
7114.167	0.9545	0.1585	3.7767
7114.334	1.0485	0.1706	5.7035
7114.5	1.1425	0.1824	8.3135
7114.667	1.1522	0.1874	9.1821
7114.834	1.1622	0.1924	10.1332
7115	1.1719	0.1974	11.1413

Depth FT-MD	FZI μm	Effective Porosity FT^3/FT^3	Permeability mD
7115.167	1.1216	0.1939	9.6634
7115.334	1.0716	0.1904	8.3401
7115.5	1.0214	0.1869	7.1556
7115.667	0.9861	0.1812	6.066
7115.834	0.9508	0.1755	5.115
7116	0.9156	0.1698	4.2844
7116.167	0.9695	0.1796	5.7086
7116.334	1.0236	0.1895	7.4974
7116.5	1.0776	0.1993	9.7073
7116.667	1.1116	0.2102	12.1743
7116.834	1.1455	0.2211	15.1116
7117	1.1796	0.232	18.6185
7117.167	1.14	0.236	18.3336
7117.334	1.1007	0.2397	17.9518
7117.5	1.0612	0.2431	17.4414
7117.667	1.0065	0.2325	13.6546
7117.834	0.9516	0.222	10.5646
7118	0.8967	0.2114	8.0602
7118.167	0.9413	0.2152	9.395
7118.334	0.9858	0.2188	10.8329
7118.5	1.0303	0.2219	12.3781
7118.667	1.0599	0.2206	12.8595
7118.834	1.0897	0.2191	13.3111
7119	1.1192	0.2174	13.703
7119.167	1.129	0.2193	14.3281
7119.334	1.1387	0.2212	14.9644
7119.5	1.1483	0.2231	15.6244
7119.667	1.1007	0.213	12.4443
7119.834	1.053	0.2029	9.7952
7120	1.0052	0.1927	7.6153

Table 13 FZI, effective porosity, and permeability logs of Gamma-4

Depth FT-MD	FZI μm	Effective Porosity FT ³ /FT ³	Permeability mD
7172	0.5984	0.093	0.2949
7172.167	0.644	0.1059	0.5057
7172.334	0.6899	0.1189	0.8235
7172.5	0.7357	0.1319	1.2808
7172.667	0.8335	0.146	2.2401
7172.834	0.9313	0.1601	3.7059
7173	1.0291	0.1742	5.8592
7173.167	1.1473	0.1874	9.1106
7173.334	1.2653	0.2006	13.6512
7173.5	1.3832	0.2137	19.8431
7173.667	1.5972	0.2392	37.573
7173.834	1.8111	0.2631	65.0885
7174	2.0248	0.2855	105.337
7174.167	1.9807	0.2871	102.6499
7174.334	1.9365	0.2887	99.8595
7174.5	1.8923	0.2903	97.0296
7174.667	1.7532	0.2706	66.6686
7174.834	1.6141	0.251	44.5898
7175	1.475	0.2313	28.8511
7175.167	1.3686	0.2099	18.3821
7175.334	1.2625	0.1886	11.2442
7175.5	1.1561	0.1672	6.5189
7175.667	1.1017	0.1522	4.441
7175.834	1.0471	0.1371	2.9217
7176	0.9926	0.1221	1.8462
7176.167	0.973	0.1158	1.5118
7176.334	0.9532	0.1095	1.2234
7279	0.9183	0.106	1.0296
7279.167	0.9939	0.1125	1.4435
7279.334	1.0697	0.1189	1.9799
7279.5	1.1453	0.1253	2.6572
7279.667	1.1699	0.1262	2.8332
7279.834	1.1949	0.1271	3.0209

Depth FT-MD	FZI μm	Effective Porosity FT ³ /FT ³	Permeability mD
7280	1.2197	0.1279	3.2103
7280.167	1.2595	0.1296	3.5584
7280.334	1.2995	0.1312	3.9365
7280.5	1.3395	0.1328	4.3328
7280.667	1.3697	0.1353	4.7959
7280.834	1.3997	0.1378	5.2965
7281	1.4298	0.1403	5.8343
7281.167	1.4649	0.1442	6.6671
7281.334	1.5004	0.1483	7.607
7281.5	1.5356	0.1523	8.6438
7281.667	1.5549	0.1549	9.3427
7281.834	1.5742	0.1576	10.0841
7282	1.5936	0.1602	10.8695
7282.167	1.5734	0.16	10.5516
7282.334	1.5533	0.1597	10.2305
7282.5	1.5331	0.1594	9.9107
7282.667	1.5206	0.1572	9.3364
7282.834	1.5083	0.155	8.7958
7283	1.4959	0.1528	8.2818
7283.167	1.4901	0.1531	8.2792
7283.334	1.4844	0.1535	8.2759
7283.5	1.4787	0.1539	8.2801
7283.667	1.4784	0.155	8.46
7283.834	1.4783	0.1562	8.6488
7284	1.478	0.1573	8.8328
7284.167	1.4658	0.1571	8.6685
7284.334	1.4538	0.1571	8.5123
7284.5	1.4416	0.1569	8.3504
7284.667	1.3707	0.1535	7.0549
7284.834	1.2999	0.1498	5.8933
7285	1.2292	0.1458	4.8565
7285.167	1.1386	0.1394	3.6303
7285.334	1.048	0.1324	2.6326
7287.334	0.9489	0.125	1.8108

Depth FT-MD	FZI μm	Effective Porosity FT ³ /FT ³	Permeability mD
7287.5	1.0449	0.1339	2.7053
7287.667	1.0957	0.1385	3.296
7287.834	1.1465	0.143	3.9751
7288	1.1975	0.1473	4.7543
7288.167	1.1985	0.148	4.8223
7288.334	1.1994	0.1486	4.8911
7288.5	1.2007	0.1492	4.9702
7288.667	1.1877	0.1492	4.8592
7288.834	1.1748	0.1492	4.7508
7289	1.1619	0.1491	4.64
7289.167	1.1453	0.1476	4.3757
7289.334	1.1285	0.1461	4.1175
7289.5	1.1117	0.1446	3.8701
7289.667	1.1079	0.1441	3.8027
7289.834	1.104	0.1435	3.7321
7290	1.1001	0.143	3.6626
7290.167	1.1256	0.1435	3.8791
7290.334	1.1514	0.144	4.0993
7290.5	1.1768	0.1444	4.3147
7290.667	1.2652	0.1495	5.5513
7290.834	1.3539	0.1542	6.9824
7291	1.4425	0.1584	8.6055
7291.167	1.5084	0.1621	10.0878
7291.334	1.5739	0.1654	11.6929
7291.5	1.6395	0.1686	13.4376
7291.667	1.6548	0.1699	14.0335
7291.834	1.6701	0.1713	14.6502
7292	1.6856	0.1727	15.2991
7292.167	1.7203	0.174	16.2934
7292.334	1.7552	0.1752	17.3202
7292.5	1.7898	0.1763	18.3692
7292.667	1.827	0.1779	19.6922
7292.834	1.864	0.1795	21.0562
7293	1.9009	0.1811	22.4826

Depth FT-MD	FZI μm	Effective Porosity FT ³ /FT ³	Permeability mD
7293.167	1.9287	0.1821	23.5553
7293.334	1.9564	0.1831	24.6607
7293.5	1.984	0.1841	25.7734
7293.667	1.9957	0.1849	26.4299
7293.834	2.0071	0.1857	27.0755
7294	2.0186	0.1864	27.7269
7294.167	2.0111	0.1851	26.9351
7294.334	2.0036	0.1838	26.1602
7294.5	1.9962	0.1825	25.4021
7294.667	1.9855	0.1821	24.9706
7294.834	1.9751	0.1817	24.5585
7295	1.9648	0.1814	24.1695
7295.167	1.9504	0.181	23.6637
7295.334	1.936	0.1807	23.1802
7295.5	1.9217	0.1803	22.6986
7295.667	1.9235	0.1807	22.8837
7295.834	1.9257	0.1811	23.105
7296	1.9278	0.1815	23.3082
7296.167	1.9322	0.1797	22.6991
7296.334	1.9366	0.1779	22.0977
7296.5	1.9409	0.176	21.504
7296.667	1.921	0.1739	20.2908
7296.834	1.9013	0.1718	19.1458
7297	1.8816	0.1697	18.0527
7297.167	1.7966	0.1642	14.8944
7297.334	1.7119	0.1586	12.1655
7297.5	1.6272	0.1529	9.8179
7297.667	1.5729	0.1521	9.0443
7297.834	1.5185	0.1513	8.2936
7298	1.4643	0.1504	7.5649
7298.167	1.4385	0.1501	7.253
7298.334	1.413	0.1497	6.9527
7298.5	1.3871	0.1493	6.6381
7298.667	1.353	0.1488	6.2542

Depth FT-MD	FZI μm	Effective Porosity FT^3/FT^3	Permeability mD
7298.834	1.3187	0.1482	5.8632
7299	1.2847	0.1474	5.4771